Politecnico di Torino

Master of Science program in
BUILDING ENGINEERING
A.a. 2025/2026
March 2026

Energy geostructures for heating and cooling of a sports center in Turin

Supervisors:
Prof. MARCO **BARLA**
Ing. MARIA ROMANA **ALVI**

Candidate:
BASIL MARZOUG MOHAMED **MUSA**

Abstract

As the building sector increasingly shifts toward net-zero energy targets, energy geostructures present a promising solution for sustainable heating and cooling. This thesis investigates the design and thermal performance of an integrated geothermal skin and slab system for a new sports center in Turin, Italy, operating within a cold climate context. The primary objective is to evaluate the feasibility and energy contribution of these shallow energy geostructure technologies toward achieving Near Zero Energy Building (NZEB) standards.

The research methodology encompasses a comprehensive literature review identifying current advancements and knowledge gaps in energy geostructure applications. The theoretical framework further examines low-enthalpy geothermal mechanisms and heat pump integration across four primary geostructure types: tunnels, piles, walls, and geothermal skins. After that, the energy performance model is developed to simulate the building's thermal behavior and demand. The geothermal skin and slab configurations have been specifically engineered for the case study, with their thermal yields quantified through detailed performance calculations. At the end, the percentage of the building's total energy requirements supplied by the proposed geothermal system is determined.

Results demonstrate that the integrated geothermal system meets about 18.2 % of the sports center's total heating demands, demonstrating significant potential for reducing conventional energy consumption. This research provides a practical framework for the implementation of energy geostructures in cold climates and offers a scalable strategy for advancing NZEB objectives in the building sector.

Acknowledgement

*I would like to express my sincere gratitude to my supervisor, Professor Marco **Barla**, for his continuous guidance, valuable suggestions, and unwavering support throughout the development of this thesis. His expertise and constructive feedback greatly contributed to improving the quality of this work.*

*I would also like to thank Ing. Maria Romana **Alvi** for her patience, helpful suggestions, and steady support during this journey. Her assistance made a real difference.*

*My deep appreciation goes to **Politecnico di Torino** for providing an excellent academic environment and all the resources necessary to complete my studies and research.*

To my professors and colleagues who shared knowledge and encouragement along the way — thank you for being part of this academic journey.

Finally, my deepest gratitude goes to my family, cousins, and friends. You have stood by me through one of the hardest times — while facing the weight of war in Sudan, you never stopped encouraging me, believing in me, and holding me up. Your strength is beyond words, and this work belongs to you as much as it belongs to me.

.

Table of contents

List of Figures

List of Tables

Chapter 1.

Introduction

1.1. Research Aims and Objectives

The primary goal of this research is to design and evaluate an energy geostructure solution — specifically integrating a geothermal skin and slab—for a new building in Turin, Italy. This study assesses the thermal performance and feasibility of such systems in a Cold climate.

To achieve this, the following objectives have been established:

- **Literature Synthesis**: Conduct a comprehensive review of the current scientific research, focusing on geothermal and solar energy advancements, while identifying critical knowledge gaps in energy geostructure integration.
- **Energy Modeling:** Develop a performance model to simulate the building's thermal behavior and energy demands.
- **System Design:** Design geothermal skin and slab geostructures.
- **Performance Quantification:** Calculate the thermal energy provided by the proposed geostructures.
- **Comparative Analysis:** Evaluate the system's efficacy by determining the percentage of the building's total energy requirements met by the geothermal solution.

1.2. Thesis Structure

The thesis is organized into four primary chapters, detailed as follows:

Chapter 2 | Fundamentals of Renewable Energy: Provides a theoretical foundation in renewable energy systems, with a specialized focus on low-enthalpy geothermal systems and the mechanics of geothermal heat pumps.

Chapter 3 | Energy Geostructures & State-of-the-Art: Examines the functional mechanisms of energy geostructures. This chapter includes a comparative analysis of four distinct types— tunnels, piles, walls, and geothermal skins— validated through established case studies and previous research.

Chapter 4 | Case Study & Methodology: presents the geometry and properties of this case study, including the energy performance analysis model, geothermal design for the building, and performance calculations for the geothermal system and results.

Conclusions and Future Outlook: In the concluding chapter, the key findings of the study are presented and recapped, and recommendations for further developments are suggested.

Chapter 2.

Renewable energy

2.1. Introduction to Renewable Energy in the Built Environment

The building sector remained a prime energy consumer in 2022, accounting for 30% of the worldwide very last-strength demand, mainly for operational activities, including heating and cooling. This parent rises to 34%, including the strength used to supply construction materials, as shown in Figure 1. Over time, the sector's electricity call has step by step improved by means of simply over 1% yearly. A notable improvement has been the developing share of strength in homes' energy mix, which rose from 30% in 2010 to 35% in 2022, observed by using a gradual shift toward renewable electricity resources (United Nations Environment Programme, 2024).

Error! Reference source not found. shows that the buildings sector became liable for a full-size portion of world carbon dioxide emissions, accounting for 37% of the total, which corresponds to nearly 10 billion tonnes. This consists of 6.8 billion tonnes from indirect emissions, mostly stemming from energy use, in addition to three billion tonnes from direct emissions. Additionally, the manufacturing of critical construction materials, which includes cement, steel, and aluminium, contributed an extra 2.5 billion tonnes, whilst the production of bricks and glass brought about 1.2 billion tonnes (United Nations Environment Programme, 2024).

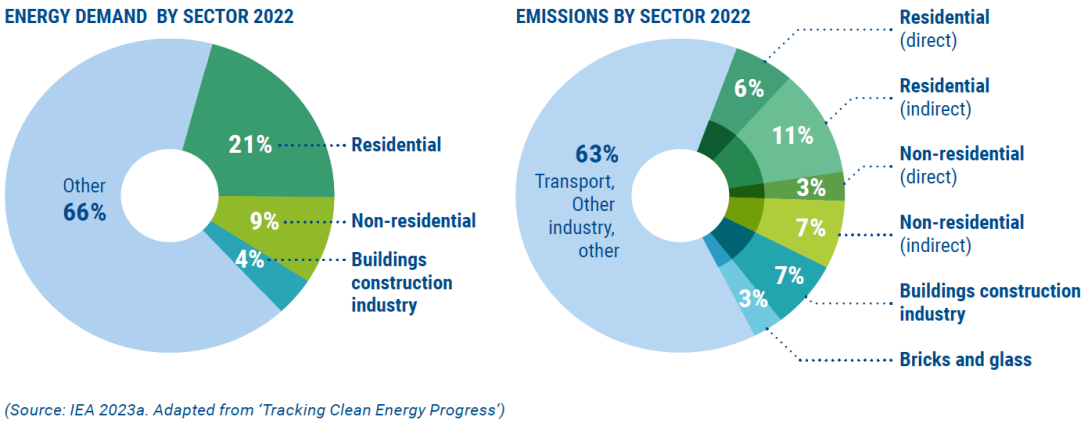

Figure 1:share of buildings in total energy consumption in 2022(left) and share of total CO_2 emissions in 2022(right)(IEA, 2023)

2.1.1. The Importance of transitioning to renewable energy in buildings

The transition to renewable energy sources in the construction sector is important for addressing climate change, decreasing energy intake, and promoting sustainability. The construction area is a good-sized contributor to worldwide energy use and greenhouse gas emissions, necessitating a shift toward renewable energy sources. This transition is not the most effective in mitigating environmental influences; however additionally complements power performance and financial viability in constructing projects. The following sections define the key elements of this alteration.

Environmental Impact Reduction: Buildings consume 30-40% of global energy and generate approximately one-third of greenhouse gas emissions (IEA, 2023). Implementing renewable energy sources such as solar, geothermal, and wind can substantially reduce building carbon footprints(Reddy et al., 2024).

Economic Benefits: Renewable energy technologies can yield long-term cost savings through reduced electricity bills and potential government incentives (Yang et al., 2023). Renewable energy integration in buildings can stimulate green finance opportunities, promoting investment in sustainable construction practices (Yang et al., 2023).

Technological Advancements: Innovations in renewable energy technologies, including geothermal systems and biomass, are increasingly implemented in construction designs (Reddy et al., 2024).

While the advantages of transitioning to renewable energy in buildings are undeniable, demanding situations consisting of preliminary investment charges and the need for regulatory frameworks remain vast obstacles to massive adoption. Addressing those challenges is important for knowing the full capacity of renewable energy within the building sector.

Challenging to integrate renewable energy in buildings

Integrating renewable energy systems into building design and construction faces numerous obstacles that obstruct widespread implementation. From a financial standpoint, the substantial initial investment required to deploy renewable technologies, including solar panels and geothermal systems, persists as a significant hurdle. This challenge is exacerbated by the fact that, although financial incentives and subsidies are accessible, they frequently prove inadequate to offset the initial capital outlay, thereby constraining their influence on promoting the adoption of renewable energy (Chen et al., 2024; Sonal Vaghela et al., 2024).

Aside from financial obstacles, integrating renewable energy systems into buildings presents technical challenges. Adapting existing structures to accommodate these technologies necessitates specialized expertise and meticulous planning to ensure compatibility and

operational efficiency (Sonal Vaghela et al., 2024). Additionally, the variability of renewable energy sources, such as solar and wind, requires reliable energy storage solutions to manage the balance between supply and demand (ZANELDIN, 2024), introducing further complexity to the system's design and operation.

Moreover, standards, regulatory (ZANELDIN, 2024) and policy-related challenges (Sonal Vaghela et al., 2024) hinder the widespread incorporation of renewable energy in building construction. Many countries lack explicit and consistent policies that encourage the integration of renewable technologies into buildings. The need for well-defined regulatory frameworks and standards in this domain generates uncertainty for project developers, ultimately discouraging large-scale implementation.

2.2. Overview of Solar Energy

2.2.1. Principles of Solar Energy

The magnitude and distribution of solar radiation incident upon Earth's atmosphere can be broadly categorized into absorbed and reflected components. Approximately 52 PW (10^{15} W) of incoming solar radiation is reflected into space, constituting about 30% of the total incident solar energy, a fraction commonly referred to as Earth's planetary albedo. This significant reflected component has spurred interest in the exploration of space-based solar energy collection, including concepts involving satellite-mounted photovoltaic arrays capable of harvesting solar radiation and transmitting the captured energy to Earth via microwave or laser beams for terrestrial use. At the top of the atmosphere, when the Sun is positioned directly overhead, the incident solar radiation flux reaches approximately 1.36–1.40 kW/m², a value known as the solar constant. In contrast, the total global human energy consumption—accounting for all primary energy sources such as fossil fuels, nuclear power, and renewables—amounts to approximately 18 TW. Given that nearly 174 PW of solar radiation continuously impinges on Earth's sunlit hemisphere, the available solar energy exceeds current global energy demand by roughly four orders of magnitude. Consequently, the interception and conversion of even a small fraction of this incoming solar radiation could, in principle, satisfy present and future global energy requirements (Rhodes, 2010).

The spectral distribution of solar radiation closely resembles that of a blackbody radiator with an effective temperature of approximately 5,800 K. Consequently, emitted energy is predominantly concentrated in the visible range (400–700 nm) and near-infrared region, with a smaller but significant ultraviolet (UV) contribution. Total electromagnetic radiation reaching Earth's atmospheric boundary spans wavelengths from approximately 100 nm to 10^6 nm and is commonly classified into five functional spectral regions according to wavelength. The ultraviolet spectrum is subdivided into UVC (100–280 nm), which exhibits strong germicidal properties but is almost entirely absorbed by atmospheric oxygen and the ozone

layer; UVB (280–315 nm), which plays a critical role in photochemical processes responsible for ozone formation and maintenance; and UVA (315–400 nm), which penetrates deeper into the atmosphere and is widely used in medical and cosmetic applications due to its comparatively lower potential for direct DNA damage. The visible spectrum accounts for roughly 50% of total solar radiation and represents the portion detectable by the human eye. Radiation at longer wavelengths constitutes the infrared (IR) region (700 nm–10^6 nm), which is the principal contributor to solar thermal energy. The infrared spectrum is further divided into Infrared A (700–1,400 nm), Infrared B (1,400–3,000 nm), and Infrared C (3,000–10^6 nm), with increasing wavelength corresponding to decreasing photon energy and deeper relevance for thermal interactions with terrestrial materials (Rhodes, 2010).

Solar energy technologies are generally classified as active or passive, based on their mechanisms for capturing, converting, and using solar radiation. Active solar technologies, often considered supply-side systems, use mechanical and electrical components—such as photovoltaic (PV) modules and solar thermal collectors—to convert solar radiation into electricity or usable thermal energy. Conversely, passive solar technologies serve as demand-side strategies, leveraging architectural and urban design principles—including building orientation, optimized glazing, thermal mass selection, shading devices, and natural ventilation—to minimize external energy demand without active mechanical systems. Solar technologies specifically designed for electricity generation, whether through direct photovoltaic conversion or indirect solar thermal power cycles (e.g., steam turbines driven by concentrated solar power), are collectively known as solar power technologies (Rhodes, 2010).

From an environmental standpoint, about 70% of incoming solar radiation is absorbed by the Earth's atmosphere and surface, maintaining a global mean surface temperature of approximately 14 °C and fueling critical geophysical and biological processes. This absorbed energy drives the hydrological cycle through atmospheric convection, evaporation, and latent heat release, and supports photosynthesis, which annually converts solar energy into around 3,000 EJ of biomass. The Earth system absorbs an estimated 3.85×10^6 EJ per year of solar energy, a quantity so immense that the energy received in just one hour surpasses current annual global human energy consumption. These statistics highlight the enormous potential of solar energy technologies as a foundation for future sustainable energy systems (Rhodes, 2010).

2.2.2. Types of Solar Technologies

Photovoltaic (PV)

The term photovoltaic combines the Greek word Phos (light) and voltaic (electric), the latter named in honor of Alessandro Volta, and describes the generation of electricity from light. The photovoltaic effect was first observed by A. E. Becquerel in 1839; however, early experimental devices, such as Charles Fritts' selenium-based solar cell developed in 1883, had very low

conversion efficiencies of about 1%. A significant technological advance occurred in 1946 when Russell Ohl patented the semiconductor p–n junction solar cell. Building on this, in 1954, Chapin, Fuller, and Pearson at Bell Laboratories fabricated the first silicon photovoltaic cell, which achieved approximately 6% efficiency and marked the beginning of practical solar electricity generation (Rhodes, 2010). The successful deployment of photovoltaic cells on the Vanguard 1 satellite in 1958 demonstrated their reliability in space and enabled long-term power for satellite systems. This milestone spurred substantial public investment in photovoltaic research and development. Over the following decades, technology progressed from a specialized solution for aerospace and telecommunications to a mature and widely used option for large-scale, grid-connected terrestrial electricity production (Rhodes, 2010).

Photovoltaic (PV) technology is a widely adopted method for directly converting solar radiation into electrical energy. PV systems offer high energy potential, silent operation, and comparatively low installation, operational, and maintenance costs. The core element of a PV system is the PV cell, which functions as a p–n junction diode. PV cells are manufactured from semiconductor materials and typically range in size from 0.5 to 4 inches. When sunlight strikes the p–n junction, incident photons generate electron-hole pairs by exciting electrons within the semiconductor structure. The released electrons then migrate toward the treated front surface. With the front and rear contacts connected through an external conductor, current flows and power are generated, as illustrated in Figure 2. Incident radiation also raises the surface temperature of the PV module. This temperature increase elevates circuit resistance, which in turn reduces electron mobility. Consequently, the open-circuit voltage is lowered, negatively influencing both the electrical performance and material behavior of the PV cell (Yousef et al., 2023)

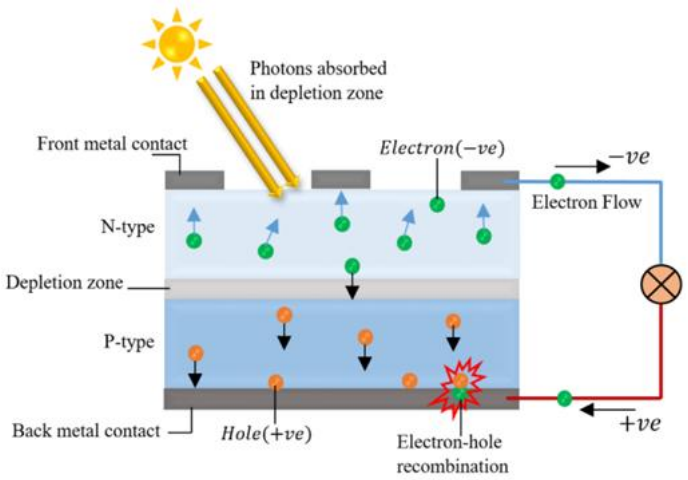

Figure 2 Working principle of photovoltaic (Yousef et al., 2023)

While photovoltaic applications are diverse, the overall system configuration is structurally straightforward. The central component is the PV array, which consists of interconnected PV modules sized to achieve the required power capacity. The balance of systems (BOS) includes

power conditioning units, energy storage devices, mounting and support structures, monitoring instruments, and safety components. System performance primarily refers to the quantity and temporal distribution of energy production and depends on both operational conditions and detailed system design. Operational conditions are site-specific and include solar irradiance, ambient temperature, and other climatic parameters that directly affect output. System performance determines technical reliability and economic viability, and it defines whether PV technology represents the most suitable electricity supply option for a given application (Pearsall, 2017).

A (PV) system converts solar energy into electrical energy, beginning with the PV cell, which captures solar radiation and generates an electrical current. These individual cells are interconnected to form a module, and several modules are then combined to create a larger array, thereby increasing the overall power output, as shown in Figure 3. The direct current (DC) energy generated by the array is converted into alternating current (AC) by a Sun Tie Inverter, making it compatible for use in households and the electrical grid. The AC power is subsequently routed through an AC Utility Meter and integrated into the main electrical grid via the Main Utility Breaker Panel, thus supplying electricity to the surrounding area if needed (Energy Information Administration, 2026).

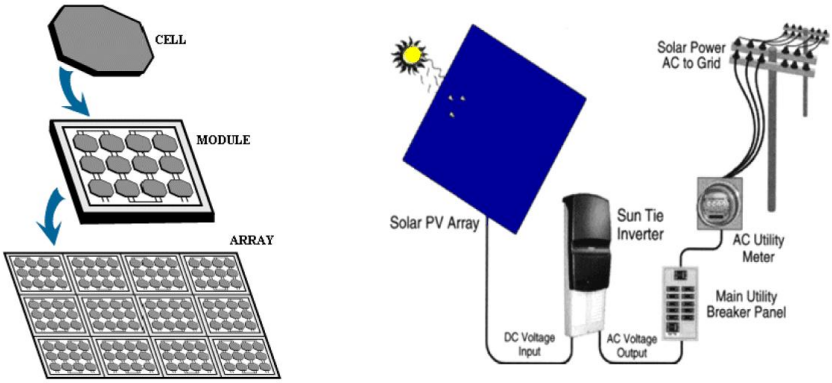

Figure 3 PV Systems Illustration on the right, and PV array configuration starts from the cell on the left (Kumar & Shekhar, 2014)

There are various types of (PV) technologies, each distinguished by unique characteristics, efficiency levels, and applications.

Semi-Transparent (PV) Modules: Advances in semi-transparent (PV) modules, particularly thin-film technologies, have facilitated their integration into building-integrated photovoltaic (BIPV) systems. These modules, which combine electricity generation with partial transparency and thermal insulation, can be incorporated into skylights, windows, and architectural façades. PV glass retains the mechanical characteristics of conventional architectural glazing while producing clean energy, enhancing the functional performance of the building envelope (Kurian & Karthi, 2023; Pandey et al., 2021). For example,semi-transparent thin film Cadmium telluride (CdTe) modules with 50% transparency(Sun et al.,

2020) show lower performance compared with CdTe semi-transparent PV windows with 10% transparency, which demonstrate improved operating hours within the 500 to 2000 irradiance range.

Bifacial Modules: As the photovoltaic sector continues to develop, bifacial PV modules have emerged as a widely adopted solution, particularly in ground-mounted systems (Wilson et al., 2020).These modules generate electricity from both front and rear surfaces by capturing direct and reflected radiation, thereby increasing total energy yield. However, soiling on either surface can significantly reduce performance and should be considered in system design (Raina & Sinha, 2023).

Perovskite Solar Cells: Perovskite solar cells represent a high-efficiency technology with the potential for low-cost manufacturing. Current research focuses on integrating perovskite materials into commercial PV modules. Organic–inorganic metal halide perovskite solar cells (PSCs) constitute a major research direction (Anoop & Ahipa, 2023). While many high-performance PSCs have been fabricated on rigid glass substrates, recent investigations propose durable PSC configurations on steel substrates (Zheng et al., 2023), enabling applications beyond glass-based systems. Furthermore, positive aging effects in perovskite materials can increase photoluminescence (PL) intensity and carrier lifetime (Shin & Shin, 2023).

Thin-Film Solar Cells: Thin-film technologies, including cadmium telluride (CdTe) and copper indium gallium selenide (CIGS) cells (Zhao et al., 2023), are attracting interest due to their low weight, flexibility, and potential cost advantages. CdTe modules with 50% transparency (Sun et al., 2020) exhibit lower operational performance than CdTe semi-transparent PV windows with 10% transparency, which achieve longer working hours within the 500 to 2000 irradiance range. Recent approaches focus on developing hole-transport materials with high work function (WF) and optical transmittance, such as transparent Cu-based selenides. These materials support high-efficiency bifacial CdTe cells and expand their application potential (Wang et al., 2023).

In summary, PV modules have progressed in efficiency, geometry, and aesthetic adaptability to meet diverse building skin requirements. This flexibility supports architectural design freedom in façade integration (Hemmerle, 2017). The report by Smith, (2021) outlines the minimum sustainable price (MSP) benchmark and technological development of PV modules in 2020. With the advancement of c-Si-based technologies, photovoltaic systems are becoming the most economically competitive renewable energy source (Li, 2023).

Thermal solar system

In a solar thermal system, the sunlight is converted to heat. Solar thermal collectors are a special kind of heat exchangers that convert solar radiation into thermal energy through a transport medium or heat transfer fluid, typically water or air (Sarbu & Sebarchievici, 2016). The absorbed heat is then transferred to the designated application point. The possible solar collector configurations for buildings include flat-plate, evacuated tube, and air- or water-based (connecting directly to the building) systems. The schematic illustrates the conversion

of solar radiation into mechanical work. To accurately design such a system, one must evaluate several factors, including the type of solar thermal collector, storage configuration, working fluid, installed capacity, load characteristics, and site location for the intended application (Kalogirou, 2003; Mekhilef et al., 2011).

The performance of solar thermal collectors depends on thermal efficiency, optical absorptance, hydraulic behavior, and environmental response. Reliable evaluation of these parameters requires calibrated sensors, robust data acquisition systems, and standardized testing procedures such as ASHRAE 93–2003 or ISO 9806 (Smaisim et al., 2022; Ziyadanogullari et al., 2018)

The common configuration of a solar thermal system, as shown in Figure 4 Provide the following equipment: solar collectors to capture solar radiation, heat storage device (like thermal storage tanks), circulation pumps, distribution network to convey the heat to the desired locations, a temperature regulation system to control the system's operation, and auxiliary components to guarantee uninterrupted functioning during intervals of diminished solar energy availability. If insufficient solar energy is available, an auxiliary energy source is used (Sarbu & Sebarchievici, 2016).

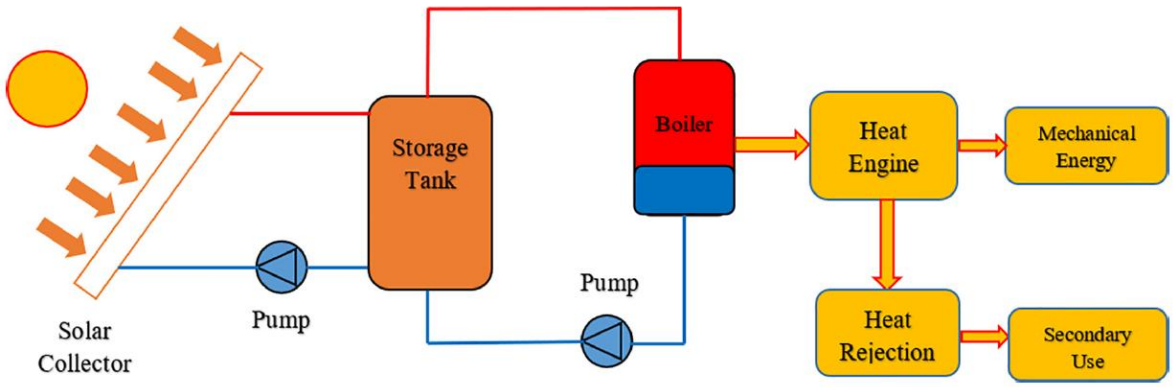

Figure 4 Schematic of a solar-thermal conversion system(Kalogirou, 2004)

Solar thermal collectors can be divided into two main categories: non-concentrating and concentrating collectors. Non-concentrating collectors directly capture and absorb solar energy from the incident sunlight, while concentrating collectors utilize mirrors or lenses to focus sunlight onto a smaller area, thereby increasing the intensity of the solar radiation. These two main categories are further subdivided into various specific collector designs, each with unique functions, as shown in the Figure 5 (Kalogirou, 2004; Suman et al., 2015).

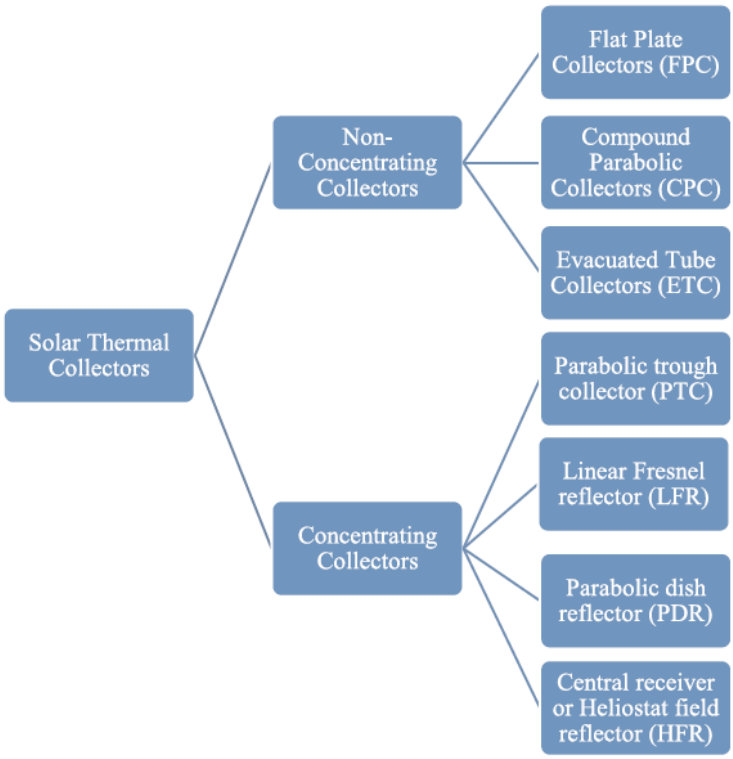

Figure 5 Solar thermal collectors (Kalogirou, 2004; Suman et al., 2015)

Non-concentrating solar thermal collectors are widely utilized across numerous applications, encompassing domestic hot water generation, space heating, and industrial heating. These collectors can be categorized into three primary types:

Flat Plate Collectors (FPC)

They are designed to absorb both direct and diffuse solar radiation. They are further categorized into glazed and unglazed versions. Glazed flat plate collectors feature a transparent cover, typically made of glass or similar materials, which helps minimize heat loss through conduction, convection, and radiation. In contrast, unglazed collectors lack this cover, leading to increased convective losses but eliminating optical losses. The efficiency of FPCs is influenced by several factors, such as the collector's aspect ratio (length to width), tilt, and orientation. The optimal tilt angle is generally set to match the geographical latitude of the location, with minor adjustments based on the specific application (Suman et al., 2015).

Stationary Compound Parabolic Collectors (CPC)

They are non-imaging concentrators with a low concentration ratio of up to two. These collectors utilize a stationary parabolic reflector to capture solar radiation from a wide range of angles, enhancing their ability to gather more solar energy compared to flat plate

collectors(Winston, 1974). The reflective surfaces of the CPC are often covered with glass to protect them from dust and environmental factors, ensuring consistent performance over time. Due to their ability to capture radiation across a broad range of angles, CPCs are more efficient in conditions where solar radiation is scattered or diffused (Suman et al., 2015). Stationary Compound Parabolic Collectors (CPC) are generally not as commonly used in typical building applications as flat plate or evacuated tube collectors. However, they may be utilized in specific situations, such as when there is a need to capture solar radiation from a wider range of angles, or in systems designed for more specialized industrial applications integrated into building infrastructures.

Evacuated Tube Collectors (ETC)

They offer higher efficiency than FPCs, particularly in colder or cloudier climates. These collectors consist of a series of vacuum-sealed glass tubes, each containing a copper pipe connected to an absorbent plate. The vacuum layer significantly reduces heat loss through conduction and convection, enabling ETCs to operate efficiently at higher temperatures. The ability of ETCs to capture both direct and diffuse solar radiation, coupled with their reduced heat losses, makes them an ideal choice for high-temperature applications such as industrial process heating and high-efficiency residential systems (Engeland et al., 2017; Suman et al., 2015). In the Table 1 summarize the general Features of the three types mentioned above.

Table 1 Overall, typical features of FPC, CPC and ETC(Kumar et al., 2019)

Parameter	Value		
	FPC	ETC	CPC
Absorber Type	Flat	Flat	Tabular
Concentration Ratio	1	1	1–5
Temperature Range (°C)	30–80	50–200	60–240

Concentrating solar thermal collectors (CSTC)

are designed to focus solar radiation onto a smaller, more efficient absorber surface, substantially enhancing the intensity of captured solar energy. These collectors typically have a higher concentration ratio compared to non-concentrating systems, enabling them to operate at elevated temperatures and achieve greater efficiency, particularly in applications demanding high thermal energy. However, concentrating solar collectors, such as parabolic troughs, solar power towers, and parabolic dish collectors, are generally not well-suited for direct integration within buildings due to their sizable scale, elevated costs, and complexity. These systems are more appropriate for large-scale industrial or utility-grade applications, like concentrated solar power plants. The need for precise tracking and higher operational temperatures makes these systems optimal for large-scale deployments. Their requirement for extensive areas and sophisticated infrastructure renders them impractical for typical residential or commercial building settings (Kalogirou et al., 1994).

In addition to these, some buildings may also incorporate **photovoltaic thermal (PVT)** collectors, which combine both solar thermal and photovoltaic technologies. PVT systems are increasingly being adopted for integrated solutions, where both electricity and thermal energy are needed for building operations, offering a dual-purpose approach to energy generation and efficiency.

2.3. Overview of Geothermal Energy

2.3.1. Principles of Geothermal Energy

Geothermal energy is thermal energy stored within the Earth's interior, originating from the planet's internal structure and physical processes. The Earth's crust and deeper layers contain vast and nearly inexhaustible thermal reserves. However, this energy is irregularly distributed, rarely concentrated, and often located at depths that hinder economic extraction (Barbier, 2002). Heat continuously flows from the Earth's interior toward the surface, where it dissipates. This transfer is generally imperceptible, though evidenced by the increase in rock temperature with depth. The geothermal gradient averages approximately 30 °C/km (Barbier, 2002).

In certain regions accessible through drilling, the geothermal gradient exceeds the global average. This occurs where magma bodies exist a few kilometers below the surface, either in a molten state or during solidification, releasing significant heat. In areas without active magmatism, elevated gradients result from geological configurations that promote heat accumulation within the crust (Barbier, 2002).

Effective geothermal energy extraction requires a carrier to transport heat from depth to accessible zones. Generally, heat transfers by conduction through rock, followed by convection through geothermal fluids. These fluids mainly consist of rainwater that infiltrates the crust in recharge zones, heats upon contact with hot rock formations, and accumulates in permeable aquifers. In some reservoirs, temperatures exceed 300 °C, and pressures are high. Such geothermal reservoirs constitute the primary exploitable component of most geothermal systems (Barbier, 2002).

The Earth's structure is composed of three concentric layers: the crust, mantle, and core. The crust, the outermost layer, is thin relative to the other layers, comparable to the skin of an apple. Its thickness averages about 7 km beneath ocean basins and ranges from 20 to 65 km beneath continents, minor compared to the Earth's mean radius of 6,370 km. Drilling operations only access the crust, rarely exceeding depths of 10 km. Seismic investigations reveal that oceanic crust is thinner than continental crust and that seismic waves propagate faster through oceanic crustal material. This velocity contrast indicates differences in composition: oceanic crust consists mainly of dense basalt, while continental crust is predominantly granitic.

The mantle begins at the base of the crust and extends to a depth of approximately 2,900 km. It is closer to the surface beneath oceans (about 7 km depth) than beneath continents (20–65 km). The prevailing model suggests that the mantle is composed primarily of ultrabasic rocks rich in iron (Fe) and magnesium (Mg), such as peridotite, which contains abundant ferromagnesian minerals. Together, the crust and uppermost mantle form the lithosphere, a rigid and brittle outer shell. According to plate tectonic theory, the lithosphere is subdivided into large lithospheric plates, with an average thickness of about 70 km beneath oceans and 100–125 km beneath continents. The lower boundary of the lithosphere corresponds to a seismic low-velocity zone within the upper mantle, known as the asthenosphere, which may extend to depths greater than 200 km. Rocks in this zone approach their melting temperature, resulting in ductile behavior, which allows the lithospheric plates to move over the asthenosphere, acting mechanically as a weak layer. The core extends from a depth of 2,900 km to the Earth's center at 6,370 km, giving it a radius of approximately 3470 km. Core temperatures are estimated to be near 4,000 °C, and pressure at the center reaches about 3.6 million bar (360,000 MPa) (Barbier, 2002).

Plate tectonic theory offers a comprehensive explanation for various geological processes. The lithosphere is divided into distinct plates that move across the Earth's surface at rates of a few centimeters per year. These plates, composed of both continental and oceanic crust, move over the underlying asthenosphere. Plate interactions primarily occur at three types of boundaries, as illustrated in Figure 6.

Divergent boundaries: Plates move apart, allowing magma to rise and form new lithosphere. These zones are associated with mid-ocean ridges, which are generally submarine but occasionally emerge above sea level, as exemplified by Iceland.

Convergent boundaries: Plates collide, with one plate subducting beneath the other. This process leads to the formation of oceanic trenches and subduction zones. When an oceanic plate converges with a continental plate, the denser oceanic plate descends beneath the less dense continental plate. As the descending slab sinks, it heats up and may partially melt within the mantle.

Transform boundaries: Plates slide past each other horizontally without creating or destroying the lithosphere. The relative motion is parallel to the fault plane. These transform boundaries are found in both oceanic and continental regions, such as the San Andreas Fault in California, where plate displacement causes seismic activity.

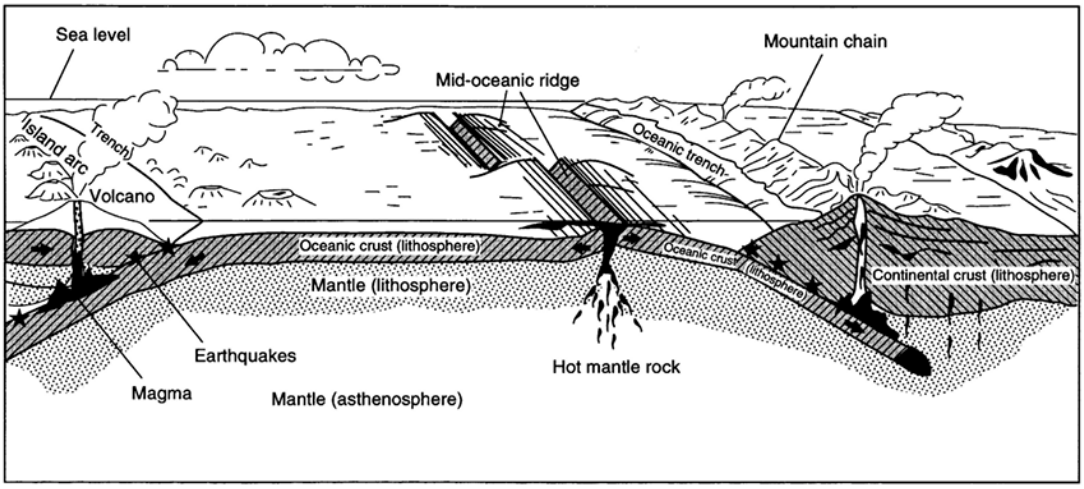

Figure 6 Schematic cross-section showing plate tectonic processes(Barbier, 1997)

Earthquake distribution is strongly correlated with plate boundaries. The majority of seismic events occur along these margins, reflecting mass transfer within the mantle. This movement necessitates ductile behavior, indicating that mantle materials exhibit fluid-like mechanical properties over geological timescales (Barbier, 2002).

The Earth possesses considerable thermal energy, with estimates suggesting approximately $12.6*10^{12}$ EJ overall, and around $5.4*10^{9}$ EJ within the crust down to a depth of 50 km, as outlined by (Dickson & Fanelli, 2003). This thermal energy primarily originates from the heat of the Earth's core and mantle, as well as the radioactive decay occurring within the crust. Conduction is the primary mechanism by which heat is transferred to the Earth's surface, at rates of 65 mW/m² on continental surfaces and 101 mW/m² beneath the ocean, contributing to a global terrestrial heat flow of around 1,400 EJ/year. According to Stefansson, (2005) The continents, which cover approximately 30% of the Earth's surface, account for approximately 315 EJ/year of this total heat flow.

At a depth of 3 kilometers, the Earth's continental regions are estimated to contain $42.67*10^{6}$EJ of stored thermal energy, with 80% originating from hot dry rock formations and 20% from hydrothermal resources, according to (EPRI, 1978). Extending to a depth of 10 kilometers, the estimated thermal energy increases significantly to $403*10^{6}$ EJ, composed of $110.4*10^{6}$ EJ from hot dry rocks and only $0.14*10^{6}$ EJ from hydrothermal sources, as noted by (Tester, 2005). Based on these estimates, theoretical potential clearly does not constitute a limiting factor for global geothermal deployment. However, practical deployment is limited by current drilling technology and geological conditions. As a result, commercial geothermal development has primarily focused on areas with suitable geological characteristics for accessing convective hydrothermal reservoirs, where drilling to depths up to 4 kilometers allows access to fluids ranging in temperature from 180°C to over 350°C (Goldstein et al., 2011).

On a global scale, the technical potential for generating electricity from geothermal energy ranges from 118 (EJ/yr) for resources accessible up to 3 km deep, to 1,109 EJ/yr for those at depths of up to 10 km (Goldstein et al., 2011). For direct thermal applications, the potential varies between 10 and 312 EJ/yr. This geothermal potential is sustained by a continuous continental heat flow of 315 EJ/yr(Stefansson, 2005), suggesting that geothermal energy's capacity exceeds global energy demands, although regional utilization will depend on the advancement and availability of Enhanced Geothermal Systems technology (EGS) (Goldstein et al., 2011)

Geothermal energy utilization generally produces limited negative environmental impacts. The production of geothermal fluids may release small quantities of greenhouse gases (GHGs), primarily CO_2 of natural origin. These emissions originate from geological sources that would eventually discharge into the atmosphere through natural surface venting. Geothermal operations do not generate additional subsurface CO_2, as no combustion occurs; however, production activities may modify the rate of natural gas release depending on plant design. Water availability does not typically constrain geothermal power generation because produced fluids are commonly saline brines and do not compete with potable water resources. Flash power plants do not require drinking water for cooling and generating condensate that can be reused for agricultural or industrial applications after appropriate treatment. Binary cycle plants further reduce water consumption by employing air-cooling systems. Potential impacts related to fluid and gas disposal, induced seismicity, and ground subsidence can be mitigated through appropriate engineering and operational practices. Proper management strategies also enhance sustainable resource use, optimize land and water efficiency, and preserve natural geothermal features that hold environmental and social value (Goldstein et al., 2011).

The primary greenhouse gas (GHG) emitted by geothermal operations is CO_2. Geothermal fluids contain minerals leached from reservoir rock and variable quantities of gas, mainly CO_2, with smaller amounts of hydrogen sulfide. The composition and quantity of these gases depend on the geological conditions of the specific field. Depending on the technology used, most of the mineral content of the fluid, along with some gases, is injected back into the reservoir. Gases are often extracted from a steam turbine condenser or two-phase heat exchanger and then released through a cooling tower. On average, CO_2 constitutes 90% of these non-condensable gases (Bertani, 2002). A 2001 field survey of operating geothermal power plants revealed a wide range of direct CO_2 emission rates. The generation-weighted average was 122 g CO_2/kWh, with individual values ranging from 4 to 740 g CO_2/kWh (Bertani, 2002). Closed-loop binary-cycle power plants, where extracted geothermal fluid is passed through a heat exchanger and then completely injected, have near-zero operational CO_2 emissions. Similarly, direct heating applications typically have negligible CO_2 emissions (Fridleifsson, 2008).Enhanced Geothermal System (EGS) power plants are likely to be designed as liquid-phase closed-loop circulation systems, resulting in zero direct emissions. However, if gas separation occurs within the circulation loop, some gas extraction and emission is likely. The current trend toward increased use of lower-temperature resources and binary plants suggests a future reduction in average emissions (Goldstein et al., 2011)

2.3.2. High enthalpy and Low enthalpy geothermal systems

Geothermal resource classification is primarily based on the fluid's enthalpy, that express the quality of its energy content on the basis of its temperature and pressure. Geothermal resources are typically divided into three categories—low, medium, and high enthalpy—that are related to the thermal energy contained in the fluids and their potential uses. However, due to the absence of a standardized classification system, these terms can often be ambiguous. To avoid confusion, it is important to specify the temperature ranges associated with each category until a uniform classification system is established.

Geothermal systems can be installed in various geological settings, depending on the temperatures and depths of their reservoirs. Systems with high temperatures, typically over 180°C, are usually associated with recent volcanic activity and are located near tectonic boundaries such as subduction zones, rifts, spreading centers, transform faults, or near crustal and mantle hot spots. Systems with intermediate temperatures, ranging from 100 to 180°C, and low-temperature systems, below 100°C, are generally found in continental regions. These areas may exhibit higher heat production due to the decay of radioactive isotopes or contain aquifers heated by water circulating through deep fault zones. Based on their thermal properties, these geothermal fields can be utilized for both power generation and direct heating applications, demonstrating the flexibility and potential of geothermal energy (Tester, 2005). Table 2 and Figure 7 summarize the resources and utilization technologies.

Table 2 Types of geothermal resources, temperatures, and uses. (Goldstein et al., 2011).

Type	In-situ fluids	Subtype	Temperature Range	Utilization	
				Current	Future
Convective systems (hydrothermal)	Yes	Continental	H, I & L	Power, direct use	
		Submarine	H	None	Power
Conductive systems	No	Shallow (<400 m)	L	Direct use (GHP)	
		Hot rock (EGS)	H, I	Prototypes	Power, direct use
		Magma bodies	H	None	Power, direct use
Deep aquifer systems	Yes	Hydrostatic aquifers	H, I & L	Direct use	Power, direct use
		Geo-pressured		Direct use	Power, direct use

Note: Temperature range: H: High (>180°C), I: Intermediate (100-180°C), L: Low (ambient to 100°C). EGS: Enhanced (or engineered) geothermal systems. GHP: Geothermal heat pumps.

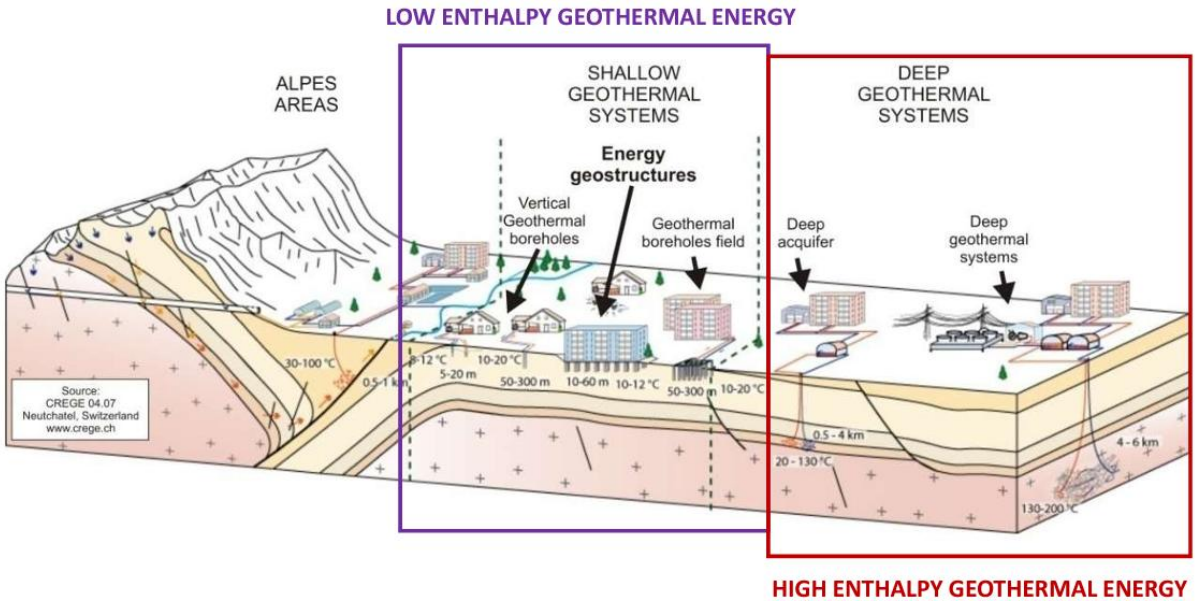

Figure 7 low and high enthalpy geothermal energy systems

High enthalpy geothermal energy

High enthalpy geothermal resources tap into this deep underground heat, where temperatures are much higher than at the surface. High-temperature resources suitable for power generation (above 150°C) are typically found in geologically active areas where crustal movements bring magma close to the surface. The most significant and widespread of these areas is the "Pacific Ring of Fire," which encircles the Pacific Ocean along the American and Asian continental borders. This region is characterized by compressional tectonics, often associated with subducting crustal plates. It includes all Latin American geothermal fields, from Chile to Mexico, as well as those in California, Kamchatka, Japan, and the Philippines. Similar conditions exist in Indonesia and the central Mediterranean, from Turkey through Greece to Italy. Geothermal resources are also favored in areas of active continental spreading, such as the mid-oceanic rifts (extensional tectonic regimes). Examples include Iceland and the Azores in the Atlantic Ocean, and Hawaii in the Pacific. Mid-continental rifting, such as the African rift system, also offers geothermal potential. Conventional electric power production typically requires fluid temperatures above 150°C; however, binary fluids can be used at considerably lower temperatures. Cascade systems, in which high-enthalpy fluid is used for electricity generation, and the resulting lower-temperature fluid is then used for other applications, are employed in many countries, including Iceland, Italy, and Japan, significantly increasing overall energy efficiency. In Figure 8, The major uses of geothermal resources are summarized in the diagram are shown (the European Commission, 1999).

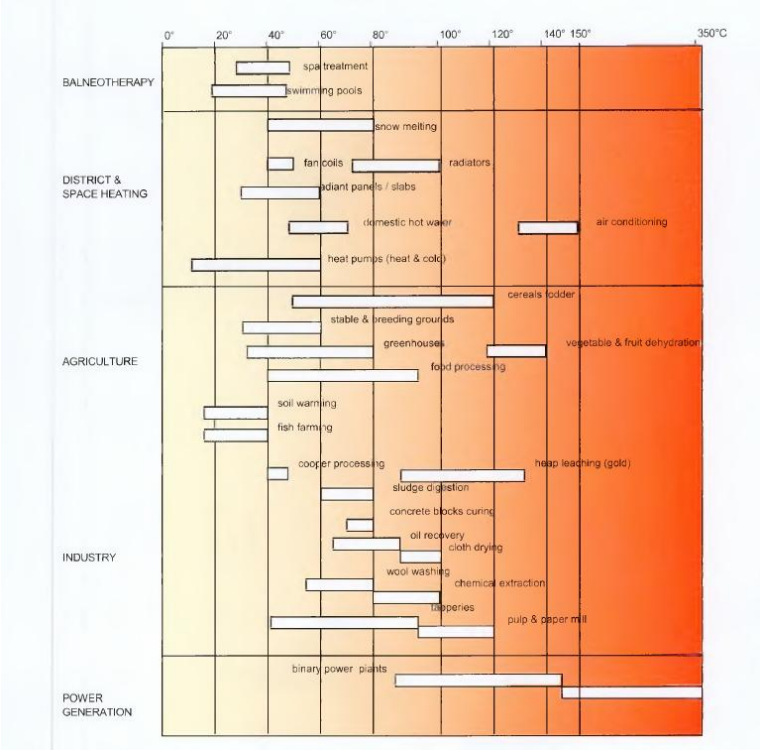

Figure 8 The major uses of geothermal resources at low - high temperatures(the European Commission, 1999)

Low-enthalpy geothermal energy

Low-enthalpy resources, which are mainly used for heat production (with temperatures below 150°C), can be found in most countries. These are formed by deep circulation of meteoric water along faults and fractures, and by water residing in high-porosity rocks, such as sandstone and limestone, at sufficient depths for water to be heated by Earth's geothermal gradient. Direct heat use is one of the oldest, most versatile, and most common forms of geothermal energy utilization. Space and district heating, agricultural applications, and aquaculture are the best-known and most widespread forms of utilization. Industrial applications are also widespread and become typical for specific aims where geothermal resources meet local needs. In recent years, significant advances have been made in applying heat pumps for extracting energy from very low-temperature resources (<20°C) for heating and cooling. Seasonal storage in shallow formations (<200 m) makes use of rock energy storage capacities. This adaptation has multiplied the number of countries and regions that can harness geothermal energy (the European Commission, 1999).

Beyond depth, shallow and deep geothermal resources differ primarily in the origin of their usable heat. Deep geothermal systems exhibit high temperatures resulting from heat flux from the Earth's interior, thermal energy that derives from the planet's formation, and the decay of radioactive elements. Shallow and very shallow geothermal systems, however, operate at relatively low temperatures and are directly influenced by solar radiation. Consequently, subsurface temperature stabilizes at depths of approximately 5–10 m, where it is no longer

affected by daily or seasonal air temperature variations (see Figure 9). At depths of approximately 10–15 m, soil temperature typically corresponds to the mean annual surface air temperature; this depth is known as the homeothermic level. Below this zone, temperature progressively increases according to the geothermal gradient, which typically ranges from 1 °C to 3 °C per 100 m due to internal heat flux from the Earth's interior (Barbero et al., 2016).

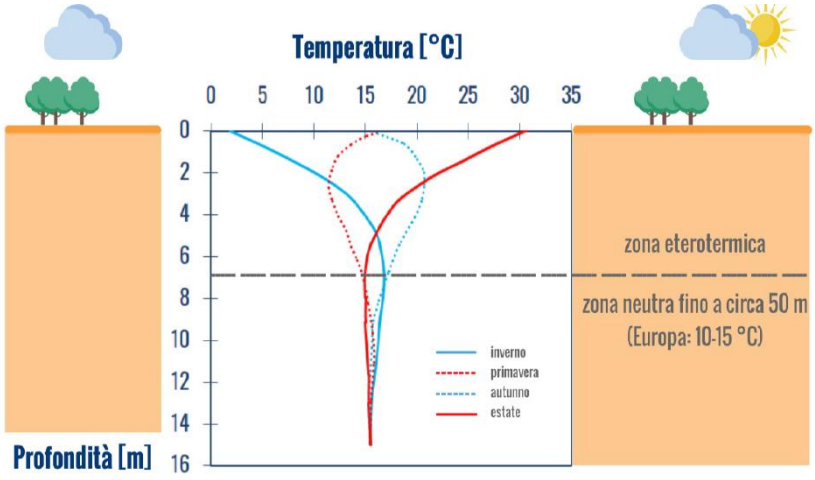

Figure 9 Diagram of the subsoil Temperature according to the depth of the soil layer (source: Politecnico di Torino)

Heat pump

Global assessments of direct geothermal applications show that Ground Source Heat Pumps (GSHPs) are the predominant use for space heating and cooling, with an installed capacity exceeding 50 GWt in 2015 (Lund & Boyd, 2016) Shallow geothermal energy is therefore mainly used for heating and cooling buildings and infrastructure. Because low-temperature heating systems typically operate between 35 °C and 45 °C, and shallow geothermal resources generally offer temperatures between only 5 °C and 15 °C, direct heating is not feasible. Consequently, these systems incorporate heat pumps to raise the temperature from the ground-side circuit to the building-side circuit, necessitating two separate hydraulic circuits (Baralis, 2020).

The primary circuit exchanges heat, and sometimes mass, with the subsurface, while the secondary circuit transfers heat to the building. Given the low heat source temperature, the secondary distribution system usually operates at low to medium temperatures, as in radiant heating networks (Brandl, 2006). Primary systems are classified as either Closed Loop (CL) or Open Loop (OL). Open-loop systems exchange both heat and groundwater mass with the subsurface, whereas closed-loop systems involve only heat transfer. Both configurations fall under the broader category of Geothermal Heat Pump (GHP) systems and encompass various technological designs (Figure 10). Closed-loop systems are commonly referred to as Ground Source Heat Pump (GSHP) or Ground Coupled Heat Pump (GCHP) systems (Baralis, 2020).

Open-loop systems are further distinguished by their water source:

- Groundwater Heat Pumps (GWHPs) directly extract and reinject groundwater from the subsoil.
- Surface Water Heat Pumps (SWHPs) utilize surface water bodies in either open loop or closed loop configurations.

.

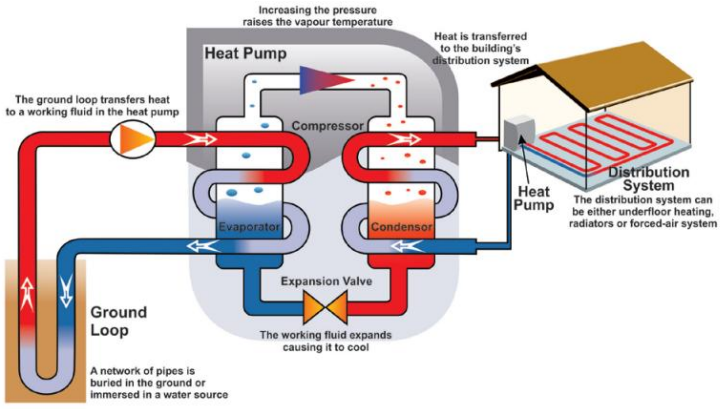

Figure 10 Scheme of a Geothermal heat pump (in heating mode).(Lind, 971)

Heat pump efficiency

When assessing the efficiency of a heat pump, it is essential to compare the quantity of energy transferred and the energy provided to the heat pump. This efficiency is quantified by the coefficient of performance (COP), which denotes the ratio of beneficial heating or cooling produced by the heat pump to the energy consumed by the compressor. COP Equ.1 is utilized for heating applications, while the Energy Efficiency Ratio (EER) Equ.2 is employed to evaluate cooling efficiency.

$$COP = \frac{\text{Heating capacity from heat pump [kW]}}{\text{energy input from source [kW]}} \qquad (1)$$

$$EER = \frac{\text{Cooling capacity from heat pump [kW]}}{\text{energy input from source [kW]}} \qquad (2)$$

Geothermal installation requires electricity not only to operate the heat pump but also to power circulation pumps that drive the heat carrier fluid within the primary circuit. To account for total electrical consumption, the Seasonal Performance Factor (SPF) is defined as:

$$SPF = \frac{\text{exploitable energy output [kWh]}}{\text{energy input of the plant [kWh]}} \qquad (3)$$

Groundwater Heat Pump (GWHP) and Ground Source Heat Pump (GSHP) systems exhibit different typical values of Coefficient of Performance (COP) and SPF due to differences in system configuration. The theoretical upper limit of both COP and SPF is determined by the Carnot cycle efficiency, which describes the ideal thermodynamic cycle of a heat pump:

$$COP_{th} = \frac{T_H}{T_H - T_C} \qquad (4)$$

where T_H and T_C represent the absolute temperatures of the hot and cold reservoirs, respectively, under heating mode conditions. The efficiency of a heat pump, therefore, depends on the temperature difference between the heat source and the user side.

2.3.3. Shallow geothermal systems (open & close loop)

Closed-loop geothermal systems

Closed-loop systems represent the most widespread geothermal utilization technology because they can be implemented at most sites (Link, 2015; Raymond, 2015; Sanner, 2016). These systems are divided into two main types: vertical and horizontal. Vertical systems are designed to reach deeper into the Earth to access more stable year-round temperatures, making them more suitable for areas with limited space, such as densely inhabited urban environments. Conversely, horizontal systems are installed a few feet below the ground surface and are better suited for areas with ample land. The pipe layout, whether in straight lines or slinky coil patterns, is designed to optimize heat transfer within the available soil volume. The different types of closed-loop shallow geothermal energy systems are shown in Figure 11.

Ground Source Heat Pump (GSHP) systems employ buried pipe networks, commonly grouted in boreholes or embedded in shallow ground, which act as heat exchangers with the subsurface. Because only heat is exchanged and no groundwater is abstracted, the environmental risk during operation is lower than in open-loop systems. In addition, GSHP installations face limited technical constraints. However, their overall efficiency is generally lower than that of Groundwater Heat Pump (GWHP) systems due to the multiple heat transfer steps between the ground and the end user. Closed-loop pipe configurations vary according to installation layout. Main categories include horizontal collectors, geothermal baskets, pond or lake collectors, and borehole heat exchangers (BHE) (see Figure 11). Pipes are typically manufactured from cross-linked polyethylene (PE-Xa). The circulating heat carrier fluid consists of water or a water–glycol mixture to prevent freezing. Among these configurations, BHE systems are the most established. They consist of vertical boreholes equipped with single U-tube (1U) or double U-tube (2U) pipes. Coaxial borehole heat exchangers, with annular (CXA) or centered (CXC) inlet arrangements, are also available but less frequently adopted (Baralis, 2020).

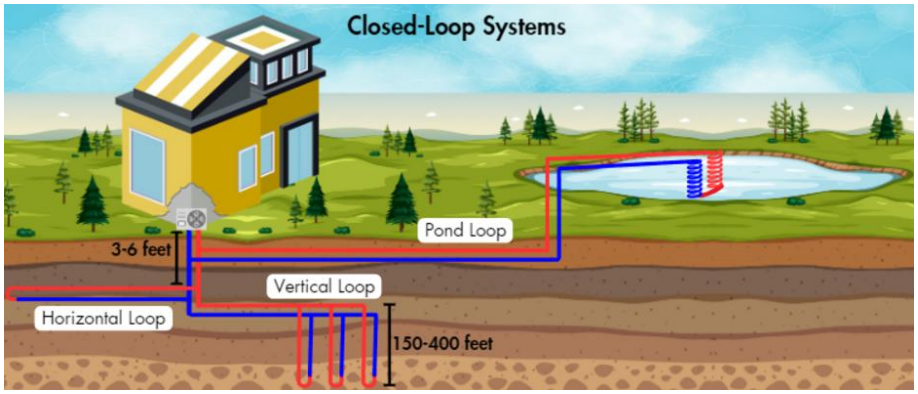

Figure 11 Different types of Close-loop shallow geothermal energy systems(Georgette Kilgore, 2024)

The initial investment cost, particularly drilling expenses, represents a significant limitation for BHE systems. Horizontal or shallow installations involve lower drilling costs but require extensive surface area, which restricts application in urban environments. Moreover, their limited depth increases exposure to seasonal air temperature variations, reducing thermal stability and efficiency. In GSHP systems, heat transfer occurs across the pipe walls between the ground and the circulating fluid. The fluid then flows to the heat pump, which adjusts the temperature level—raising it in heating mode or lowering it in cooling mode—before delivering energy to the building through the secondary circuit (Baralis, 2020).

Because the heat source interacts indirectly with the heat pump, GSHP systems typically achieve lower COP values than open-loop configurations. Heat pump performance depends primarily on the temperature difference between the source and the load. For this reason, GSHP systems are best suited to low- or medium-temperature heating systems operating between 35 °C and 45 °C. To prevent freezing, the primary circuit temperature should be maintained above approximately 0–5 °C (Anstett, 2005).

Open-loop geothermal systems

Open-loop geothermal systems use natural water bodies, such as groundwater and lakes, as heat transfer media. In these systems, water is pumped from the source, directed through a heat exchanger where it either gains or releases thermal energy, and then discharged into a reinjection well, surface water body, or onto the ground. A typical Groundwater Heat Pump (GWHP) installation consists of at least two wells that extract and reinject water into an aquifer (Baralis, 2020). As illustrated in Figure 12 The heat pump extracts thermal energy from the flowing water between these wells.

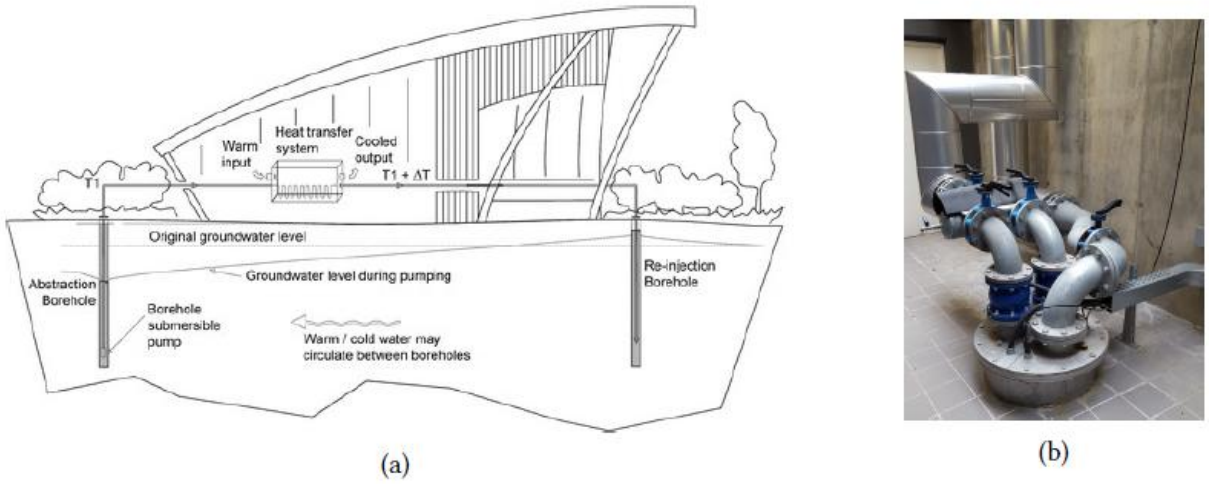

Figure 12 (a) Scheme of a groundwater heat pump system with a single abstraction borehole well and a single re-injection borehole well (Arola et al., 2014) (b) An injection well head as part of a groundwater heat pump system in Politecnico di Torino.

GWHP systems allow for direct heat exchange between groundwater and the heat pump, followed by transfer to the secondary building circuit. This direct interaction generally leads to higher performance than closed-loop systems operating under the same temperature difference. However, their implementation requires specific hydrogeological conditions, including a shallow aquifer with adequate hydraulic conductivity to sustain the required pumping rate. Conductivity values ranging from 10^{-5} to 0.1 m/s are considered appropriate for installation (Arola et al., 2014). Hence, only geological formations with a high proportion of coarse-grained materials, such as gravel and sand deposits, are appropriate for groundwater heat pump systems. Many large urban centers are located above accessible aquifers, reflecting the historical importance of water supply for human settlement. However, aquifer productivity does not always meet the long-term operational demands of GWHP systems (Baralis, 2020).

Besides hydraulic properties, groundwater quality must also satisfy technical requirements. Elevated concentrations of iron (Fe), manganese (Mn), carbon dioxide, and chloride can induce corrosion and scaling within system components. These constraints often limit GWHP applications, particularly in urban and industrial regions where shallow aquifers may be contaminated by past or ongoing activities. Furthermore, regulations frequently restrict installations in aquifers designated for potable water supply (Baralis, 2020).

Chapter 3.

Energy geo-structures

3.1. General overview

Energy geostructures (EG), also known as thermo-active geostructures, are a novel engineering idea that combines the structural support functions of geostructure with geothermal energy systems using low-enthalpy geothermal resources. These systems use the Earth's shallow subsurface as a reliable thermal energy source. Initially conceived in the 1980s, energy geostructures use the ground's consistent temperature profile to satisfy the heating and cooling requirements of buildings. This multifunctional technology enhances sustainability in urban construction by performing both structural and thermal energy functions. EGs include energy piles, walls, tunnels, and other geostructural elements equipped with ground heat exchangers. This dual-purpose design offers significant advantages, such as minimized land use, enhanced energy efficiency, and reduced environmental impact compared to traditional heating and cooling systems (Adinolfi et al., 2021; Ayaz et al., 2024).

The idea of energy geostructures was first applied in Austria in 1984 with the introduction of energy piles, followed by the construction of diaphragm walls in 1996 (Brandl, 2006). The conceptual basis for EGs was established by Brandl, who demonstrated the feasibility of integrating heat exchange systems into load-bearing structural elements. Technically, EGs encompass various ground-embedded structures, including deep foundations (piles, barrettes), shallow foundations (footings, base slabs), tunnel linings, anchors, and earth-retaining structures (diaphragm walls, quay walls). EGs leverage the ground's thermal properties, obviating the need for additional excavation or drilling solely for geothermal installations, resulting in considerable cost savings. EGs serve two main functions beyond structural support, which are the main functions:

Heat exchange – EGs transfer thermal energy between the ground and the building. In cold periods, the ground acts as a heat source, supplying warmth to maintain indoor comfort. In warm periods, excess building heat is rejected into the ground for cooling.

Heat storage – EGs use the subsurface as a thermal reservoir, smoothing seasonal temperature swings. During summer, surplus heat from internal loads or solar gain can be stored underground; the stored energy is later reclaimed in winter to supplement heating (Salciarini et al., 2026).

Energy geostructures are typically built of reinforced concrete, with the main distinction being in the pipes incorporated in the reinforcing cage or inside the infill material. Pipes are often connected to the reinforcing cage on the ground-facing side of energy walls and tunnels to prevent maintenance concern unintentional damage. Embedding pipes within the concrete offer's better protection, as the concrete cover provides adequate safeguarding over the reinforcing cage. Figure 13 shows a variety of configurations of EGs (Salciarini et al., 2026).

Pipes can be installed either in a factory or on-site, with on-site installation being more common (Brandl, 2006). During on-site installation, pipes are delivered on reels and prepared in a designated work area. During construction, locking valves and manometers are fitted at each piping system's inflow and outflow locations to maintain the test pressure (typically 8 bar) and leak-tightness testing. This pressure testing is required before and after concreting a building (Brandl, 2006).

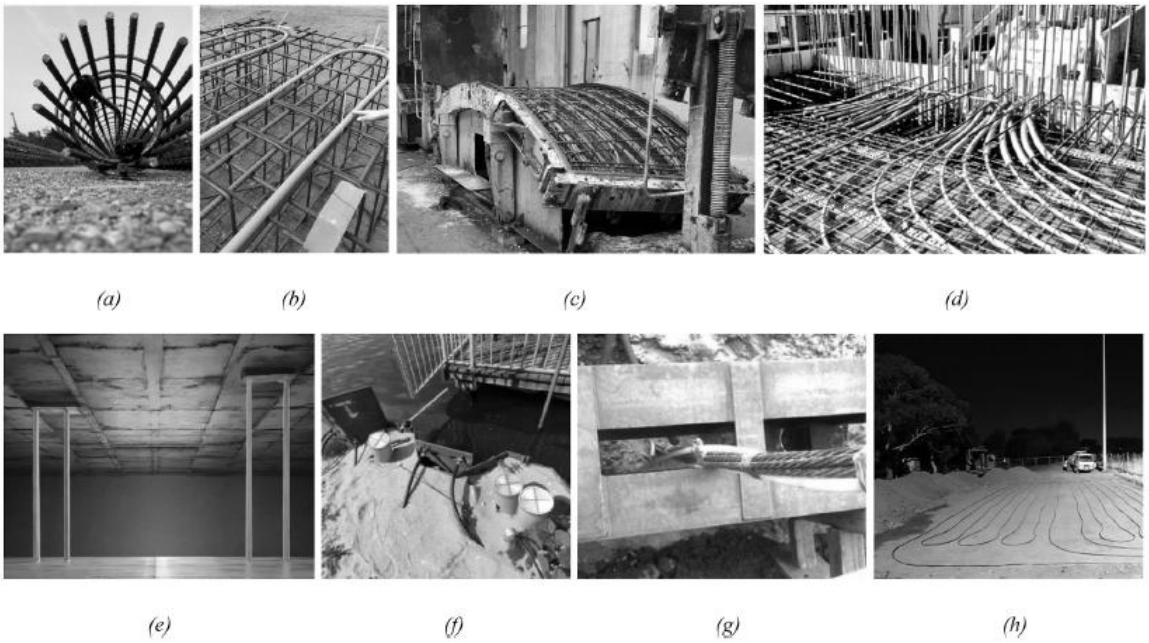

Figure 13 Pictures of the different types of EGs (real installations): (a) Energy Pile; (b) Energy Wall; (c) Energy Tunnel; (d) Energy Slab; (e) Energy Barrette; (f) Energy Quay Wall; (g) Energy Anchor; (h) Energy Pavement.(Salciarini et al., 2026)

Pipes used in energy geostructures are typically made of high-density polyethylene, with diameters ranging from 10-40 mm and wall thicknesses of 2-4 mm to improve heat exchange efficiency; thermal insulation is applied to the first few meters of the pipes to reduce the effects of external climatic conditions (Batini et al., 2015; Gao et al., 2008) . The heat transfer fluid that flows through these pipes might be water combined with antifreeze or saline solutions. Antifreeze chemicals, such as ethylene glycol or propylene glycol, are commonly used to avoid freezing and extend system life. While ethylene glycol is toxic, propylene glycol is considered safer and more often utilized (Salciarini et al., 2026).

The design and arrangement of an energy geostructure's pipe system substantially impact its efficiency. Standard configurations for energy piles include U-shaped, W-shaped, and coaxial layouts, with multi-U designs frequently used in larger-diameter piles to enhance thermal energy transmission. Similarly, energy walls and slabs utilize U-shaped or repeatedly bent pipe layouts to enhance heat exchange surface area while minimizing pressure drops. In energy tunnels, the orientation of the pipes can be either parallel or perpendicular to the tunnel's axis, depending on the structural and thermal requirements of the project (Salciarini et al., 2026).

Due to this multifaceted role, (EGs) require an integrated design framework that balances thermal performance with structural and geotechnical stability. This distinguishes them from traditional ground heat exchangers, such as Borehole Heat Exchangers (BHEs) or horizontal loop systems.

From an energy perspective, the design must account for fundamental soil thermal parameters, including thermal conductivity, heat capacity, and ambient ground temperature, as well as hydrogeological variables like groundwater depth and seepage velocity. Furthermore, the system's specific configuration, including pipe geometry, material selection, and fluid flow rates, is critical for successful operation. While some design principles can be adapted from BHE technologies, EGs possess unique attributes—specifically shorter vertical dimensions, significantly greater capacity to absorb and store heat, and inherent structural limitations—necessitating specialized analytical models and experimental validation (Salciarini et al., 2026).

From both geotechnical and structural standpoints, EGs must maintain their load-bearing capacity while withstanding thermal stresses caused by cyclic heating and cooling. Key considerations include evaluating axial deformations, thermally induced stress fluctuations, and their effects on structural integrity (Laloui & Rotta Loria, 2020) Therefore, the viability of EGs as thermal exchangers must be validated through rigorous thermo-mechanical assessments, considering both Ultimate Limit States (ULS) and Serviceability Limit States (SLS). Mechanical loading typically governs ULS compliance, while thermal effects are more significant in assessing SLS requirements (Rotta Loria, 2020).

3.1.1. Global spread of EGs

Recently comprehensive investigation by Salciarini et al. (2026) presents an extensive analysis based on a global database of 972 EG case studies from 27 countries, mainly in Europe. The database, which includes real-scale installations, experimental sites, and numerical simulations, represents the most comprehensive collection of EG data currently available. The study focuses primarily on energy piles (EPs, 789 cases), energy walls (EWs, 79 cases), and energy tunnels (ETs, 27 cases), providing a detailed evaluation of their development and performance. Some of these aspects addressed are as follows:

Geographical coverage: The database includes EG installations from 27 countries worldwide Figure 14a. The data were compiled from more than 80 peer-reviewed journal articles and

contributions from over 20 industrial partners, reflecting a strong interdisciplinary effort. Figure 14 illustrates the global distribution of EG installations, which are concentrated in Europe, highlighting the dominant role of European countries in the adoption and implementation of EG technologies.

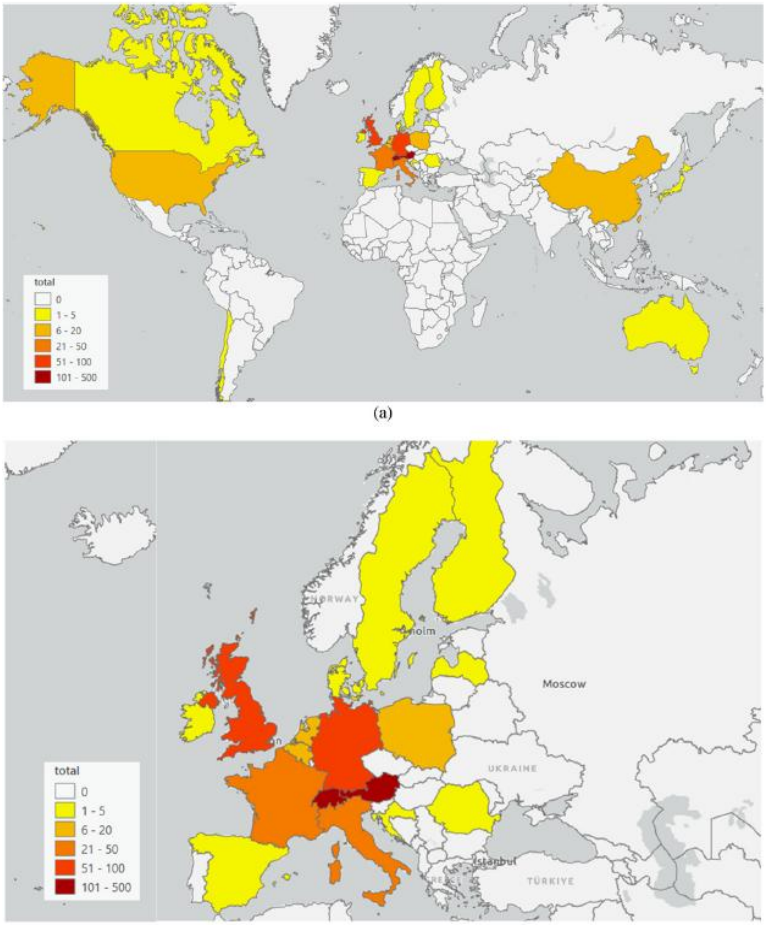

Figure 14 Map of the (a) worldwide, and (b) European distribution of the energy geostructures collected in the database.(Salciarini et al., 2026).

Technology diffusion: Figure 15 depicts the temporal evolution of EG installations between 1984 and 2023, focusing on the most common systems: EPs, EWs, ETs, and energy slabs. Figure 15a presents data for all four categories, whereas Figure 15b excludes EPs to emphasize trends in the remaining systems. The figures illustrate the long-term growth and increasing diversification of EG applications over nearly four decades. Figure 15a shows a marked rise in EP installations, particularly between 2001 and 2017, a trend linked to stricter planning regulations and incentives promoting renewable energy technologies, especially in countries such as the UK (Di Donna & Barla, 2017b, 2017a) This pattern confirms the technological maturity and reliability of EPs. Figure 15b highlights a sharp increase in EW installations from 2017 onward, indicating growing interest in this EG type. Energy slabs exhibit generally stable growth from 1995, followed by a

slight decline. After 2015, about 50% of new installations were combined with EPs or EWs, leading to a reduction in standalone energy slab applications.

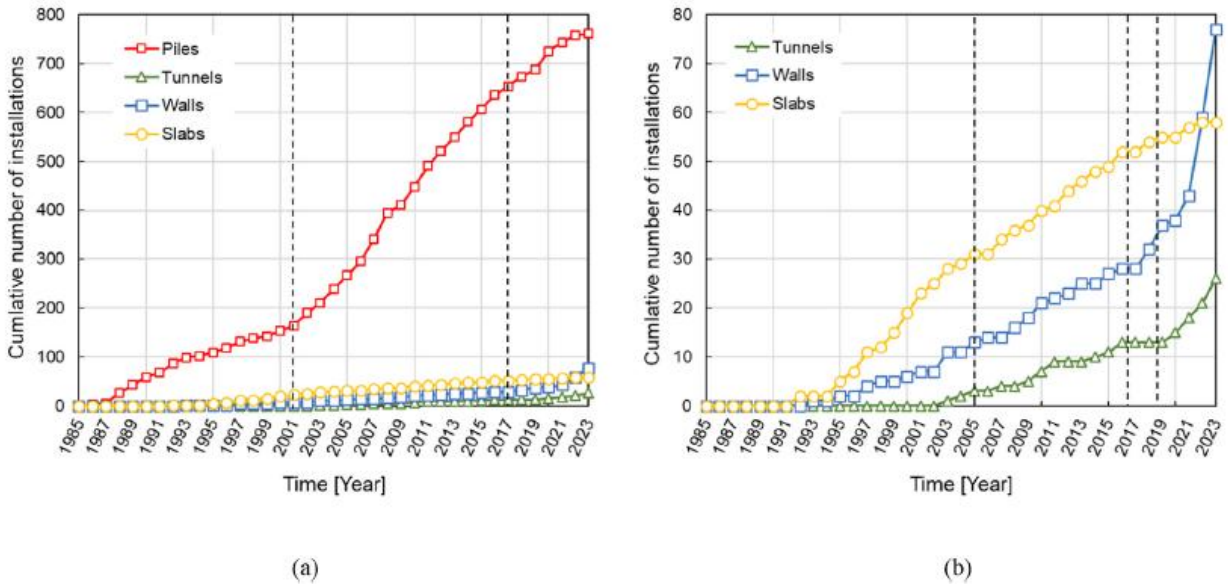

Figure 15Evolution of EGs (based solely on actual installations) over time of: a) all four prevalent types of installations (EPs, EWs, ETs, energy slabs); (b) excluding piles.(Salciarini et al., 2026)

Geographical distribution of installations and studies: Figure 16 compares the spatial distribution of EG installations with related studies and design projects. The figure identifies Austria, Switzerland, Germany, and the United Kingdom as major hubs, with Italy and France also contributing significantly to cumulative installations. These countries demonstrate broad adoption of multiple EG types, including EPs, EWs, and ETs. In contrast, most other countries predominantly rely on EP installations, reflecting the widespread applicability and advanced maturity of this technology. Six countries—Austria, France, Italy, Germany, Switzerland, and China—also show a stronger focus on EW and ET research and development, indicating ongoing efforts to advance these systems.

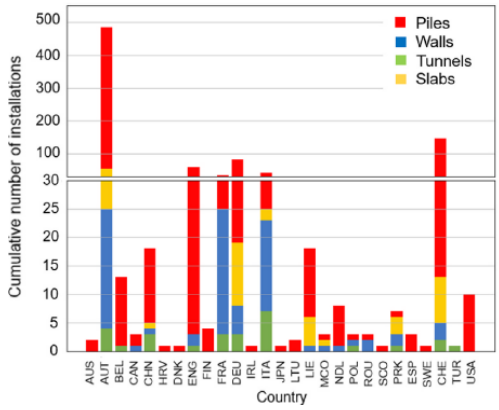

Figure 16: Geographical distribution of EGs across various countries. AUS = Australia, AUT = Austria, BEL = Belgium, CAN = Canada, CHE = Switzerland, CHL = Chile, CHN = China, DEU = Germany, DNK = Denmark, ENG = England, ESP = Spain, FIN = Finland, FRA = France, HRV = Croatia, IRL = Ireland, ITA = Italy, KOR = Korea, JPN = Japan, LTU = Lithuania, MCO = Principality of Monaco, NDL = Netherlands, POL = Poland, PRK = Czech Republic, ROU = Romania, SCO = Scotland, SWE = Sweden, USA = United States of America.(Salciarini et al., 2026)

Emerging EG types: Figure 17a illustrates the increasing interest in newer EG solutions, such as energy barrettes, energy quay walls, energy pavements, and energy anchors, through the growing number of installations. Energy pavements were the first of these systems to be implemented. The current database records four energy quay walls, three energy barrettes, and one energy anchor installation. Although these technologies remain at an early development stage, they offer innovative approaches for exploiting shallow geothermal energy. Figure 17b shows their geographical distribution, indicating that while Europe remains the main center of deployment,

adoption has also begun in regions such as Chile, Australia, and Japan. These figures highlight the initial phase of global dissemination and the potential for wider future application.

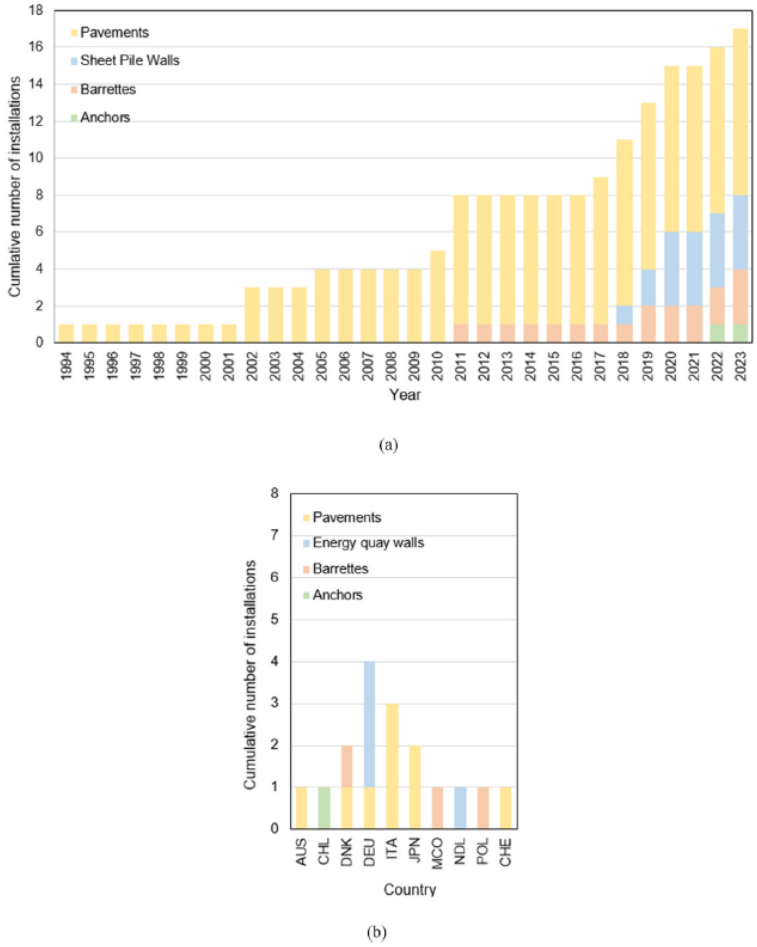

Figure 17: Evolution of emerging EG types: (a) over time; (b) across different countries.(Salciarini et al., 2026)

Geometric characteristics: Figure 18 summarizes the geometric and dimensional features of EPs, EWs, and ETs across real-world installations and prototypes, as well as feasibility studies and numerical investigations. The total number of case studies for each EG type, including the number of full-scale applications (reported in brackets), is indicated above each group. This figure demonstrates the wide range of geometries explored in EG projects. The x-axis categories represent key geometric or dimensional parameters, while higher percentages associated with specific configurations suggest preferred solutions due to their effectiveness in particular applications.

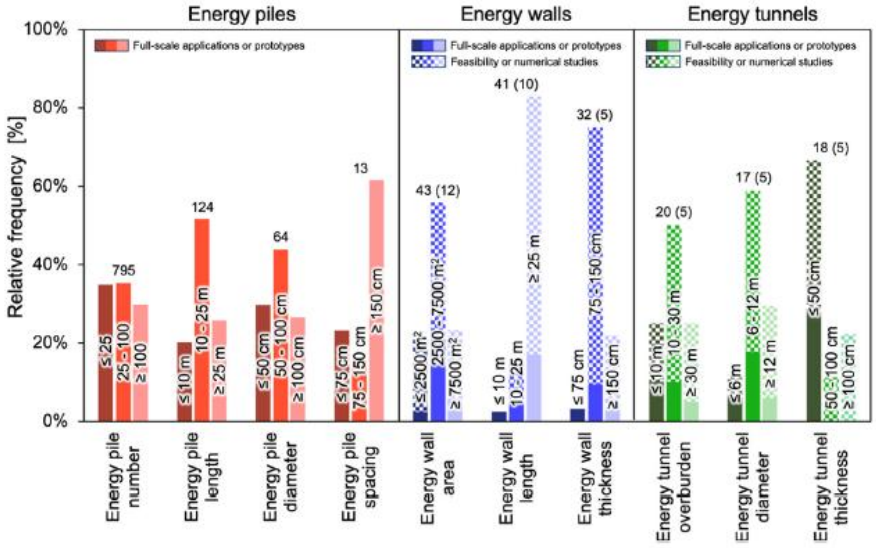

Figure 18: Geometry and size of the EPs, EWs and ETs full-scale applications or prototypes, as well as feasibility and numerical studies, gathered in the database (the total number of case studies and, within brackets, full-scale applications or prototypes for which that specific information was available is shown above each group of columns)(Salciarini et al., 2026)

Salciarini et al. (2026) also address the environmental and economic implications of energy geostructures, identifying the reduction in CO_2-equivalent emissions achieved by geothermal energy, relative to alternative energy sources, as the primary indicator of environmental benefits.

To quantify this reduction, data on CO_2-equivalent emission reductions associated with EGs were gathered from existing studies or calculated when necessary. The assessment considered the hypothetical annual geothermal energy production of each EG in the database, combined with emission factors derived from British guidelines *(British Research Establishment (BRE), Standard Assessment Procedure 10.2 - the Government's Standard Assessment Procedure for Energy Rating of Dwellings, 2022., 2022)* These factors, which quantify CO_2-equivalent emissions per unit of thermal energy, vary depending on the energy source, as shown in Table 3. For each reference technology, CO_2-equivalent savings were calculated by multiplying the annual energy production of the EG installations by the corresponding emission factors and comparing the results with those of geothermal energy. EGs lacking sufficient data on geothermal energy production were conservatively excluded from the analysis.

Table 3: Emission factors for different thermal energy sources(British Research Establishment (BRE), Standard Assessment Procedure 10.2 - the Government's Standard Assessment Procedure for Energy Rating of Dwellings, 2022., 2022)

Thermal energy source [–]	CO_2 eq. emission factor [kg/kWh]
Natural gas	0.210
Liquefied petroleum gas	0.241
Heating oil	0.298
House coal	0.395
Ambient energy	0.055
Shallow geothermal energy	0.034

For geothermal systems, the emission factor was calculated using an electricity emission factor of 0.136 kg/kWh and assuming an average coefficient of performance (COP) of 4.0 for geothermal heat pumps. Based on this COP, 75% of the usable energy is supplied by the ground, with the remaining 25% provided by electricity, resulting in emissions of 0.034 kg CO_2-equivalent per kWh of geothermal energy produced. A similar approach, consistent with that proposed by (Blum et al., 2010), was applied to ambient energy and air-source heat pump systems, assuming a COP of 2.5. Figure 19 presents the resulting cumulative annual CO_2-equivalent savings, comparing geothermal energy with other commonly used thermal energy sources, including natural gas, liquefied petroleum gas, heating oil, house coal, and ambient energy.

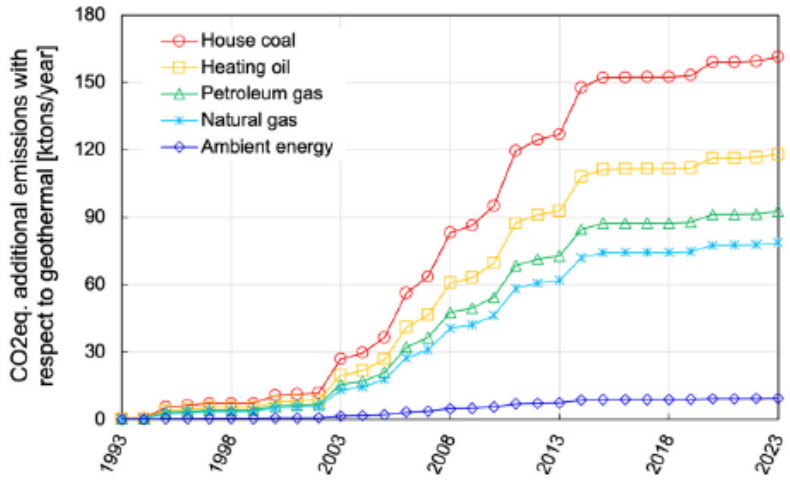

Figure 19: CO2 equivalent emissions for thermal energy production from fuels (house coal, heating oil, petroleum, and natural gases) or air source heat pumps with respect to geothermal energy.(Salciarini et al., 2026)

From an economic perspective, available data remain limited. The cost-effectiveness of EGs is typically evaluated using three indicators: the additional cost relative to the base construction cost of the geotechnical structure, the payback period, and the Levelized Cost of Energy (LCOE). The additional cost associated with installing heat exchanger pipes in geotechnical structures generally ranges from 1.0 % to 2.0 % of the total construction cost, accounting for both extra materials and increased labor for pipe installation (Barla & Insana, 2023a; Schneider, 2010) The payback period, defined as the time required to recover the initial

investment, typically varies between 2 and 15 years, depending on the thermal extraction and injection capacity of the geostructures (Barla et al., 2019; Brandl, 2006; Moormann et al., 2016).

3.2. Energy Piles

The adoption of energy piles has expanded globally, with over 100,000 units installed in Austria alone (Brandl, 2006).

Energy piles are the most common type of energy geostructure used for ground heat exchange. The application of energy piles has increased rapidly, particularly in the UK and Austria. However, installation remains challenging due to the interaction between thermal and geotechnical behavior (Laloui & Di Donna, 2011).

Understanding heat transfer is crucial for designing effective energy piles. Similar to borehole heat exchangers, heat transfer in an energy pile occurs in sequential stages:

- Heat transfer in the surrounding soil.
- Heat conduction through the pile's concrete and the heat exchanger pipes.
- Heat convection within the fluid and at the inner surface of the pipes.

These stages, illustrated in Figure 20, governs the overall rate of heat exchange between the pile and the ground.

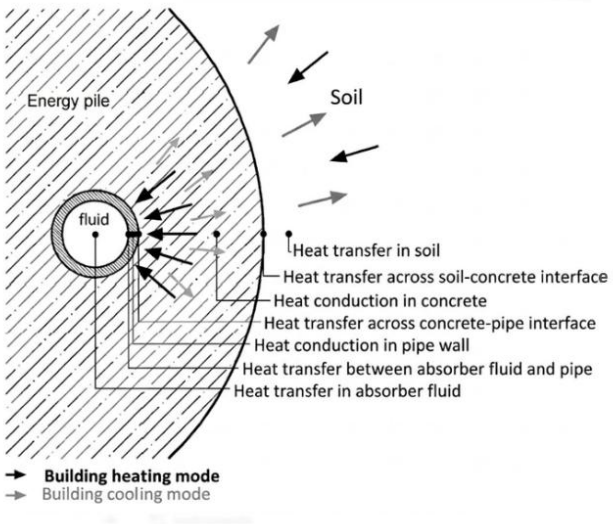

Figure 20 : Heat transfer stages in an energy pile(Mohamad et al., 2021)

Regarding the thermo-mechanical behaviour of energy piles, temperature variations from geothermal processes pose significant challenges for structural and geotechnical engineers. Heating and cooling cycles induce thermal expansion and contraction in piles, altering their bearing capacity and generating stresses and strains within the pile section (Bourne-Webb, 2013; Laloui et al., 2003). Experimental studies on energy piles—including full-scale, small-scale, and centrifuge model tests—provide insights into the behaviour of pile foundations under thermal loading. These studies demonstrate that temperature changes induce thermal stresses in energy piles. The magnitude of these stresses is influenced by:

- The extent of the temperature changes.
- The distribution of load carried by the pile (shaft resistance versus base resistance).
- The restraint conditions at the pile head and base.

These factors govern the pile's deformation and the development of stress along its length during heating and cooling cycles Figure 21.

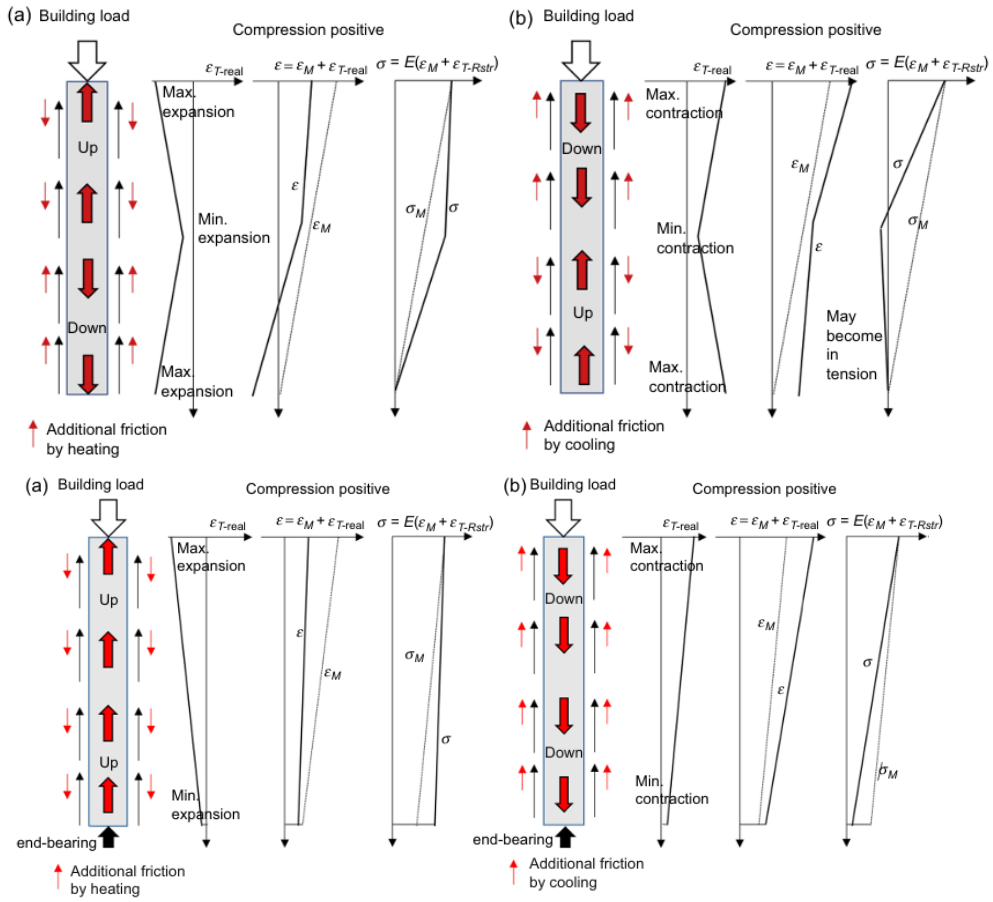

Figure 21: Thermomechanical performance of the friction pile above & the end-bearing pile below. (a) Heating and (b) cooling(Soga & Rui, 2016).

Heating energy piles during the cooling season increases compressive stresses, with reported increases ranging from approximately 40 kPa per °C to 360 kPa per °C. Conversely, cooling them during the heating season reduces compressive stresses, with decreases ranging from approximately −15 kPa per °C to −180 kPa per °C (Lyesse Laloui, 2020).

Di Donna & Laloui, (2015) reported that heating energy piles generate compressive stresses that remain below the limit state. During cooling, compressive stresses can create tensile stress zones near the pile tip. This is most likely to occur when piles are strongly restrained at their ends and subjected to significant cooling loads. Thermal loading also mobilizes shaft resistance along the pile, increasing it in both the upper and lower sections of the energy piles and altering their overall bearing capacity.

Regarding the analysis approaches of energy piles, full-scale experiments accurately represent the behaviour of energy piles under thermal and mechanical loads (Faizal et al., 2018). However, numerical studies offer an alternative when in situ tests are unavailable. Numerical modelling employs two main approaches: simplified one-dimensional load-transfer methods or complex three-dimensional finite element/difference methods.

Load-Transfer Method

Load-transfer (t-z) methods estimate the axial behaviour of energy piles by discretizing the pile into rigid elements connected by springs. Bourne-Webb et al., (2016a) summarized studies on load-transfer methods, noting their simplicity for practical design applications. However, the inherent assumptions can limit the accurate representation of real energy pile response. These models often assume minor ground temperature changes, which is problematic for long-term analysis. Furthermore, they typically disregard the impact of thermal loading on soil mechanical properties. While this simplification may be acceptable for granular and stiff soils, it is unsuitable for clayey soils where thermal consolidation can occur due to heating.

Numerical Method

A comprehensive numerical thermo-hydro-mechanical model is essential for considering all design aspects, including mechanical boundary conditions, system element behaviour, groundwater conditions, and material parameters. However, the substantial computational time required often leads researchers to simplify element modelling and boundary conditions (Bao et al., 2018; Saggu, 2019).

The foundation layout determines the arrangement of energy piles. Closely spaced piles can develop thermal interference between adjacent ones. During the ground heat extraction process, the temperature of the soil surrounding energy piles decreases with respect to the ground, pile, and circulating fluid. Conversely, soil temperature increases during heat injection. Unbalanced operation, where more heat is extracted than injected, can lower long-term energy performance. Incorporating seasonal thermal storage can maintain stable energy pile operation. Thermal interaction also occurs between the pile field, the ground surface boundary, and the building's floor structure (Bourne-Webb et al., 2016). In cold climates, heat loss from the

building floor can gradually warm the ground. This process creates natural thermal storage and can improve the thermal response of energy piles over time (Mohamad et al., 2021).

A single energy pile rarely meets a building's heating and cooling demand. Therefore, a group of energy piles is typically activated to supply the required thermal load. To account for the interaction between adjacent piles, researchers modified the load–transfer method (Laloui & Sutman, 2019) The interaction factor method also estimates the displacement response of pile groups under heating and cooling by evaluating the interaction between two closely spaced piles and then superimposing individual effects to predict group behaviour. (Rotta Loria & Laloui, 2017) validated this method using a 3D numerical model. However, the formulation only applies to energy piles without a mechanical load that is free at the head and fully restrained at the tip. Applying it to floating pile groups may underestimate vertical displacement.

Energy pile design focuses on several parameters that control thermal efficiency, as shown in Figure 22 System efficiency depends on the combined performance of all these parameters. Improving the thermal properties of each parameter increases the overall thermal output of energy piles.

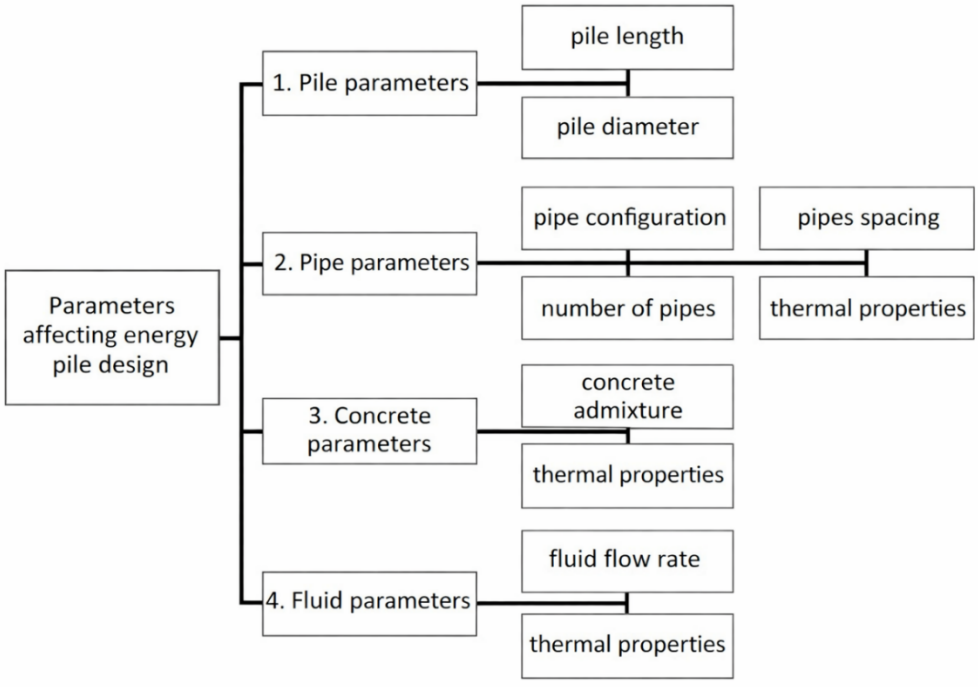

Figure 22: Parameters affecting energy piles design (Mohamad et al., 2021)

3.3. Energy tunnels

Energy tunnels represent a promising technological advancement aligned with environmental sustainability goals. Their development demonstrates the evolving role of geotechnics, traditionally considered a conservative discipline, by showing how thermal activation of geostructures can deliver innovative and substantial contributions to sustainable infrastructure development.

Interest in extracting geothermal energy from tunnel linings has grown substantially in recent years. Systems exploiting the geothermal potential of groundwater in surrounding rock masses are well-established, especially in Switzerland (Rybach, 1995; Wilhelm & Rybach, 2003) and other Alpine areas. These systems capture groundwater inflow to provide heat for adjacent buildings using principles analogous to conventional heat exchange technologies.

The Lainzer Tunnel in Vienna hosted the first full-scale implementation (Adam & Markiewicz, 2009). During tunnel excavation using the conventional NATM (New Austrian Tunnelling Method) technique, a thermal activation experiment was conducted in lot LT22 in 2003. Heat exchanger pipes were attached to geosynthetics off-site, then positioned between primary and secondary linings. By integrating pipe installation into geotextile production, this method streamlines on-site construction. The system constitutes a fully developed energy geotextile initially created at Technische Universität Wien. Energy tunnels operate through direct thermal exchange between the tunnel lining and the surrounding ground. Figure 23 illustrates this principle schematically, showing geothermal loops embedded in the lining that enable heat transfer between ground and surface according to seasonal energy requirements.

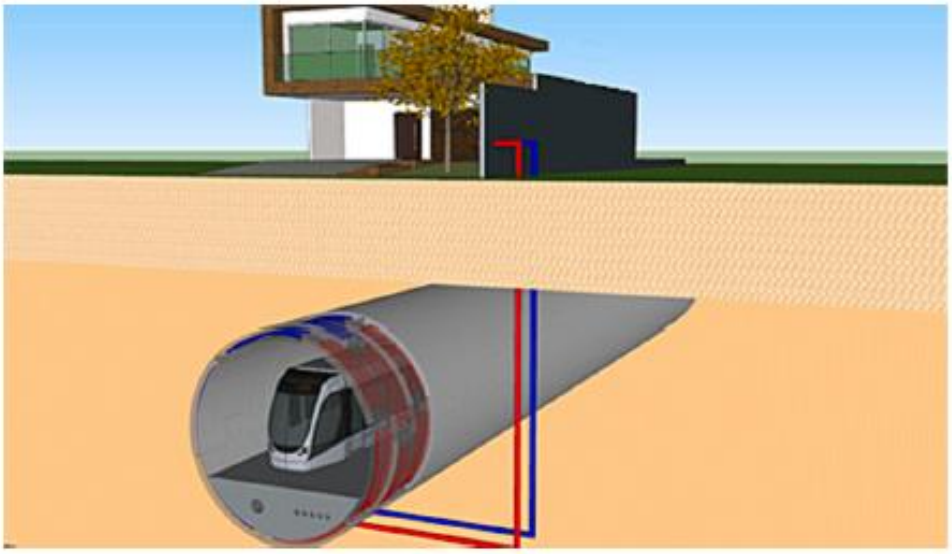

Figure 23 : Schematic view of the operation principle of energy tunnel buildings (Barla & Insana, 2023b)

Designing energy tunnels goes beyond standard code applications, necessitating broader considerations that extend conventional structural and geotechnical assessments to include urban planning and local energy supply networks (Barla et al., 2025). To fully integrate with municipal energy strategies and maximize contributions to sustainable urban development, decisions about thermal activation must be made during early feasibility studies. Thermal activation of tunnel linings addresses at least two critical technical components in the design process. First, the thermal design involves energy optimization analysis to maximize system performance at the same cost, while also assessing thermo-hydraulic interactions with the surrounding ground. Second, the structural design examines the mechanical effects of thermal loads on structural elements, as identified in the thermal design phase, to ensure long-term structural integrity. These components can be analysed using thermo-hydraulic (TH) and thermo-mechanical (TM) numerical models, respectively. Initially, fully coupled thermo-hydro-mechanical (THM) analyses may be excluded, as the increased computational demands and extended calculation times typically do not yield proportional accuracy gains. Therefore, this discussion focuses on results from coupled TH and TM (Barla, Di Donna, & Santi, 2020). Research at Politecnico di Torino (Baralis et al., 2020; Barla, Di Donna, & Baralis, 2020) established a systematic design procedure proposal for energy tunnels, later on outlined in the flow chart in Figure 24. Hydraulic circuit sizing must also be addressed and is examined in subsequent sections.

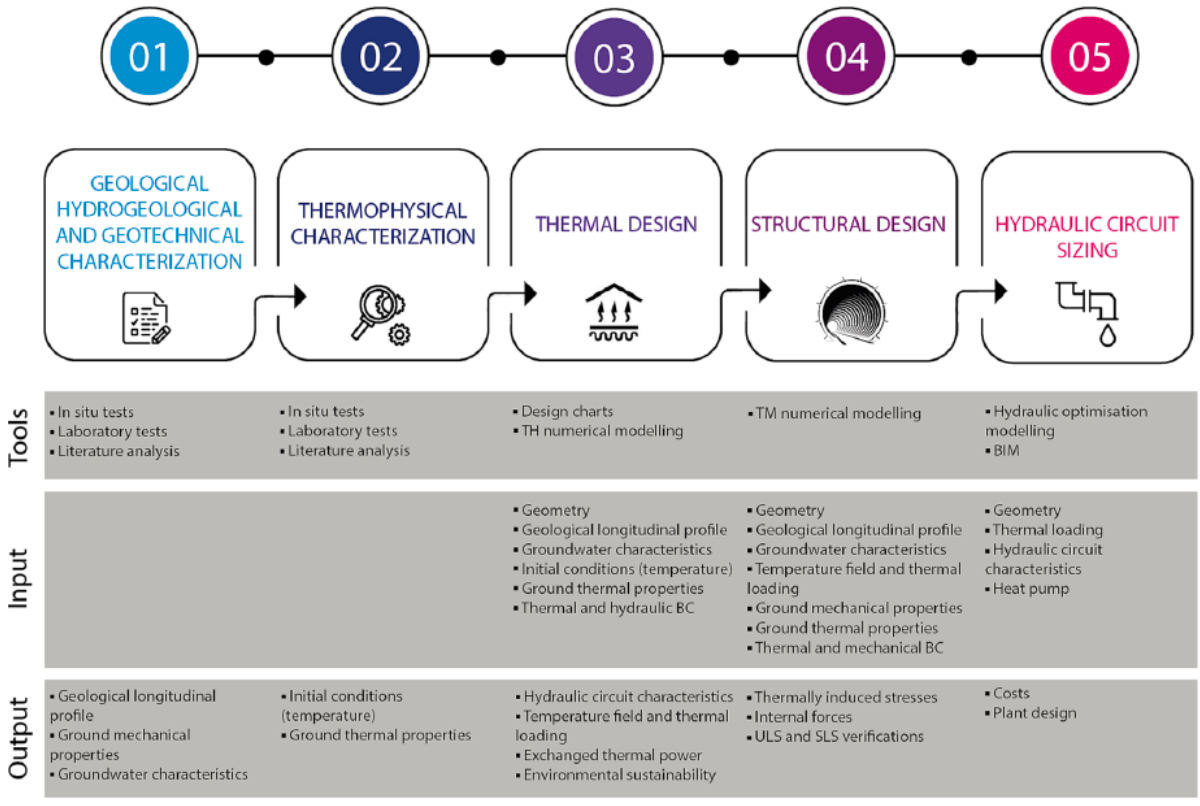

Figure 24: Design flow for an energy tunnel (Barla & Insana, 2023).

Although structural design refinement may occur at later project stages, thermal design must be considered during the initial tunnel concept phase. Thermal design aims to quantify the thermal power extractable from or injectable into the ground surrounding the geostructure via the tunnel lining. This will depend on site-specific conditions and enables assessment of both economic viability and environmental sustainability. The latter requires evaluating thermal activation impacts on the surrounding environment to minimize adverse effects.

Energy tunnels constitute relatively recent technology, lacking established methodological guidelines or regulatory frameworks for thermal sizing. Even for mature energy geostructures like energy piles, discussion regarding standardized design procedures aligned with existing regulations has only emerged recently. Preene & Powrie (2009) and Bourne-Webb et al. (2016) emphasized the necessity for design approaches consistent with limit state principles. These authors noted that the lack of formal standards stems from a historical reliance on experience with conventional geothermal systems.

The geothermal potential may be assessed by developing a three-dimensional thermo-hydraulic numerical model using finite element or finite difference numerical codes and reproducing a representative portion of the thermally activated tunnel lining. For energy segments, this may involve modelling several tunnel rings equipped with heat exchangers. The energy-lining operation should be simulated over multiple years, enabling evaluation of both short-term and long-term thermal effects.

Accurate case study geometry reproduction is essential for model development, including geothermal circuit configuration and layout, along with ground thermal and hydrogeological properties. The thermal power Q, expressed in W, exchanged during winter and summer operation can be calculated from the temperature difference between pipe inlet and outlet, T_{wi} and T_{wo}, according to Equ.5:

$$Q = mc(T_{wo} - T_{wi}) \tag{5}$$

where m represents mass flow rate in kg/s and c denotes specific heat capacity of the heat carrier fluid. Equ.5 determines the heat exchanged in a given configuration, subsequently used to estimate the geothermal potential of the considered tunnel section.

Delerablee (2019) proposed an alternative method based on Gauss's theorem, enabling evaluation of heat exchange within each control volume of the numerical model through conduction and convection mechanisms. Given the numerous parameters influencing heat transfer, simplified approaches have been explored. To reduce computational demands and avoid full numerical simulations during preliminary stages, Di Donna & Barla (2016) Conducted parametric studies investigating key variable influences, including ground temperature, groundwater flow, and ground thermal conductivity. This work produced design charts estimating system energy performance under different site conditions.

Insana & Barla (2020) Subsequently updated, these charts account for groundwater flow orientation relative to the tunnel axis and heat carrier fluid inlet temperature through a correction formulation. The resulting charts, presented in Figure 25 for winter and summer operation and three groundwater flow directions, provide specific heat power in W/m² as a function of groundwater velocity (x-axis), initial ground temperature (y-axis), and total thermal conductivity (represented by different line patterns). Predicted values demonstrate good agreement with monitoring data from the Enertun experimental site and existing case studies in the literature and can therefore support preliminary heat exchange evaluations. However, site-specific numerical analyses remain necessary at later design stages, as described above.

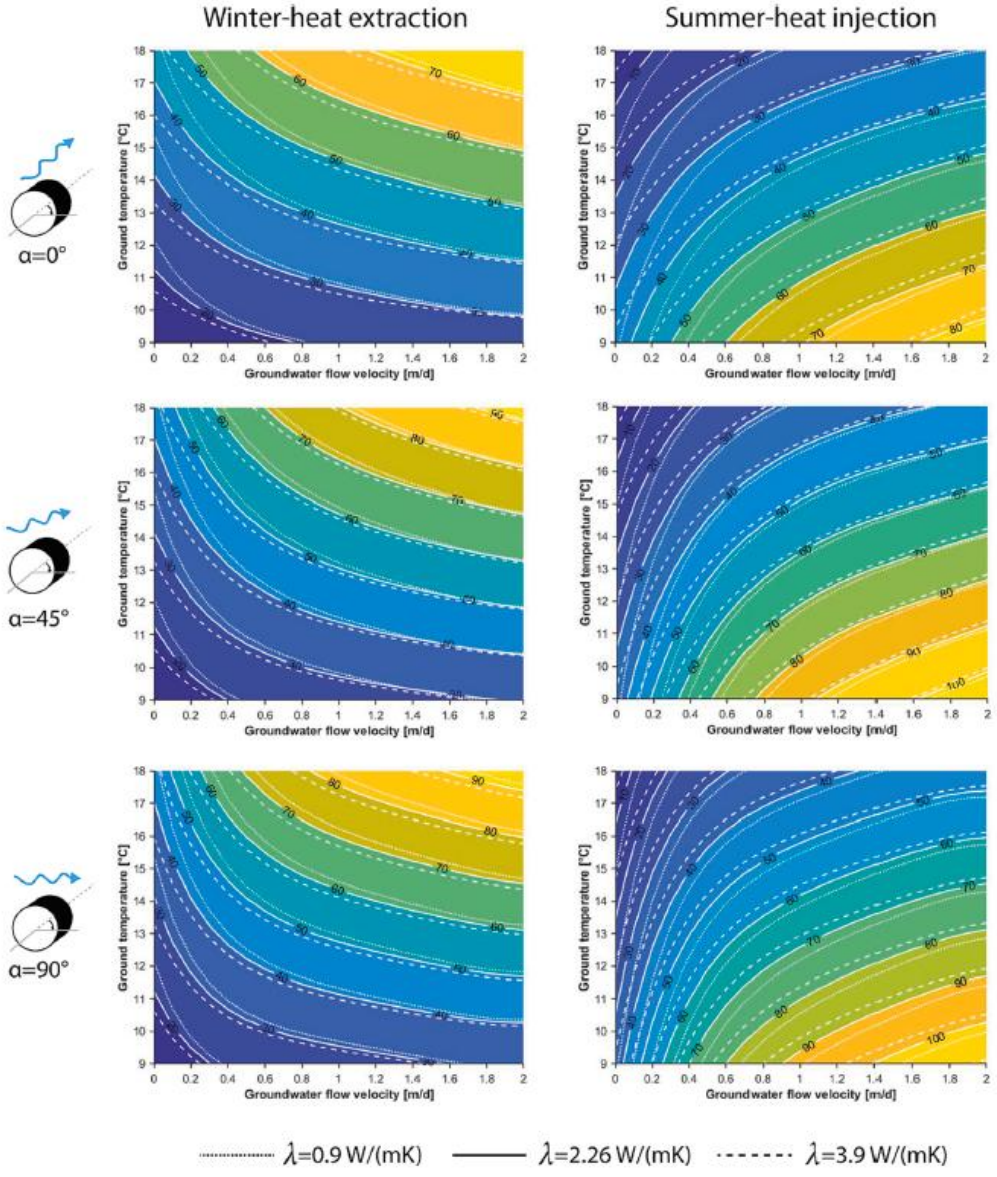

Figure 25: Example of design charts for the definition of geothermal potential in W/m2 in winter and summer for multiple groundwater flow directions (0◦, 45◦ and 90◦) (Insana & Barla, 2020)

Design chart analysis permits several general observations on energy tunnel thermal behavior. Regardless of groundwater flow direction, maximum performance occurs under high ground thermal conductivity, high groundwater velocity—due to enhanced thermal recharge accelerating recovery toward undisturbed ground temperature—and high ground temperature in winter, with opposite trends in summer. As groundwater velocity decreases, thermal conductivity influence becomes more pronounced. For perpendicular groundwater flow, winter heat exchange ranges between 10–95 W/m², while summer values fall between 10–110 W/m². Comparison of different flow orientations indicates that thermal performance increases substantially when groundwater flow is perpendicular to the tunnel axis with respect to 0° orientation, whereas only limited improvement occurs between perpendicular and oblique flow conditions. Without groundwater flow, tunnels can get specific heat power exchange rates of approximately 10–20 W/m², increasing to 50–60 W/m² when significant groundwater flow is relevant (Barla & Insana, 2023).

Regarding structural design, the objective for energy tunnels is to evaluate thermal activation effects on tunnel lining stress states and assess resulting implications for structural dimensioning. Thermal activation modifies lining stress conditions, producing internal action changes that require proper quantification. The critical aspect involves evaluating stresses induced by temperature variations generated by fluid circulation within embedded pipes. After determining thermally induced stresses, their influence on internal forces can be assessed, and the lining structural design can be updated accordingly. This update incorporates the additional loading condition associated with geothermal heat exchanger operation. Thermal activation of the lining is therefore treated as an additional load case beyond those typically considered in conventional tunnel design (Barla & Insana, 2023a).

3.4. Energy walls

A growing number of applications demonstrate the use of embedded retaining walls as energy geostructures, hereafter termed "energy walls". Brandl (2006) reported early implementations at an Austrian rehabilitation center and in Section LT24 of the Lainzer Tunnel near Vienna, both of which employed piled retaining walls. He also noted the use of diaphragm walls in the Vienna Metro U2 line underground stations. (Tony P et al., 2002) documented the first UK application at Keble College, Oxford, where a thermally activated bored pile retaining wall was installed alongside energy-bearing piles. A similar bored pile wall solution was adopted for the shallow geothermal system at the Palais Quartier development in Frankfurt, Germany (Katzenbach et al., 2013). (Amis et al., 2011) described the first thermally activated diaphragm wall in the UK, constructed for the Bulgari Hotel in Knightsbridge, London. In China, diaphragm walls and bearing piles were thermally activated during the construction of the Shanghai Museum of Natural History to provide space heating and cooling (Xia et al., 2012). Furthermore, several underground stations along the new London underground railway line incorporate thermally activated retaining walls and bearing piles to supply energy to future over-site developments (Amis et al., 2011).

Unlike energy piles, energy walls are not fully encased in soil but are partially exposed to the built environment, such as in underground stations. This exposure disturbs heat exchange efficiency and temperature recovery through the combined interaction of soil and rock deposits, structural elements, groundwater, and airflows (Amis et al., 2011). Consequently, the design of energy walls requires more complex thermal and mechanical assessments than energy piles, as the interaction between the structure and the surrounding environment must be explicitly considered. These effects include the thermally induced responses of both the surrounding soil and the structural components, influenced by combined airflow and groundwater flow. Beyond axial forces, thermally induced bending moments and flexural deformations must also be addressed in wall analysis (Lam, 2010).

Previous studies on energy walls can be broadly classified into two categories. The first focuses on thermal behaviour, including energy production, heat exchange efficiency, temperature field evolution, pipe configuration, and operational modes. The second investigates mechanical behaviour, such as thermally induced stresses and strains, wall displacements, and ground settlements. Thermal analyses typically simulate heat exchange between circulating fluid and the surrounding environment—such as airflow, groundwater flow, and adjacent soil—using coupled TH approaches implemented in numerical platforms like FEFLOW and COMSOL Multiphysics. Mechanical performance is generally assessed through coupled TM or THM analyses using software such as Abaqus and PLAXIS (Dai et al., 2023).

The mechanical response of energy walls has received comparatively limited attention, as most existing research emphasizes the thermal performance. While several countries, including Germany, Switzerland, the United Kingdom, and France, have issued recommendations or guidelines for energy geostructures, these documents rarely define standardized design procedures or assessment criteria for energy walls, particularly regarding mechanical behavior. (Lam SY, 2010). More recently, Loveridge et al., 2020 presented a comprehensive review of energy geostructure research, summarizing current knowledge, while (Di Donna et al., 2021) developed design charts for the preliminary evaluation of the energy capacity of energy walls embedded in different ground conditions, using a TM-based approach.

Analysis methods for energy walls

(Sun et al., 2013) introduced the first analytical approach for energy wall design, assuming two 2D heat transfer models developed for heat exchangers in the diaphragm wall: one for the section above the excavation line and the other for the section below the excavation line, with a convective boundary condition for the inside face of the retaining wall. Heat transfer pipes are idealized as point heat sources, and Green's functions are used to solve the heat diffusion equation. The model was validated against field measurements from the Shanghai Natural History Museum project (Xia et al., 2012); however, agreement between model predictions and field data was unsatisfactory for short time periods (less than approximately 12 h), which are representative of realistic step changes in thermal demand.

Kürten et al. (2015)subsequently developed and validated an analytical model based on a thermal resistance–capacitance network that explicitly represents pipe layout within the wall. While effective, this approach still requires numerical simulations to derive resistance parameters. (Shafagh et al., 2020) adopted a similar network-based methodology using the Dynamic Thermal Network (DTN) method. This technique employs response factors to describe relationships between temperatures and heat fluxes at thermal network boundaries. However, the weighting factors required for heat flux calculations must be obtained numerically, limiting the method's applicability for routine design despite successful validation against full-scale experimental data.

Further developments include the thermal resistance model proposed by Shafagh I, (2019), which introduces analytical shape factors for a rectangular wall containing an offset cylindrical heat exchanger pipe. The method allows for either isothermal or convective boundary conditions and can be coupled with step-response methods to account for ground thermal behaviour. An initial attempt to extend step-response modelling to energy walls was presented by (Shafagh & Loveridge, 2020), though this approach remains a preliminary study and requires further validation before practical application.

Despite these advancements, none of the aforementioned analytical methods have achieved widespread adoption in engineering practice. Except for the thermal resistance model of Shafagh I, (2019), Most approaches involve complex mathematical formulations or depend on numerical calibration. Consequently, most existing energy wall studies rely predominantly on numerical 3D modelling. In these models, heat transfer pipes and circulating fluid are commonly represented using one-dimensional specialized pipe elements (Di Donna et al., 2021).

Di Donna et al., (2021) adopted a similar numerical strategy, developing a set of design charts to support preliminary energy wall performance assessments. These charts, presented in Figure 26 and Figure 27 , correspond to constant temperature and convective heat transfer boundary conditions on the excavation side, respectively. Based on site-specific parameters—such as undisturbed ground temperature, soil thermal conductivity, and groundwater flow velocity—the charts provide estimates of achievable heat extraction or injection rates, expressed in W/m² of wall surface. While results inherently depend on underlying model assumptions and geometry, they represent a useful tool for preliminary feasibility evaluations.

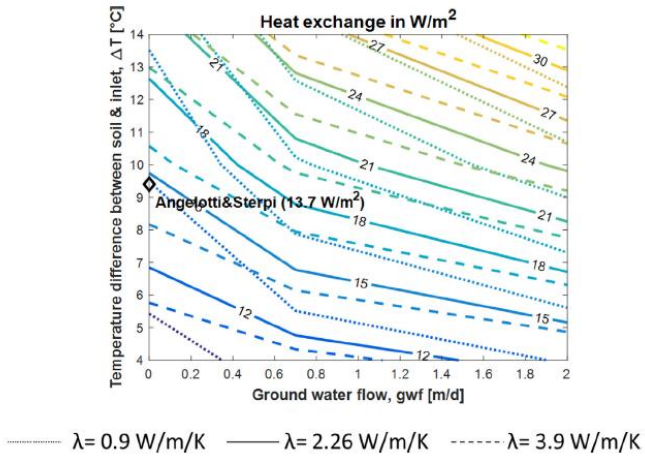

Figure 26 : Design charts for constant temperature BC (values in W/m2).(Di Donna et al., 2021)

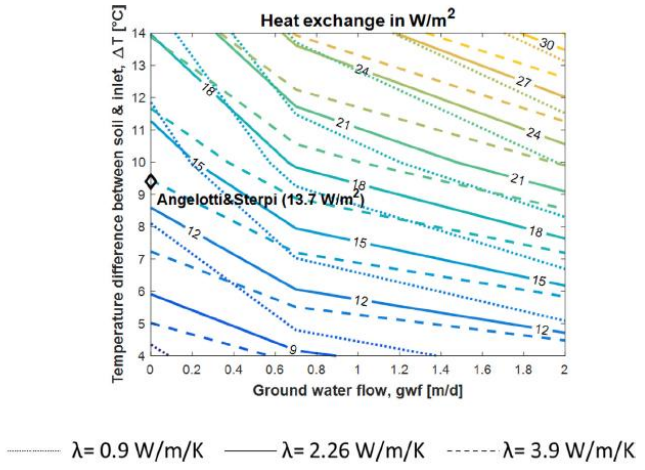

Figure 27 : Design charts for heat transfer BC (values in W/m2).(Di Donna et al., 2021)

3.4.1. Energy Geothermal skin: a very shallow energy wall

Very shallow geothermal systems can be installed in existing buildings, but they typically require Th extensive surface areas for installation, which must remain free from future use due to the presence of buried pipe networks. —such as sewer networks, district heating, or gas distribution lines (Tsagarakis et al., 2020). This constraint poses a significant limitation in densely populated urban environments, where land scarcity heavily influences planning strategies and infrastructure development.

To address these limitations, Baralis & Barla (2021) patented Geothermskin, a novel, very shallow energy wall system developed at the Politecnico di Torino. This system was designed to overcome some of the limitations affecting traditional energy geostructures and horizontal ground heat collectors. The technology was named Geothermskin to emphasize its ability to enhance a building's "underground skin" as an active interface for geothermal heat exchange.

The proposed solution can be applied to both new constructions and existing projects under or needing refurbishment, utilizing the earth-contact surfaces of basement retaining walls without requiring additional land.

Table 4 provides a schematic comparison between the Geothermskin system and other existing closed-loop shallow geothermal technologies, together with gas boiler technology. Economically, the Geothermskin solution is notably more cost-effective than traditional shallow geothermal energy (SGE) systems, especially in urban contexts, due to the absence of extensive excavation—both in depth and surface area.

Table 4 : Comparison of advantages and disadvantages of the Geothermskin system compared to direct market competitors. " + " symbols represent (Baralis & Barla, 2021).

	Gas boiler	Horizontal collectors	Geothermal "Baskets"	Borehole Heat Exchangers	Energy Geo-structures	GeothermSkin
Energy efficiency	+	−	±	+	±	±
Applicability to existing structures	+	+	+	+	−	+
Free land consumption	+	−	−	±	+	+
Initial costs	+	+	+	−	±	+
Running costs	−	+	+	+	+	+
Environmental costs	−	+	+	±	±	+
Cost per unit power [€/W]	~0.17	~0.5	~0.5	~0.8	N.A	~0.3

The Geothermskin system is a type of energy geostructure. Unlike conventional energy walls, it is designed as an external system applied to the earth-contact surface of the structural wall rather than being embedded within it. For new constructions, installation can occur using open excavations available during early construction phases. For existing buildings—such as in energy retrofitting applications, localized excavation may be required to expose the wall surface before installation.

The hydraulic circuit consists of polymeric pipes, which can be made of cross-linked polyethylene (PE-Xa), selected over high-density polyethylene (PE-HD). These pipes are fixed directly to the external wall surface after bearing the wall. Pipe deployment consists of straight segments and bends with a minimum radius of 15 cm, corresponding to the maximum allowable bending curvature of the selected pipe material. Clamps anchored to the wall provide temporary fixation, serving as support elements during installation. After pipe placement, the excavation is backfilled, and the ground surface is restored (Baralis & Barla, 2021).

The system is designed as a modular external component, ensuring operational flexibility, redundancy, and the ability to isolate individual heat exchanger sections in the event of local damage or leakage without compromising the overall system performance. Consequently, pipe deployment is independent of the wall's structural configuration, unlike traditional energy geostructures, where the heat exchanger layout is constrained by reinforcement cage arrangement (CFMS&SYNTEC, 2017). These characteristics make the Geothermskin system particularly suitable for energy retrofitting applications in existing buildings.

For new constructions, this system can be adopted at any design process stage, unlike classical energy geostructures that must be integrated from the earliest design phases. Each module constitutes an independent hydraulic circuit, with pipes preferably arranged horizontally rather than vertically Figure 28. The two layouts offer distinct advantages and limitations related to pipe routing. Horizontal deployment facilitates air bubble removal during circuit filling, while vertical deployment slightly reduces bend quantity and, consequently, associated hydraulic head losses. In both configurations, the inlet and outlet of each module are positioned at opposite edges of the upper portion of the equipped wall area, minimizing thermal short-circuiting risk between adjacent branches. This arrangement also allows both sequential and parallel hydraulic connections between neighbouring modules (Baralis & Barla, 2021).

Figure 28: Geothermskin energy wall heat exchanger conceptual application(Baralis & Barla, 2021)

3.5. Thermo-Hydro-Mechanical coupling

To evaluate the behavior of energy geostructures in general, it is necessary to understand thermo–hydro–mechanical processes in soils and rocks. Heat transfer in soil and rocks occurs through conduction, convection, and radiation; however, for most shallow geothermal applications, conduction governs the thermal response (Rees et al., 2000). Bulk thermal conductivity depends primarily on the properties of the solid matrix, pore fluid, and pore air, commonly expressed through density and moisture content. Empirical correlations have historically been applied to estimate soil thermal conductivity (De Vries, 1958; Farouki, 1981), yet these approaches may introduce significant uncertainty (Rees et al., 2000) and often neglect structural features such as soil structure, heterogeneity, and anisotropy (Midttømme & Roaldset, 1999).

Figure 29 shows the conditions under which convection and radiation may occur and become relevant in soils. Identifying soil types and environmental conditions prone to these mechanisms is essential, as their presence can affect parameter estimation and compromise system design accuracy.

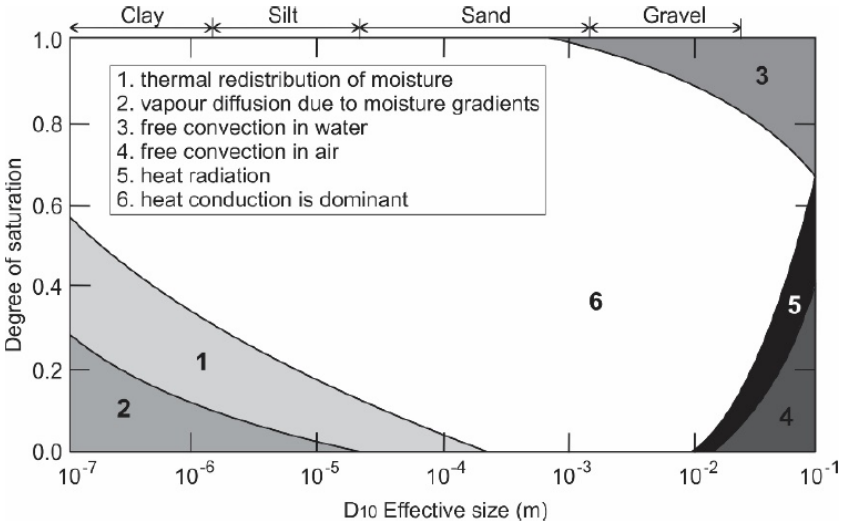

Figure 29: Main heat transfer processes in soils (Farouki, 1981).

According to Hellstrom (1991) Free convection may influence shallow energy geothermal system performance when soil hydraulic conductivity exceeds approximately 10^{-5} m/s in both vertical and horizontal directions. In most soil and rock types, reduced vertical permeability or the presence of low-permeability layers typically limit this mechanism. Forced convection is generally more relevant and occurs under groundwater flow. Its impact is often amplified in fractured rock masses, where thermal dispersion may also contribute to heat transport (Liebel, 2012).

Moisture movement is particularly relevant in fine-grained unsaturated soils (Farouki, 1981). Heating can induce pore water evaporation, which consumes latent heat. The resulting vapor migrates along vapor pressure gradients toward cooler zones, where condensation releases latent heat. This process can enhance heat transfer and alter thermal properties by changing phase distribution. Under strong thermal gradients, soil drying reduces thermal conductivity. Hellstrom (1991) indicates that this effect becomes significant in highly porous soils with low saturation when temperatures exceed 25 °C. The magnitude of the effect depends on soil type and boundary conditions (e.g., humidity/ventilation) and remains an active research topic example (Laloui et al., 2006).

Moisture move represents thermo–hydraulic coupling in soils. For energy geostructures, thermal loading must also be evaluated in terms of mechanical response, because temperature changes can alter pore pressures, effective stresses, and deformation. Coupled THM analysis provides a consistent framework to quantify the magnitude and temporal evolution of these coupled effects and to support (Figure 30).

Temperature effects on soil mechanical behavior are well established and can be complex, as confirmed by extensive experimental evidence (e.g., Campanella & Mitchell, 1968). In shallow geothermal applications, the interaction is predominantly one-directional, since mechanical

loading typically has negligible influence on the temperature field. In contrast, thermal and hydraulic processes are strongly coupled: temperature variations alter pore pressures and flow regimes, while hydraulic conditions influence heat transport through fluid conduction and advection. Mechanical and hydraulic responses are also interdependent, as pore pressure changes modify effective stress and deformation behaviour.

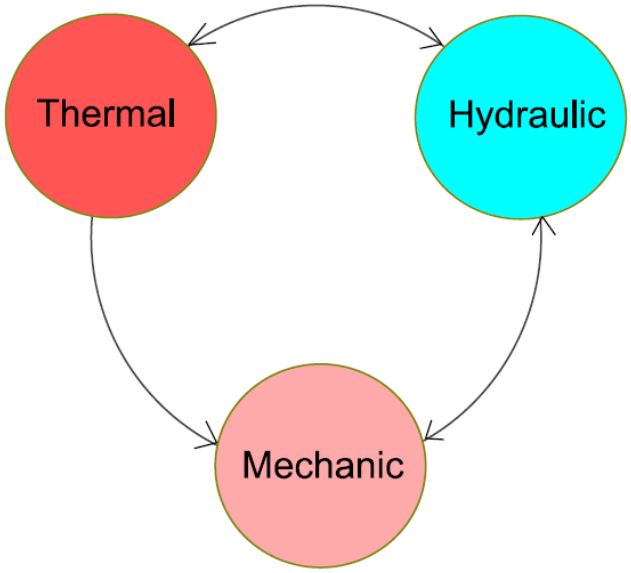

Figure 30. Schematic representation of relevant couplings in shallow geothermal energy system(Vieira et al., 2017).

Chapter 4.

Case Study

4.1. General overview

For nearly two centuries, Reale Mutua Assicurazioni has played a prominent role in Turin's economic and business landscape. In recent years, the Group has pursued an extensive program of development and refurbishment of its real estate assets, supported by a widespread territorial presence that includes more than 2,000 agencies operating in the city of Turin alone. Within this strategic framework, Reale Group set the objective of relocating the CRAL (Circolo Ricreativo Aziendale Lavoratori) to a more central and accessible urban location. An approximately 18,000 m² site was identified within the city, already designated for sports-related functions and well connected by public transportation, ensuring ease of access for all users. As part of the Group's internal social initiatives, the new CRAL was conceived as a multifunctional hub where innovation and environmental sustainability could be seamlessly integrated with Reale Group's core value: the centrality and well-being of people. Aligned with the thesis's focus on Nearly Zero-Energy Buildings (NZEB), the project was developed to meet stringent energy performance requirements, incorporating passive design strategies, high-performance building envelopes, and renewable energy systems to minimize primary energy consumption and achieve near-zero energy demand in accordance with the European Directive 2010/31/EU and Italian national standards. The geographical location of the selected case study area is illustrated in Figure 31.

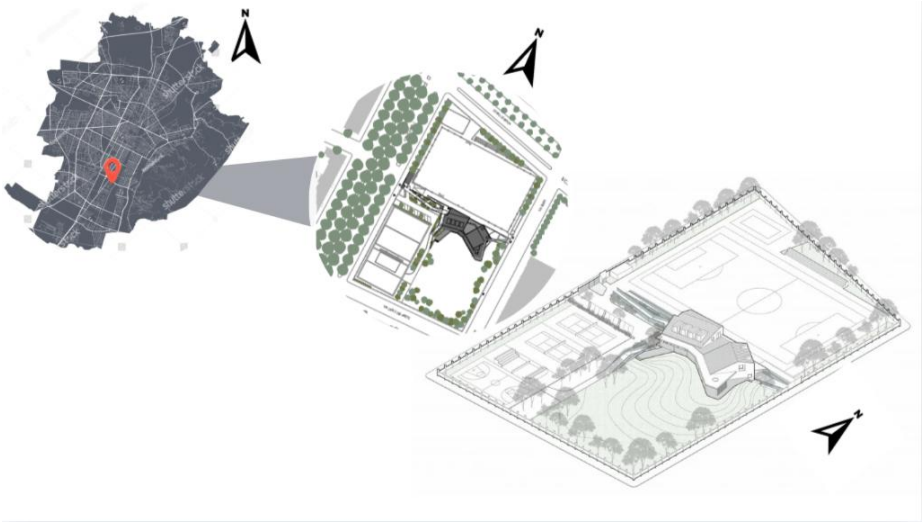

Figure 31: Location and site Boundary of the case study Torino, Italy.

For the project's realization, the company relied on the expertise of PICCO Architetti, who, for years, have combined research and practice in urban and architectural design within the complex contemporary European landscape. The program called for the construction of various spaces for recreational and social activities, a gym, multiple sports fields, and a large green area suitable for outdoor activities. The design followed this plan, placing the main building of the Club in a central position on the site, with an open green area occupying the southeast quadrant of the lot. Sports fields were located to the southwest and north of the building.

The building is composed of three interconnected volumes—two with pitched roofs and one with a flat roof—arranged to create a fan-shaped configuration opening toward the south. Along the western façade, an architectural screen reinforces the concept of "embracing" the adjacent green area, generating a protected outdoor space clearly separated from the sports fields and suitable for summer camp activities for employees' children. The volumes are defined by clean geometries and a differentiated façade articulation, with openings alternately flush with the exterior surface or recessed with splayed reveals. These architectural choices are consistent with NZEB design principles. The south-oriented layout enhances passive solar gains during winter, while recessed openings and the continuous portico limit excessive solar exposure in summer, thereby reducing cooling demand. The roofs are finished with double-seamed metal sheets, which also clad the projecting dormers that introduce daylight into the gymnasium and office areas. This strategy increases natural lighting availability and contributes to lowering artificial lighting demand and associated energy consumption. Figure 32 below shows the building elevation.

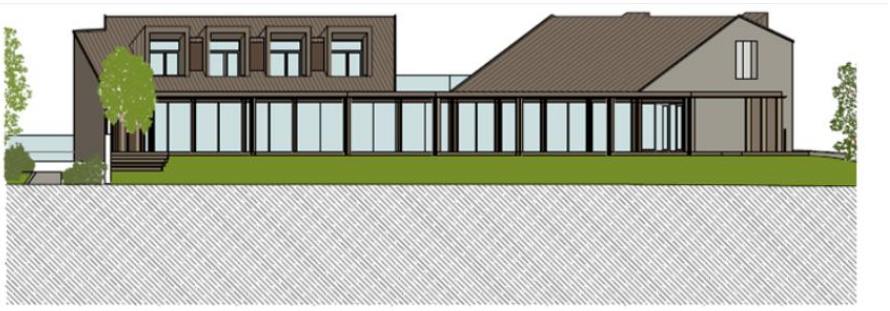

South Elevation

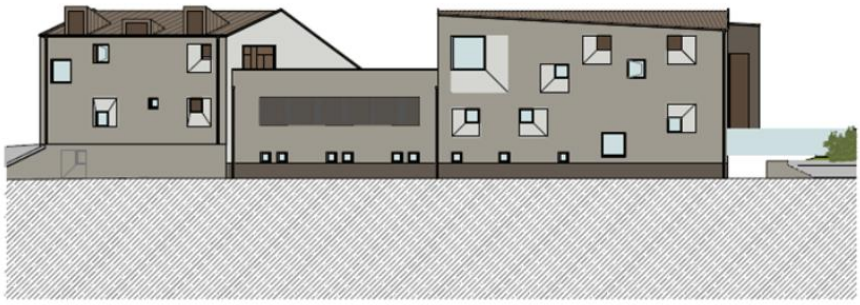

North Elevation

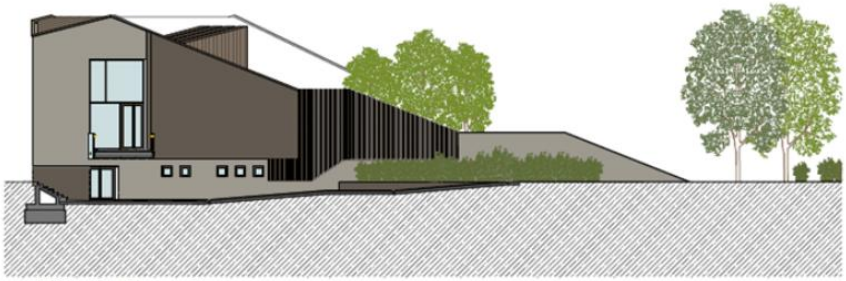

West Elevation

East Elevation

Figure 32: General view of the Four Building Elevations.

The basement level accommodates the locker rooms serving both sports activities and service personnel. The ground floor, positioned slightly above the surrounding outdoor areas, hosts

the main public functions, including the reception area, bar, restaurant, members' lounge, and a multipurpose space. These functions are organized in a semicircular layout around large, glazed openings facing a continuous portico along the southern green area. This configuration provides a sheltered transitional outdoor space and limits direct solar gains within the interiors, acting as a passive cooling strategy that supports the achievement of NZEB performance targets. The first floor contains the Club's administrative offices, a gym equipped with a sun terrace, and a small service apartment for the caretaker. Figure 33 below illustrates the building floor plans.

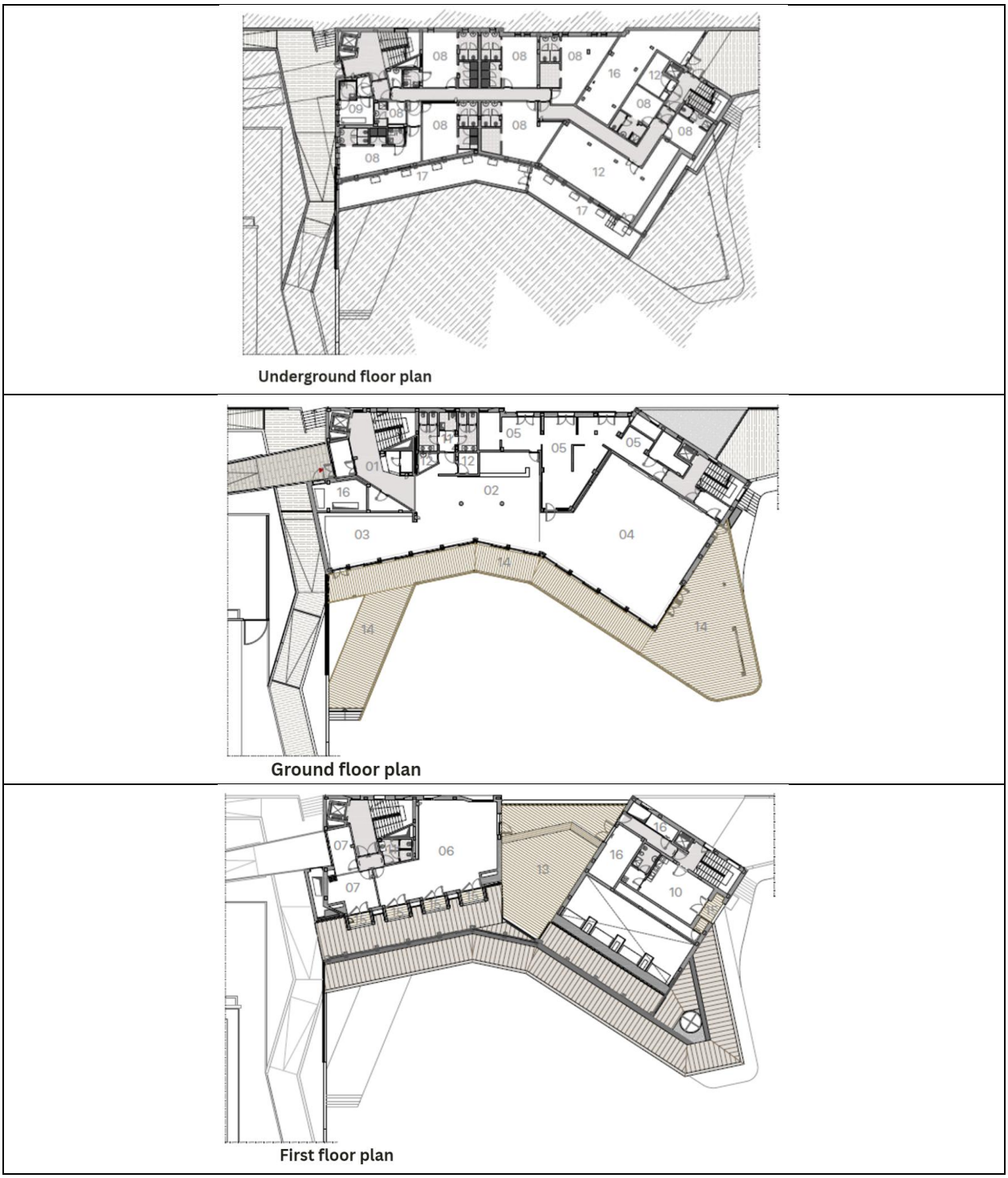

Figure 33. General floor plan and functional distribution of the building: 01–Entrance and Reception; 02–Bar; 03–Members' Lounge; 04–Multipurpose Hall; 05–Kitchen; 06–Gym; 07–Office; 08–Changing and Locker Rooms; 09–Infirmary; 10–Caretaker's Apartment; 11–General Restrooms; 12–Storage and Warehouse; 13–Terrace and Solarium; 14–Portico; 15–Balcony; 16–Technical Room (HVAC and Geothermal Manifold); 17–Ventilated Crawl Space.

The building volumes exhibit clear, rational geometries and a diversified façade composition, with selected openings aligned flush with the external wall and others recessed with splayed reveals. These solutions are consistent with NZEB design principles: the south-oriented

configuration enhances passive solar gains during winter, while recessed openings with splayed geometries improve daylight penetration and mitigate excessive solar radiation in summer, thereby reducing cooling demand.

The roofing system consists of double-seamed metal sheets, which also clad the projecting dormer elements. These dormers introduce natural daylight into the gymnasium and office areas, decreasing reliance on artificial lighting and the associated energy consumption, in line with nearly zero-energy performance objectives. The façades are finished with plaster applied over an external thermal insulation system, ensuring high thermal efficiency and limiting thermal bridging, which is fundamental to the NZEB envelope strategy. Window systems incorporate powder-coated aluminum frames with thermal break profiles, selected to achieve low thermal transmittance and to minimize heat losses, contributing to the building's overall energy efficiency targets in compliance with European Directive 2010/31/EU.

4.2. Energy needs

The evaluations follow the hourly and monthly methods specified in the EN ISO 52016 standard, which provides guidelines for calculating building energy performance. To comply with Italian energy efficiency regulations, procedures outlined in the UNI/TS 11300 technical standards were rigorously followed. Developed by the Italian National Unification Institute, the UNI/TS 11300 standards offer extensive guidance on energy performance calculations and efficiency measures for buildings, covering aspects such as thermal transmittance, heating and cooling systems, lighting, and renewable energy sources. Implementation of the EN ISO 52016 methods and UNI/TS 11300 procedures was facilitated by EC700 simulation software from Edilclima S.r.l., which allows analysis and evaluation of building energy performance by inserting relevant data to predict and simulate energy consumption. This software enables insight into building energy performance, facilitating decision-making for potential cost-effective measures.

According to Presidential Decree n. 412 of 26 August 1993, Annex A, and its subsequent amendments, Turin is classified within Climatic Zone E based on its heating degree days. The classification ranges from Zone A (the warmest) to Zone F (the coldest). These zones determine the heating period and duration for which heating systems can be operated within municipalities. Zone E typically includes areas with significant heating needs due to lower average temperatures. Municipalities in this zone are allowed to use heating systems for up to 14 hours daily from October 15 to April 15. This classification helps ensure that residents can adequately heat their houses during colder months while promoting energy efficiency and reducing unnecessary heating outside designated periods.

4.2.1. Input Data

Climate data

To conduct the building energy analysis, access to climatic data for the case study area is necessary. The Turin's external air temperature and solar irradiance are shown in Figure 34 and Figure 35.

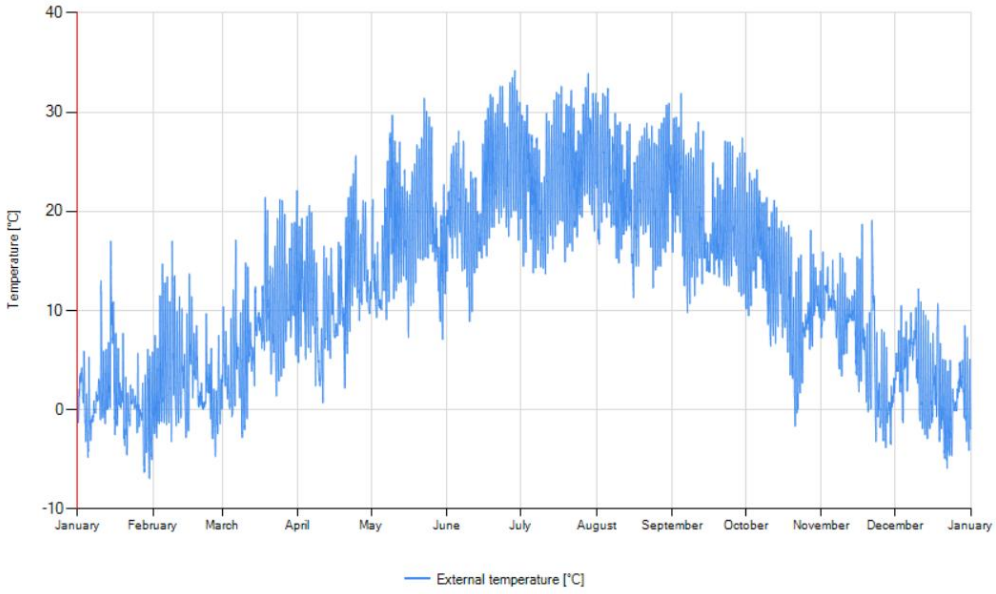

Figure 34: Annual average daily external temperature Torino, Italy 2025.

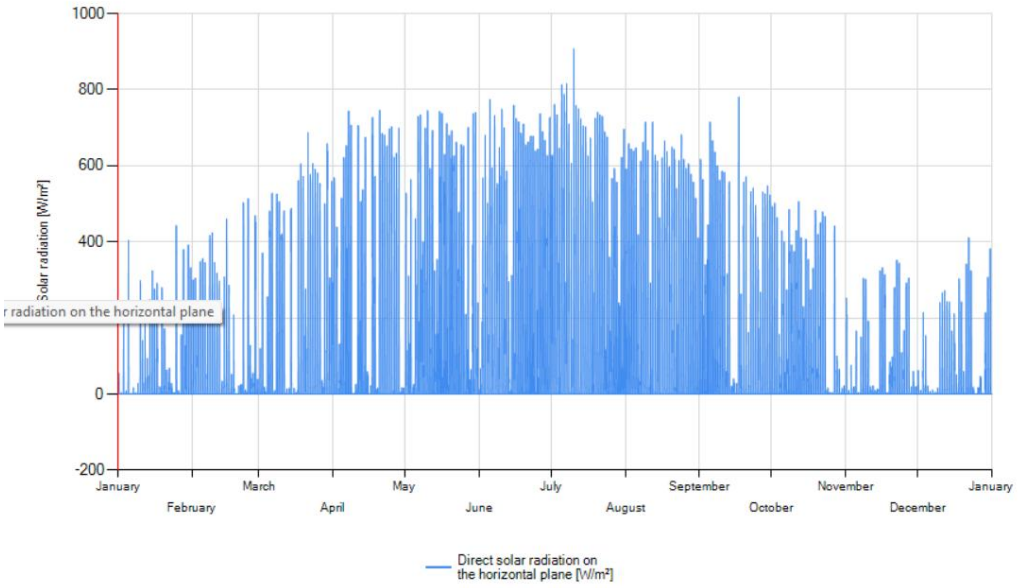

Figure 35: Annual average daily Solar irradiance Torino, Italy 2025.

When a municipality is searched in the Edilclima Archive or User Archive, both the "Monthly data" and "Hourly data" tabs are automatically populated with archive data, as shown in Figure 36. The "Monthly data" tab displays the following information: municipality name, province, degree days (according to Presidential Decree 412/93), altitude above sea level (m), latitude and longitude (with an indicative geographical position on the map of Italy), cadastral and postal codes, distance from the coast (< 20 km, < 40 km, > 40 km), wind region (according to UNI 10349 standard), prevailing wind direction, average and maximum winter wind speeds (m/s), ISTAT code, survey stations used for calculating monthly average temperatures, solar radiation and windiness, solar irradiance on a horizontal plane during the month of maximum insolation (W/m²), reference locality for design winter outdoor temperature, design winter outdoor temperature (°C) with contextual variations if applicable, climatic zone (A-F), and conventional heating period duration, including start and end dates (in days).

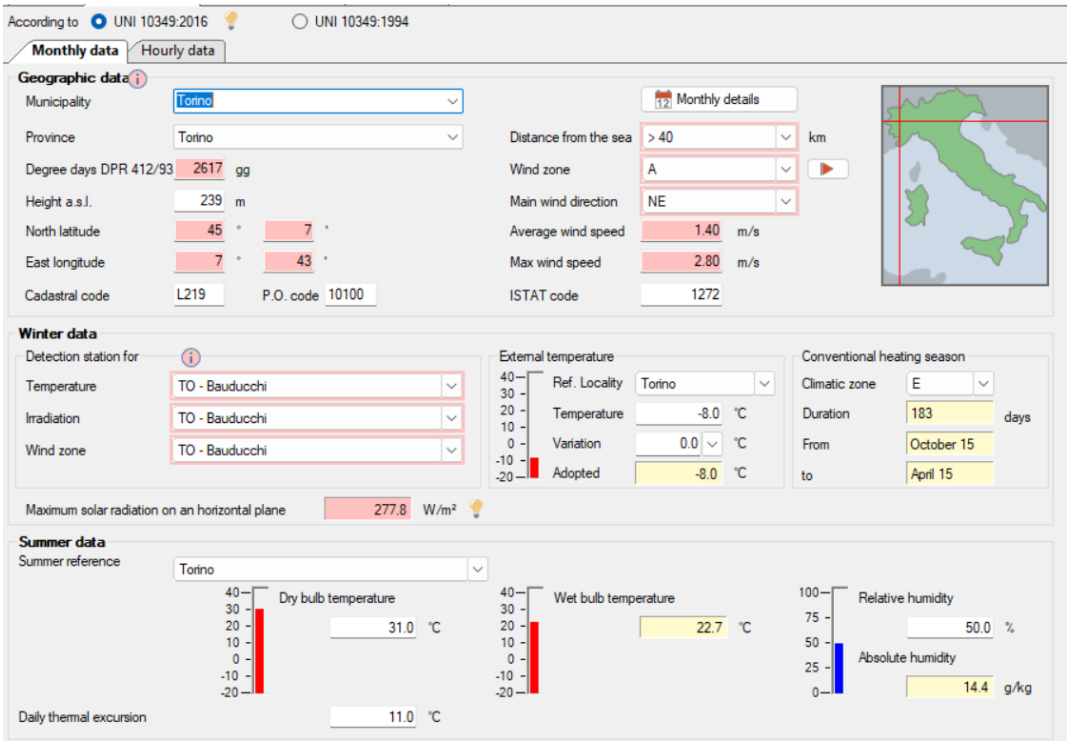

Figure 36: Input data relates to the location of the case study.

The software generates the data necessary for evaluating building performance during both winter and summer seasons. The assessment is first carried out using standard climatic data, which differ from actual conditions, to analyze potential energy performance based on data from meteorological stations. These initial assessments are then refined using actual building-specific data. For this purpose, additional hourly data were provided, including outdoor temperature (°C), solar radiation (W/m²), global radiation (W/m²), relative humidity (%), vapor pressure (Pa), and wind speed (m/s).

Thermal envelope

A building's energy performance is significantly influenced by its envelope composition, which includes both opaque and transparent components and thermal bridges. Therefore, understanding and defining the layers and materials used in these components is crucial for accurately assessing energy needs.

The Edilclima Software requires detailed input on building envelope composition for both opaque and transparent components. After a brief overview, the following sections will detail the layers and materials used within the software, with reference to the Abacus UNI/TR 11552. This abacus includes representative assemblies for walls, floors, and ceilings, derived from case studies reported in UNI technical report 11552. It allows users to select structures with known compositions and to specify layer thicknesses based on the structure's typology. Inputting each layer's thickness and thermal conductivity into Edilclima is essential for calculating the overall thermal transmittance (U-value) of the wall. This level of detail for the composition enables precise modelling of heat flow through the building envelope, facilitating accurate energy performance assessment and optimization.

Opaque Envelope

The building's components are designed to comply with Italian Ministerial Decree (M.D. 26/06/2015) limitations. The external opaque walls primarily consist of semi-hollow bricks with an insulation layer. Internally, partitions are made of hollow bricks of varying thicknesses, providing both structural integrity and sound insulation.

The building's horizontal components include underground floors, constructed on a ventilated crawl space and separated from the ground using plastic modular formwork. These floors consist of lightweight concrete slabs topped with ceramic tiles for durability and ease of maintenance. The ground floor incorporates a hollow block slab with thermal insulation. The roofing system consists of double-seamed metal sheets, while the roof structures, both sloped and flat roofs, are primarily made of hollow bricks and concrete. Thermal transmittance values for all components are presented in Table 5.

Table 5: Opaque Envelope thermal transmittance values.

	Transmittance U-value [W/m²K]	**Periodic transmittance Y_{ie} [W/m²K]**
External wall	0.226	0.03
Internal wall	0.329	0.96
Underground floor	0.240	0.039
Ground floor	0.244	0.008
Roof	0.180	0.024

Transparent Envelope

The building envelope features transparent components, including double and triple-glazed windows and sliding doors with metal thermal break frames, which were designed to comply with Italian legislation (M.D. 26/06/2015). The external shutter blinds on select openings further improve thermal comfort and reduce glare. These transparent components are modelled and analysed in detail using Edilclima software again. The workflow requires defining the typology (e.g., from a climatized room to the outdoors), geometry, frame material, and glazing details. Key thermal parameters, such as thermal transmittance (U-value) and solar heat gain coefficient (G-value), are obtained from manufacturer data or calculated in accordance with standards like UNI EN ISO 10077. Edilclima also accounts for shading effects due to overhangs or adjacent structures to increase model accuracy. Once window modules are created, each transparent component is assigned to its position on the building envelope, and the corresponding thermal bridge is associated. U-values of the transparent components pertaining to the envelope, together with their geometrical characteristics, are presented in Table 6.

Table 6: thermal transmittance of transparent components.

Code	L [cm]	H [cm]	U_w [W/m²K]
W1	220.0	220.0	1.345
W2	92.5	92.5	1,353
W3	92.5	92.5	1,338
W4	120.0	120.0	1,334
W5	152.5	152.5	1,347
W6	60.0	60.0	1.303
W7	170.0	172.5	1,333
W8	92.5	92.5	1,338
W9	120.0	150.0	1,337
W10	160.0	75.0	1,330
W11	120.0	480.0	1,344
W12	190.0	250.0	1,282
W13	90.0	250.0	1,282
W14	350.0	590.0	1,285
W15	160.0	220.0	1,253
W16	295.0	315.0	1,276

W17	225.0	150.0	1.335
W18	80.0	170.0	1,332
W19	180.0	160.0	1,333
W20	180.0	315.0	1,282
W21	160.0	315.0	1,282
W22	225.0	250.0	1,282

Thermal Bridges

Thermal bridges are localized regions of the building envelope where heat flow deviates from adjacent one-dimensional heat flow paths. These occur due to variations in material, thickness, or geometry within the building structure. If not properly addressed, thermal bridges can result in increased heat loss, higher energy consumption, and problems such as condensation and mold growth.

To accurately assess and mitigate the impact of thermal bridges, European standards recommend detailed numerical calculations and simplified approaches. Key standards include UNI EN ISO 14683, which provides simplified methods for determining the linear thermal transmittance of thermal bridges using catalogues with tabulated values. Edilclima software calculates thermal bridges using either the Mold Simulator by Dartwin or by using the EC709 catalogue (an abacus) based on finite element simulations, following procedures detailed in European standards. Utilizing the latter method, the EC709 module returns the linear thermal transmittance Ψ (referred to the external dimensions of surfaces for various thermal bridge types), based on key design parameters.

Beyond calculating linear thermal transmittance, EC709 also verifies critical temperatures at thermal bridge locations to prevent mold or condensation. Standard 'nodes' libraries in EC709 provide access to a set of typical thermal bridge scenarios, calculated and parameterized using the finite element method, able to automatically import data from other opaque components generated within EC700.

The "Type" section at the top of the interface allows users to specify the thermal bridge typology by selecting between a series of options such as: junctions between external envelope elements (wall and roof, wall and balcony, wall corners); junctions between external walls with intermediate floors and internal walls; junctions between external walls with elevated or ground-level floors; pillars in external walls; and thermal bridges around doors and windows. In UNI EN ISO 14683, each thermal bridge typology is associated with a specific code. Figure 37 illustrates a thermal bridge's example and Table 7 summarise the set of thermal bridges considered and their corresponding linear transmittances.

Table 7 : thermal bridges that considered in the case study

Type	Description	Ψ[W/mK]
Z1	W - Wall - Frame	0.092
Z2	R - Wall - Roof	0.002
Z4	GF - Wall - Slab on the ground	0.029
Z6	C - Corner between walls	0.049

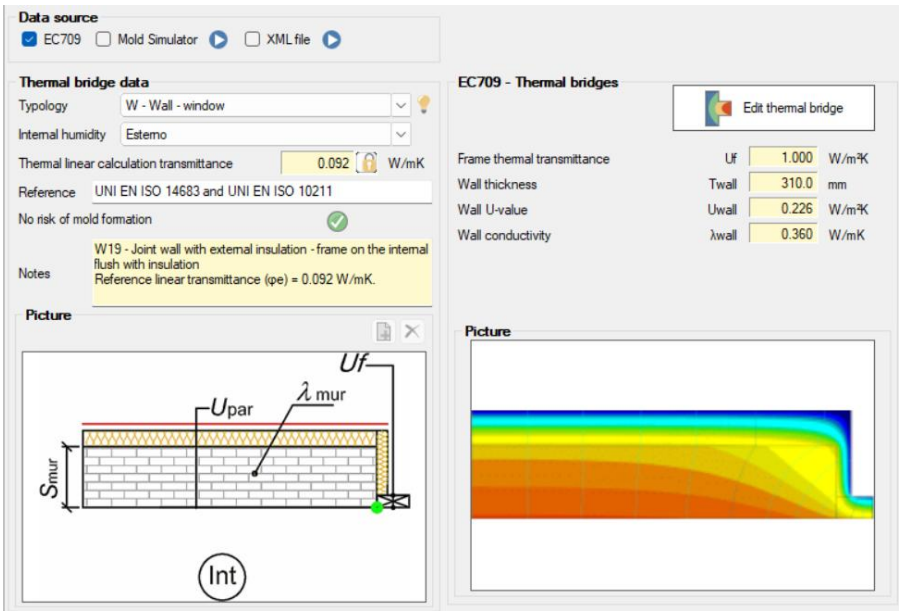

Figure 37: Thermal bridge example, connection between windows and walls.

Building Geometry & Surface Area

Once the thermal envelope was defined, the building geometric model in Edilclima software was created using information from a .dwg file containing the floor plans and storey heights. The modelling process began by importing the .dwg file with the floor plans into the software's graphical input interface. Starting from the basement level, external and internal walls were systematically traced for each constructed floor, assigning to each building component its appropriate thicknesses and specific stratigraphy previously defined. Upon completion of this representation process, a comprehensive geometric model of the building was obtained and visualized through a 3D representation (presented in Figure 38), which provides a complete spatial understanding of the building's thermal envelope layout and structural composition.

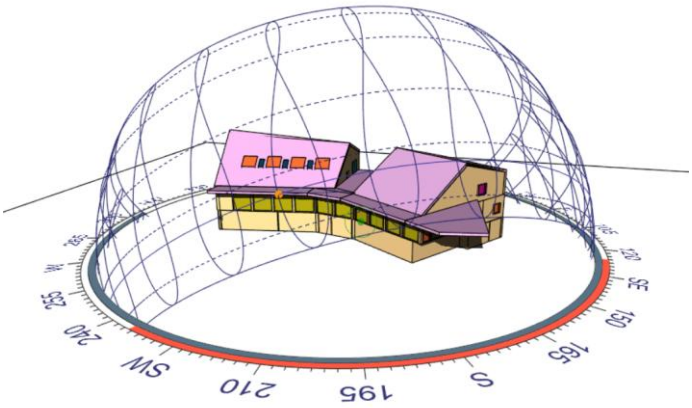

Figure 38: 3D view for the geometrical data of the case study.

As observed in the geometric model, transparent components of the building envelope have been comprehensively included within the graphical input interface. This encompasses fenestration elements such as windows and glazing systems, along with doors integrated into the building model. Additionally, shading devices and surrounding buildings have been strategically positioned around the main structure to account for solar obstruction effects on the thermal performance. The placement of these shading devices and surrounding buildings was achieved by incorporating a detailed model of the building and its surrounding urban context into the graphical input environment. The principal parameters defining the geometric input configuration are summarized in Table 8.

Table 8: Geometrical data main energy parameters.

Parameter	Net Value	Gross Value	Unit
Floor Surface	1577.61	1806.29	m^2
Volume	5379.12	7976.80	m^3
Gross External Surface (N-type)	—	7528.87	m^2
S/V Shape Factor	—	0.94	m^{-1}

Technical building systems

The building is equipped with a space heating and domestic hot water (DHW) production system, while ventilation is ensured exclusively through natural airflow, as no mechanical ventilation system is installed. Thermal energy for heating and DHW generation is supplied by two heat pumps. The installed units are two Aurax Eco AE i 290.2 heat pumps. Their general technical specifications are reported in Table 9.

Table 9: heat pump Data Aurax Eco AE i 290.2

Category	Parameter	Unit	Value
Heating	Thermal Power Range (30 Hz - 60 Hz)	kW	74.0 - 288.8
	Nominal Thermal Power	kW	288.8
	Absorbed Power	kW	72.2
	COP	W/W	4.00
	SCOP (35 °C / 55 °C)	kWh/kWh	3.80 / 3.01
Cooling	Refrigeration Power Range (30 Hz - 60 Hz)	kW	62.6 - 249.3
	Nominal Refrigeration Power	kW	249.3
	Absorbed Power	kW	84.7
	EER	W/W	2.94
	SEER (7 °C)	kWh/kWh	4.50
Hot Water (ACS)	Thermal Power (ACS Mode 1)	kW	261.2
	COP (ACS Mode 1)	W/W	2.5
	Thermal Power (ACS Mode 2 - Recovery)	kW	297.3
	COP (ACS Mode 2)	W/W	3.2
	TER (Total Efficiency Ratio)	W/W	5.3
Electrical	Power Supply	V/Ph/Hz	400/3+N+Pe/50
	Max. Absorbed Current	A	197
	Max. Absorbed Power	kW	109.2
	Starting Current (Spunto)	A	352

The EC700 software implements heat pump performance calculations in accordance with the Italian technical specification UNI/TS 11300-4, which establishes comprehensive requirements for determining energy performance in building systems. The standard requires detailed specification of both cold and hot source characteristics, with particular attention to operating temperature limits (cut-off temperatures) that define the heat pump operating domain. For performance assessment, the software offers two calculation approaches: a simplified method using single-point manufacturer data extrapolated across operating conditions, and an analytical method based on multiple performance points at standardized reference temperatures as prescribed by the norm. Critical to the calculation methodology is the application of correction coefficients (Cc, Cd, Fc) that adjust the nominal COP or gas utilization efficiency (GUE) based on part-load operation, with specific values varying according to heat pump typology (electric compression, direct-fired absorption, or engine-

driven). The software also accommodates the alternative reference climate method from UNI EN 14825 for determining part-load correction factors. Additionally, the standard requires specification of nominal conditions per Italian legislative requirements (D.Lgs. 311/06 and DPR 59/09) primarily for regulatory compliance verification, while actual energy calculations rely on the temperature-dependent performance data and the hydraulic circuit configuration that determines real operating conditions throughout the heating season.

Thermal zones

The UNI-TS 11300-1 defines a thermal zone as "a part of the conditioned environment maintained at a uniform temperature (and possibly humidity) through the same air conditioning system." While the partition of a structure into thermal zones is generally flexible, it is advisable to consider the intended use, set point temperatures, and thermal affinities of the areas within each zone. Consequently, thirteen thermal zones were taken into consideration.

For each thermal zone, it was then necessary to define:

- Winter setpoint temperature.
- Summer setpoint temperature.
- Temperature setback during the system shutdown period at night or on holidays.
- Hourly temperature schedules to maintain within the conditioned spaces.
- Hourly occupation schedules.
- Internal heat gains, including occupants (latent and sensible heat), internal equipment, and lighting contributions.

These parameters are crucial for accurately controlling the thermal conditions within each zone and optimizing the energy efficiency of the building. Inside the Edilclima software, suggested values for the previously mentioned parameters, along with pre-filled schedules, are provided from the database. These values vary depending on the type of room considered, and the most representative schedules are chosen based on the thermal zones. Specifically, the temperature parameters presented in Table 10 were selected for use.

Table 10: temperature set point for the case study.

WINTER SETPOINT TEMPERATURE [°C]	20
SUMMER SETPOINT TEMPERATURE [°C]	26
WINTER SETBACK TEMPERATURE [°C]	16
SUMMER SETBACK TEMPERATURE [°C]	32

4.2.2. Energy results

The following section presents the energy performance results obtained from the simulation of the building's heating system and domestic hot water (DHW). The results are structured across four tables, each addressing a distinct aspect of the energy balance. Table 11 traces the thermal energy flow from the initial building heating need through the several stages of emission, control, distribution, storage, and generation, accounting for the losses incurred at each stage that are not recovered back into the system (Figure 39). Table 12 details the total electrical energy required to operate the heating system, with particular focus on the electricity consumed by the heat pump generation unit, as no auxiliary electrical components or renewable electricity sources, such as photovoltaic panels or cogeneration systems, contribute to the system. Table 13 breaks down the primary energy for heating into its renewable and non-renewable fractions, reflecting the contribution of the heat pump in shifting a significant portion of the energy demand toward renewable sources. Finally, Table 14 consolidates the total primary energy consumption for both heating and domestic hot water services, providing a comprehensive overview of the building's overall energy demand.

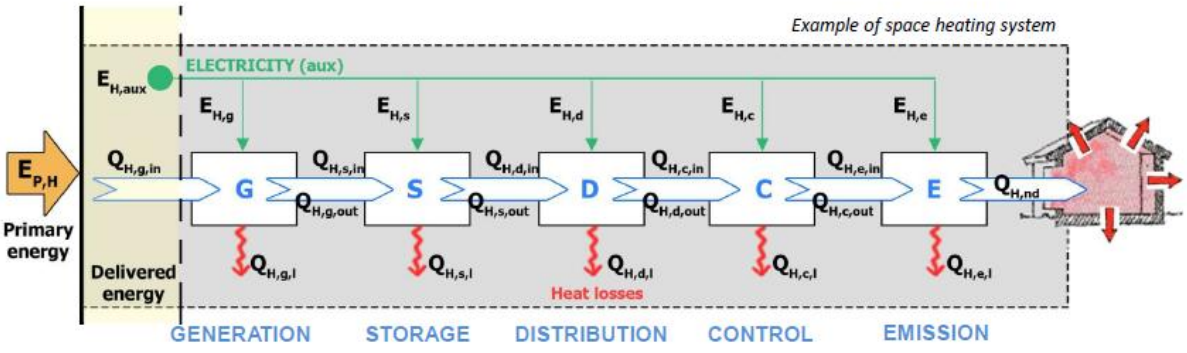

Figure 39 : energy flow graph

Table 11: Balance the thermal need for heating.

Description	Code	Value	Unit
Building needs (real ventilation)	QH,sys,out	371538	kWh
Energy recovered by the domestic hot water system	QH,W,rh	433	kWh
Net ideal energy need (deduced from recoveries)	Q'H,sys,out	371105	kWh
Energy need corrected for heat allocation costs	QH,sys,out,cont	371105	kWh
Energy need corrected for other factors	QH,sys,out,corr	371105	kWh
Emission losses not recovered	QH,em,ls,nrh	7574	kWh

Energy need entering into emissions	QH,em,in	378678	kWh
Generation losses not recovered	QH,rg,ls,nrh	19930	kWh
Energy need entering control system	QH,rg,in	398609	kWh
User distribution losses not recovered	QH,du,ls,nrh	4026	kWh
Energy need entering user distribution	QH,du,in	402635	kWh
Storage losses not recovered	QH,s,ls,nrh	0	kWh
Energy need entering storage	QH,s,in	402635	kWh
Energy produced by thermal solar	QH,sol,out	0	kWh
Thermal solar surplus	QH,sol,surplus	0	kWh
Net contribution of thermal solar	QH,sol,out,net	0	kWh
Actual energy need entering the storage	QH,s,in,eff	402635	kWh
Primary distribution losses not recovered	QH,dp,ls,nrh	0	kWh
Energy needs entering the primary distribution	QH,dp,in	402635	kWh
Energy needs are coming from the generation	QH,gen,out	402635	kWh
Losses of generation circuits are not recovered	QH,gen,circ,ls,nrh	0	kWh
Energy need entering generation circuits	QH,gen,circ,in	402635	kWh
Generation losses not recovered	QH,gen,ls,nrh	-291129	kWh
Energy need entering into generation (thermal)	QH,gen,in,t	0	kWh
Energy from outside (heat pump)	QH,gen,in,RES	291129	kWh

Table 12: Electrical Needs.

Description	Code	Value	Unit
Emission auxiliaries electrical need	QH,em,aux	0	kWh
User distribution auxiliaries electrical need	QH,du,aux	0	kWh
Thermal solar auxiliaries	QH,sol,aux	0	kWh
Primary distribution auxiliaries electrical need	QH,dp,aux	0	kWh
Generation auxiliaries electrical need	QH,gen,aux	0	kWh
Energy need entering generation of electricity	QH,gen,in,el	111506	kWh
Total electrical need	QH,el	111506	kWh
Energy produced by photovoltaic	QH,PV,out	0	kWh
Energy produced by cogeneration	QH,CG,out	0	kWh
Current electrical need (from network)	QH,el,eff	111506	kWh

Table 13: Primary Energy for heating

Description	Code	Value	Unit
Non-renewable	QH,p,nren	217437	kWh
Renewable	QH,p,ren	343537	kWh
Total Primary Energy	QH,p,tot	560974	kWh

Table 14: Total energy of Heating and DHW

Service	Non-renewable ($Q_{p,nren}$)	Renewable ($Q_{p,ren}$)	Total ($Q_{p,tot}$)	Unit
Heating	217437	343537	560974	kWh
Domestic hot water	4550	7538	12089	kWh
Total	221987	351075	573063	kWh

The total thermal energy need of the building is **371,105 kWh** (Q'H,sys,out, Table 11), and the total primary energy for heating and DHW (thermal+electric) combined is **573,063 kWh** (Table 14).

4.3. Energy geothermal systems

Having evaluated the building thermal requirements located in Torino (Italy) in the previous section, the focus now shifts to developing and defining sustainable strategies to meet these energy demands. To this end, we propose implementing the Geothermskin system and energy geo-slab: its design principles and operational framework are outlined below.

Geothermskin exploits shallow geothermal energy by utilizing the ground as a renewable thermal reservoir to satisfy the building's heating demand. The design and preliminary sizing approach adopted here follows the methodology proposed by Poveromo et al. (2023). Their approach addresses a practical gap in shallow geothermal design: the difficulty of predicting system performance without running full numerical simulations for every possible site. The solution they propose is a data-driven model trained on experimental data collected from the Turin prototype. Specifically, an artificial neural network (ANN) of the multilayer perceptron type is trained to learn the relationship between the local climatic conditions and the thermal power the system delivers. The four input variables fed into the network are external air temperature, ground temperature, global solar irradiance, and relative humidity, chosen because they are the main environmental factors governing heat exchange at shallow depth. The network processes these inputs through two hidden layers and outputs a prediction of the thermal power produced by the reference 34.5 m² wall.

Training was carried out using backpropagation with gradient descent optimization over 100 epochs, with the dataset split into batches of 64 samples per iteration. The model was validated against a withheld portion of the experimental dataset, yielding a Mean Absolute Percentage Error of approximately 7 %, which confirms acceptable predictive reliability for preliminary sizing purposes.

Once trained, the model is used together with long-term average climatic data from the ERA5-Land reanalysis dataset, a product of the Copernicus Climate Change Service that combines satellite observations with numerical weather model outputs to provide consistent historical climate records at high spatial resolution. By feeding provincial climate averages into the trained ANN, an estimate of the annual mean thermal power $Q_{forecasted}$ [W] can be obtained for any location in Italy, representing the average heat output expected from the 34.5 m² reference wall under local conditions.

System dimensioning is completed by applying the sizing equation proposed by Poveromo et al., (2023), which yields the Geothermskin surface area needed per unit of building floor area (as in Equ.6):

$$S_{\text{Geothermskin,required}} = \frac{Q_{\text{requested}}}{Q_{\text{forecasted}}} \cdot A_{\text{Geothermskin}} \left[\frac{m^2_{\text{Geothermskin}}}{m^2_{\text{building}}}\right] \quad (6)$$

where $Q_{requested}$ is the maximum annual average heating power demand per unit floor area as defined by Italian energy regulations for the building's climatic zone [W/m²], $Q_{forecasted}$ is the ANN-predicted annual mean thermal power output of the 34.5 m² reference wall for the site [W], and $A_{Geothermskin}$ is the reference area of the experimental installation, equal to 34.5 m². The ratio $Q_{requested}/ Q_{forecasted}$ essentially expresses how much wall area is needed relative to the prototype to cover the building's demand, scaled by the reference surface.

Applying this framework across all Italian provinces, Figure 40 shows that the required Geothermskin surface varies between 0.12 and 0.43 m²/m² of building floor area. The general trend is clear: moving from north to south, less wall surface is needed. This is because southern provinces combine lower regulatory heating demands with higher geothermal yields, the latter being driven by warmer and more stable ground conditions that reduce the thermal gradient the heat pump must overcome, allowing it to operate more efficiently.

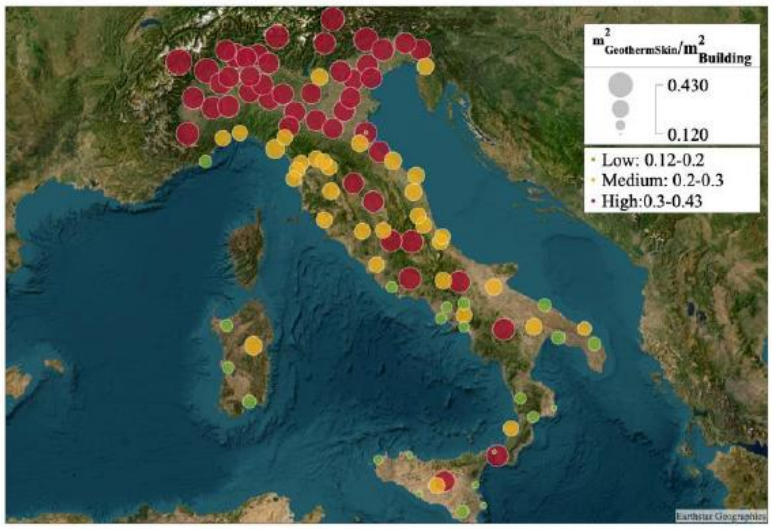

Province	$Q_{requested}$ [W/m²]	$Q_{forecasted}$ [W]	$\frac{m^2_{GeothermSkin}}{m^2_{building}}$	
Milano	13,2	1449	0,32	
Torino	13,2	1326	0,34	
Firenze	10,0	1465	0,24	
Ancona	10,0	1402	0,25	
Roma	10,0	1527	0,23	
Brindisi	7,8	1317	0,20	
Palermo	5,5	1423	0,13	
Cagliari	7,8	1363	0,20	

Figure 40: Required Geothermskin surface per unit surface of building and summary for main cities (Poveromo, 2023).

4.3.1. Technical and design description

The building aims to achieve a high-efficiency standard by utilizing the underground floor and ground slab as energy geostructures. Based on the architectural documents, the underground floor, with three sides directly connected to the ground (excluding the West side), suggests its suitability for use as an energy Geothermskin.

Geologically, the Turin metropolitan area is located at the distal end of the Dora Riparia alluvial plain. The upper 50 m of the subsoil consist primarily of sand and gravel deposits, interspersed with discontinuous cemented layers ranging from decimetric to metric thickness (Barla & Barla, 2005; 2012). These deposits exhibit significant spatial variability in density and cementation and host an unconfined aquifer with a strong groundwater flow directed toward the East/South-East. Beneath this unit, low-permeability silty-clayey deposits are encountered. At the experimental site, the groundwater table is approximately 23 m below ground level (Baralis & Barla, 2021; Bove, 2005), well below the prototype system's installation depth. Consequently, the system operation is not expected to be affected by the groundwater flow and its temperature. The site's stratigraphic profile is well constrained, owing to multiple boreholes drilled during prior geotechnical investigations for nearby construction projects (Aiassa & Antolini, 2019; Lavezzo & Monti, 2012).

The stratigraphic profile illustrated in Figure 41 was reconstructed using data from a nearby reference borehole in Torino and direct inspection of excavated material during installation (Baralis & Barla, 2021). Beneath approximately 30 cm of topsoil, a 3.8 m thick layer of gravel with pebbles in a sandy matrix, locally containing silt, is present. Deeper down, a sandy-gravel deposit with clear signs of oxidation and alteration was observed.

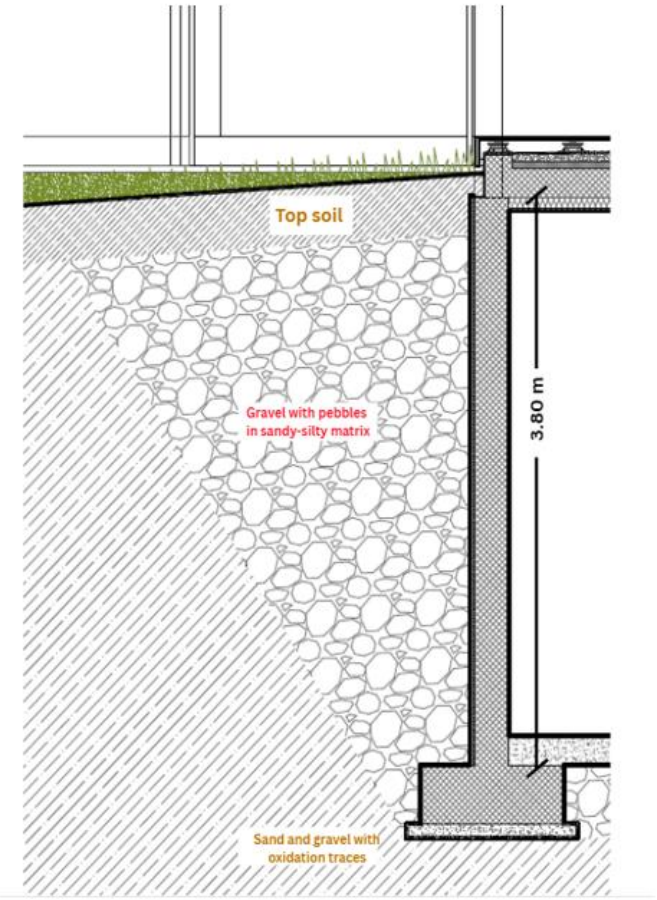

Figure 41: Stratigraphic profile.

Compared to traditional energy walls, the Geothermskin is applied to the earth-contact surface of the wall, as described in 3.4.1. For this case, the system can be implemented by taking advantage of open excavations during initial construction stages. In the case of the slab, it is implemented at the bottom of the blinding layer of the concrete slab, connecting to the reinforcement cage. Figure 42 shows the side phases of these implementations.

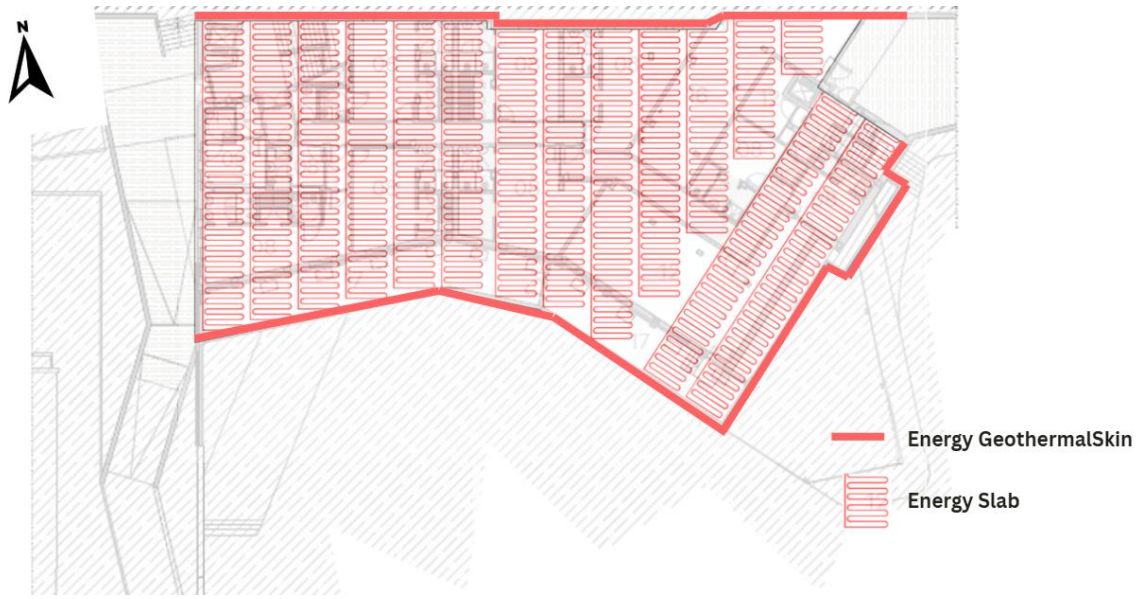

Figure 42: Energy geostructure in the case study.

In the case of the Geothermskin, the system is conceived as modular equipment to ensure end-user flexibility, redundancy, and the opportunity to exclude heat exchanger sections in case of local damage or leakage without compromising the entire system. This implies that deployment is independent of wall structural characteristics, unlike traditional energy geostructures, whose circuit deployment is based on reinforcement cage layout (CFMS&SYNTEC, 2017) .

The hydraulic circuit uses polymeric pipes (cross-linked polyethylene, PE-Xa, instead of high-density polyethylene, PE-HD) that are fixed to the external wall surface after construction. Pipe deployment includes straight sections and bends with a 15 cm radius, which is the pipe's maximum bending curvature. Clamps anchored into the wall provide temporary support and secure the pipes (see Figure 43).

Each module constitutes a hydraulic circuit where pipes are preferentially deployed horizontally rather than vertically (see Figure 43). This eases the elimination of air bubbles during circuit loading, while the horizontal orientation slightly diminishes bends and, consequently, related hydraulic head losses. Locating the ends of each module at opposite edges of the upper portion of the equipped area avoids thermal short-circuiting among different circuit branches. Furthermore, this deployment enables both sequential and parallel linking of adjacent modules. Although sequential linking allows limiting the flow rate needed at the heat pump while ensuring sufficient velocity of the heat carrier fluid in ground heat exchangers, parallel linking is expected to yield higher thermal efficiency. In all cases, heat exchanger pipes are connected to the main collector circuit on the internal wall side through appropriate holes. A manifold facilitates connection to the GSHP system.

Both ends of each module should connect to the envisaged manifold, which is supposed to be placed on the inner wall side. The manifold is designed to allow parallel or sequential

connection of modules, as well as individual module exclusion if needed. Manifold and distributor pipes connecting the geothermal circuits of Geothermskin to the system in the building and the heat pump should be heavily insulated (for instance, using closed elastomeric coating).

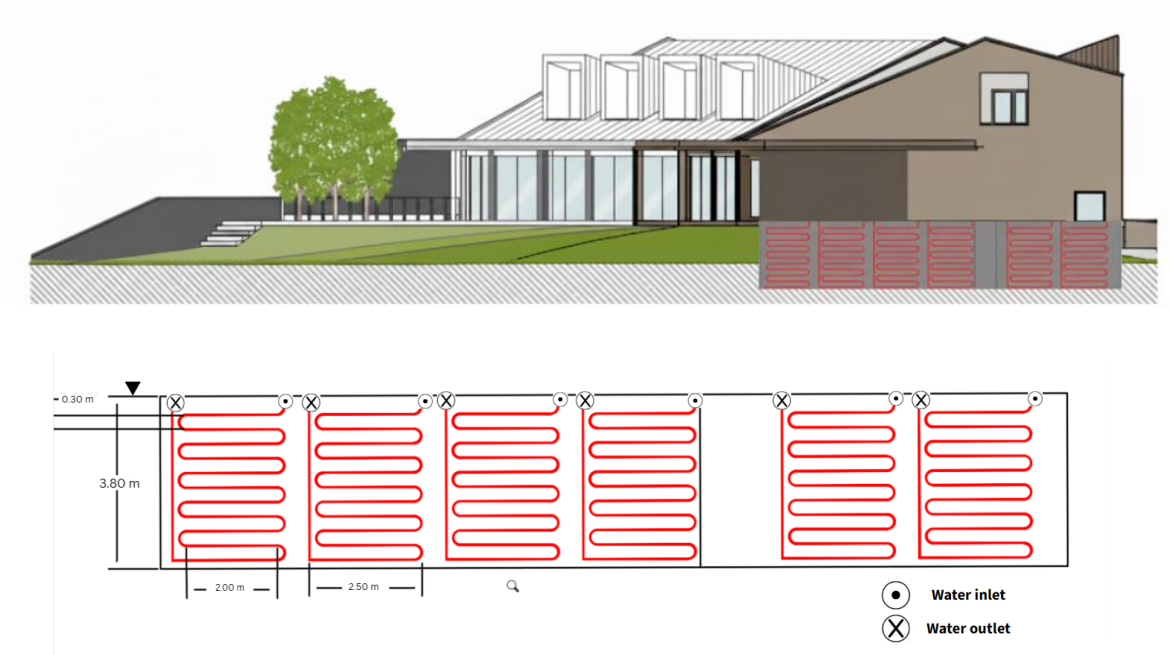

Figure 43: Energy Geothermskin for the west side of the case study.

4.3.2. Calculation and Results of EGs

Applying the methodology of Poveromo et al. (2023) to the case study building in Turin, the thermal energy contribution of the energy geostructure is estimated through the following procedure.

For Turin, the trained ANN model, supplied with ERA5-Land long-term climatic averages, predicts an annual mean thermal power output of $Q_{forecasted}$ = 1,326 W for the 34.5 m² reference wall. This represents the average continuous heat delivery capacity expected from the reference installation under Turin's typical climatic conditions. On the demand side, Turin falls within Climate Zone E under Italian energy regulations, for which the maximum permitted annual average heating power per unit floor area is $Q_{requested}$ = 13.2 W/m², in line with the European Energy Performance of Buildings Directive (EPBD 2010/31/EU).

To scale the reference wall performance to the actual components of the building's geostructure, the specific thermal power density of the equipped wall surface is first derived:

$$q_{(wall)} = Q_{(forecasted)}/A_{(GeothermSkin)} = 1326\,W/34.5m^2 \approx 38.43W/m^2$$

This value is then applied to the surface area of each geostructure component to obtain its total power output. For the north foundation wall, for instance:

$$P_{(North)} = 38.43W/m^2 \times 100.8m^2 \approx 3{,}874W$$

The same calculation is repeated for the remaining walls and the ground floor slab, and the results are converted to annual energy production based on the operational constraints applicable to Turin (Climate Zone E), where heating systems are permitted to operate for up to 14 hours per day from October 15 to April 15, corresponding to 2,548 hours per year. The full breakdown is reported in Table 15.

Table 15: Energy produced by the Energy Geostructure systems.

Component	Surface Area [m²]	Total Power [W]	System Energy for heating [kWh/year]
E Wall 1 (North)	100.80	3,874	9,871
E Wall 2 (South)	131.80	5,065	12,906
E Wall 3 (East)	76.00	2,921	7,443
E Slab	758.66	29,158	74,299
Total	**1,067.26**	**41,019**	**104,520**

The energy geostructure is estimated to deliver 104,520 kWh over the heating season. Compared to the building's total annual thermal energy need of 371,105 kWh and total primary energy demand for heating and domestic hot water of 573,063 kWh, the geostructure can cover approximately 28.2 % of the building's total thermal energy needs and 18.2 % of the total primary energy demand. These results demonstrate that, while the proposed system alone cannot fully meet the building's energy requirements, it provides a meaningful renewable

contribution, offsetting more than a quarter of the heating demand and reducing reliance on conventional energy sources.

Chapter 5.

Conclusions

This research successfully demonstrated the design, evaluation, and implementation of an integrated energy geostructure system, which includes the Geothermskin technology and slab components, for a sports center in Turin, Italy. Operating in a cold climate, the study provides comprehensive evidence that shallow energy geostructures can also substantially contribute to sustainability while maintaining structural integrity and economic viability.

The integrated geothermal system, incorporating both Geothermskin and an energy slab, achieved a reasonable energy coverage, meeting 18.2% of the building's total energy demand for heating (104,520 kWh/year from a total surface area of 1,067.26 m²), confirming that energy geostructures can serve as primary, rather than supplementary, energy sources in appropriately designed applications.

The application of the artificial neural network (ANN)-based sizing methodology developed by Poveromo et al. (2023) proved effective for preliminary design in the Turin context. This data-driven approach, trained on experimental measurements from the Turin prototype and applied using ERA5-Land long-term climatic averages, provided a reliable estimate of the annual mean thermal power output of the reference 34.5 m² wall, yielding $Q_{forecasted}$ = 1,326 W, without requiring full numerical simulations at the feasibility stage. This value was subsequently used to derive a specific power density of 38.43 W/m², which served as the basis for scaling the performance estimate to the actual geostructure components. This methodology represents a significant practical advancement for early-stage design decisions, particularly because reliable performance estimates can be obtained using only publicly available climatic data, eliminating the need for site-specific numerical modeling or extensive experimental campaigns.

The Geothermskin system demonstrated advantages for urban applications where land availability constrains traditional horizontal collectors and existing buildings are excluded from conventional energy geostructure solutions. By equipping the earth-contact area of buildings with a modular ground heat exchanger with virtually no horizontal area occupancy, the system achieved competitive thermal performance while eliminating the need for dedicated excavation. The system's modularity also allows for greater robustness through the ability to isolate damaged portions during construction or operation, reducing the risk of failing to meet expected thermal power outputs. In its two distinct configurations, the system proved to be a cost-effective solution, with preliminary assessments of cost per unit power generated showing values of approximately 30 €/kW, primarily related to labor costs during installation. Nonetheless, further investigation should be carried out considering full-scale applications and

comparison to the energy demand of existing buildings, and standardization of the construction process may further improve the cost–benefit analysis.

Comparative analysis against conventional heating systems revealed substantial reductions in CO_2 emissions. Assuming a coefficient of performance (COP) of 4.0 for the geothermal heat pump, the system achieves emission factors of approximately 0.034 kg CO_2-equivalent per kWh, representing a 79–93 % reduction compared to natural gas, heating oil, and coal-based systems.

Economic analysis indicated that the additional installation cost of integrating heat exchanger pipes into structural elements ranged from 1–2 % of the total construction cost, with projected payback periods between 2 to 15 years, depending on local energy prices and operational strategies. This wide range reflects the variability across different energy geostructure typologies (from energy piles, tunnels, and slabs to wall systems) as well as significant differences in regional energy pricing, climate conditions, and project scale.

Advanced control strategies incorporating weather forecasting, occupancy patterns, and thermal storage optimization could further enhance system performance. Research into model predictive control (MPC) algorithms specifically adapted for energy geostructures would support demand-side management objectives and grid integration of variable renewable electricity sources used to power heat pumps.

The lack of standardized design procedures and performance verification protocols poses a significant barrier to widespread adoption. Future work should focus on developing national and European standards addressing thermal sizing methodologies, structural safety factors, installation quality assurance, and performance monitoring requirements specific to energy geostructures.

This research demonstrates that integrating energy geostructures into contemporary building design represents not merely an incremental improvement, but a paradigm shift in our conceptualization of the relationship between buildings and their geological context. By transforming necessary structural elements (foundation walls, slabs, and retaining structures) into active participants in building energy systems, we unlock substantial renewable energy potential without competing for scarce urban land or requiring dedicated excavation.

The Turin sports center case study confirms that achieving meeting 18.2% of the building's total energy demand for heating through shallow geothermal systems is technically feasible, economically rational, and environmentally essential. As the building sector continues its necessary transition toward net-zero energy targets, energy geostructures should be recognized as a foundational technology rather than an optional enhancement. The challenge ahead lies not in proving feasibility but in scaling deployment through standardization, professional education, and supportive regulatory frameworks.

The convergence of structural engineering, geotechnical practice, and energy systems design embodied in energy geostructures exemplifies the multidisciplinary integration essential for sustainable infrastructure development. This research contributes both practical tools for immediate application and a foundation for continued innovation in this rapidly evolving field.

References

Adam, D., & Markiewicz, R. (2009). Energy from earth-coupled structures, foundations, tunnels and sewers. Géotechnique, 59(3), 229–236. https://doi.org/10.1680/geot.2009.59.3.229

Adinolfi, M., Rianna, G., Mercogliano, P., Maiorano, R. M. S., & Aversa, S. (2021). Behaviour of energy piles under climate-change scenarios: a case study in Southern Italy. Environmental Geotechnics, 8(8), 571–585. https://doi.org/10.1680/jenge.19.00093

Aiassa, & Antolini, F. (2019). Technical report on site investigations for "Digital revolution House." In Italian: Relazione Tecnica Sulle Indagini "Digital Revolution House."),.

Amis, T., Robinson, C. A. W., Wong, S., & Seinuk, C. (2011). INTEGRATING GEOTHERMAL LOOPS INTO THE DIAPHRAGM WALLS OF THE BULGARI HOTEL KNIGHTSBRIDGE LONDON PROJECT.

Anoop, K. M., & Ahipa, T. N. (2023). Recent advancements in the hole transporting layers of perovskite solar cells. Solar Energy, 263, 111937. https://doi.org/10.1016/j.solener.2023.111937

Anstett, M., Hubbuch, M., Laloui, L., Matthey, B., Morath, M., Pahud, D., Parriaux, A., Rybach, L., Schönbächler, M., Tacher, L., et al. (2005). SIA DO 190: Utilisation de la Chaleur du Sous-Sol par des Ouvrages de Fondation et de Soutènement en Béton–Guide Pour la Conception, la Réalisation et la Maintenance. SIA (Société Suisse des Ingénieurs et des Architects): Zürich, Switzerland.

Arola, T., Eskola, L., Hellen, J., & Korkka-Niemi, K. (2014). Mapping the low enthalpy geothermal potential of shallow Quaternary aquifers in Finland. Geothermal Energy, 2(1), 9. https://doi.org/10.1186/s40517-014-0009-x

Ayaz, H., Faizal, M., & Bouazza, A. (2024). Energy, economic, and carbon emission analysis of a residential building with an energy pile system. Renewable Energy, 220, 119712. https://doi.org/10.1016/j.renene.2023.119712

Bao, X. H., Xiong, Y. L., Mingi, H. Y., Cui, H. Z., Liu, G. B., & Zheng, R. Y. (2018). Investigation on the Thermo-Mechanical Behavior of an Energy Pile and the Surrounding Soil by Model Test and 2D Finite Element-Finite Difference Method. In Proceedings of GeoShanghai 2018 International Conference: Tunnelling and Underground Construction (pp. 696–709). Springer Singapore. https://doi.org/10.1007/978-981-13-0017-2_70

Baralis. (2020). Optimisation of geothermal resources in urban areas [Phd]. Politecnico di Torino.

Baralis, M., & Barla, M. (2021). Development and testing of a novel geothermal wall system. International Journal of Energy and Environmental Engineering, 12(4), 689–704. https://doi.org/10.1007/s40095-021-00407-y

Baralis, M., Barla, M., Bogusz, W., Di Donna, A., Ryżyński, G., & Żeruń, M. (2020). Geothermal potential of the NE extension Warsaw (Poland) metro tunnels. Environmental Geotechnics, 7(4), 282–294. https://doi.org/10.1680/jenge.18.00042

Barbero, D., De Luca, D. A., Forno, M. G., & Lasagna, M. (2016). Preliminary results on temperature distribution in the Quaternary fluvial and outwash deposits of the Piedmont Po Plain (NW Italy): a statistical approach. Rendiconti Online Della Società Geologica Italiana, 41, 272–275. https://doi.org/10.3301/ROL.2016.146

Barbier, E. (1997). Nature and technology of geothermal energy: A review. Renewable and Sustainable Energy Reviews, 1(1–2), 1–69. https://doi.org/10.1016/S1364-0321(97)00001-4

Barbier, E. (2002). Geothermal energy technology and current status: an overview. Renewable and Sustainable Energy Reviews, 6(1–2), 3–65. https://doi.org/10.1016/S1364-0321(02)00002-3

Barla, Di Donna, A., & Insana, A. (2019). A novel real-scale experimental prototype of energy tunnel. Tunnelling and Underground Space Technology, 87, 1–14. https://doi.org/10.1016/j.tust.2019.01.024

Barla, Di Donna, Alice., & Santi, Alessandro (2020). Energy and mechanical aspects on the thermal activation of diaphragm walls for heating and cooling. Renewable Energy, 147, 2654–2663. https://doi.org/10.1016/j.renene.2018.10.074

Barla, & Insana. (2023a). Energy tunnels as an opportunity for sustainable development of urban areas. Tunnelling and Underground Space Technology, 132, 104902. https://doi.org/10.1016/j.tust.2022.104902

Barla, Insana, A., & Alvi, M. R. (2025). Assessing the interaction of an energy tunnel with the underground thermal conditions in an urban area. Geothermics, 130, 103350. https://doi.org/10.1016/j.geothermics.2025.103350

Barla, M., Di Donna, A., & Baralis, M. (2020). City-scale analysis of subsoil thermal conditions due to geothermal exploitation. Environmental Geotechnics, 7(4), 306–316. https://doi.org/10.1680/jenge.17.00087

Barla, M., & Insana, A. (2023b). Energy tunnels as an opportunity for sustainable development of urban areas. Tunnelling and Underground Space Technology, 132. https://doi.org/10.1016/j.tust.2022.104902

Batini, N., Rotta Loria, A. F., Conti, P., Testi, D., Grassi, W., & Laloui, L. (2015). Energy and geotechnical behaviour of energy piles for different design solutions. Applied Thermal Engineering, 86, 199–213. https://doi.org/10.1016/j.applthermaleng.2015.04.050

Bertani, R., & Thain, I. (2002). Geothermal power generating plant CO2 emission survey. IGA News, 49, 1–3.

Blum, P., Campillo, G., Münch, W., & Kölbel, T. (2010). CO2 savings of ground source heat pump systems – A regional analysis. Renewable Energy, 35(1), 122–127. https://doi.org/10.1016/j.renene.2009.03.034

Bourne-Webb, P. (2013). An overview of observed thermal and thermo-mechanical response of piled energy foundations. In European Geothermal Congress.

Bourne-Webb, P., Burlon, S., Javed, S., Kürten, S., & Loveridge, F. (2016). Analysis and design methods for energy geostructures. Renewable and Sustainable Energy Reviews, 65, 402–419. https://doi.org/10.1016/j.rser.2016.06.046

Bourne-Webb, P. J., Bodas Freitas, T. M., & da Costa Gonçalves, R. A. (2016). Thermal and mechanical aspects of the response of embedded retaining walls used as shallow geothermal heat exchangers. Energy and Buildings, 125, 130–141. https://doi.org/10.1016/j.enbuild.2016.04.075

Bove, A., Casaccio, D., Destefanis, E., De Luca, D. A., Lasagna, M., & Masciocco, L. (2005). Piezometria della falda superficiale nel territorio di pianura della Regione Piemonte. In Regione Piemonte (Ed.), Idrogeologia della pianura piemontese (p. 10). Mariogros Industrie grafiche S.p.A.

Brandl, H. (2006). Energy foundations and other thermo-active ground structures.

British Research Establishment (BRE), Standard Assessment Procedure 10.2 - the Government's Standard Assessment Procedure for Energy Rating of Dwellings, 2022. (2022).

CFMS&SYNTEC, INGENIERIE/SOFFONS-FNTP. (2017). Recommandations pour la conception, le dimensionnement et la mise en oeuvre des géostructures thermiques. Rev. Fr. Geotech., 149(1), 1–120. https://doi.org/10.1051/geotech/2017012.

Campanella & Mitchell. (1968). Influence of temperature variations on soil behavior. J. SoilMech. Found.

Chen, L., Hu, Y., Wang, R., Li, X., Chen, Z., Hua, J., Osman, A. I., Farghali, M., Huang, L., Li, J., Dong, L., Rooney, D. W., & Yap, P. S. (2024). Green building practices to integrate renewable energy in the construction sector: a review. In Environmental Chemistry Letters (Vol. 22, Number 2, pp. 751–784). Springer Science and Business Media Deutschland GmbH. https://doi.org/10.1007/s10311-023-01675-2

Dai, Q., Zhang, D., & Li, Z. (2023). Mechanical assessment of energy wall in the long term. Acta Geotechnica, 18(1), 1–34. https://doi.org/10.1007/s11440-022-01579-5

De Vries. (1958). Simultaneous transfer of heat and moisture in porous media. Eos, Transactions American Geophysical Union, 39(5), 909–916. https://doi.org/10.1029/TR039i005p00909

Delerablee, Y. (2019). Int´egration thermique et m´ecanique des g´eostructures thermiques: de l'´echelle du bˆatiment `a l'´echelle de la cit´e. PhD thesis, Universit´e Paris-Est. In French.

Di Donna, A., & Barla, M. (2016). The role of ground conditions on energy tunnels' heat exchange. Environmental Geotechnics, 3(4), 214–224. https://doi.org/10.1680/jenge.15.00030

Di Donna, Alice., & Barla, M. (2017a). Energy geostructures: a collection of data from real applications.

Di Donna, Alice., & Barla, M. (2017b). Energy Geostructures: Analysis from research and systems installed around the World.

Di Donna, & Laloui, L. (2015). Numerical analysis of the geotechnical behaviour of energy piles. International Journal for Numerical and Analytical Methods in Geomechanics, 39(8), 861–888. https://doi.org/10.1002/nag.2341

Di Donna, Loveridge, F., Piemontese, M., & Barla, M. (2021). The role of ground conditions on the heat exchange potential of energy walls. Geomechanics for Energy and the Environment, 25, 100199. https://doi.org/10.1016/j.gete.2020.100199

Dickson, M. H., & Fanelli, M. (2003). Geothermal Energy. Routledge. https://doi.org/10.4324/9781315065786

Energy Information Administration. (2026). Solar explained Photovoltaics and electricity. https://www.eia.gov/energyexplained/solar/photovoltaics-and-electricity.php

Engeland, K., Borga, M., Creutin, J.-D., François, B., Ramos, M.-H., & Vidal, J.-P. (2017). Space-time variability of climate variables and intermittent renewable electricity production – A review. Renewable and Sustainable Energy Reviews, 79, 600–617. https://doi.org/10.1016/j.rser.2017.05.046

EPRI. (1978). Geothermal Energy Prospects for the Next 50 Years.

Faizal, M., Bouazza, A., Haberfield, C., & McCartney, J. S. (2018). Axial and Radial Thermal Responses of a Field-Scale Energy Pile under Monotonic and Cyclic Temperature Changes. Journal of Geotechnical and Geoenvironmental Engineering, 144(10). https://doi.org/10.1061/(ASCE)GT.1943-5606.0001952

Farouki, O. T. (1981). Thermal Properties of Soils.

Fridleifsson, I. B., Bertani, R., Huenges, E., Lund, J. W., Ragnarsson, A., & Rybach, L. (2008). The possible role and contribution of geothermal energy to the mitigation of climate change. In O. Hohmeyer & T. Trittin (Eds.), IPCC Scoping Meeting on Renewable Energy Sources, Proceedings (pp. 59–80). Luebeck, Germany.

Gao, J., Zhang, X., Liu, J., Li, K., & Yang, J. (2008). Numerical and experimental assessment of thermal performance of vertical energy piles: An application. Applied Energy, 85(10), 901–910. https://doi.org/10.1016/j.apenergy.2008.02.010

Georgette Kilgore. (2024, February 15). Carbon Offsets Credits. Https://8billiontrees.Com/Carbon-Offsets-Credits/Geothermal-Energy/.

Goldstein, B., Hiriart, G., Bertani, R., Bromley, C., Gutiérrez-Negrín, L., Huenges, E., Muraoka, H., Ragnarsson, A., Tester, J., Zui, V., Blackwell, D., Demayo, T., Heath, G., Lee, A., Lund, J. W., Mongillo, M., Newell, D., Sanyal, S., Williamson, K. H., … Wratt, D. (2011). Geothermal Energy. In Renewable Energy Sources and Climate Change Mitigation (pp. 401–436). Cambridge University Press. https://doi.org/10.1017/CBO9781139151153.008

Hellström, G. (1991). Ground heat storage: Thermal analyses of duct storage systems. University of Lund, Sweden.

Hemmerle, C. (2017). Solar PV building skins - Structural requirements and environmental benefits. Journal of Facade Design and Engineering, 5(1), 93–106. https://doi.org/10.7480/jfde.2017.1.1528

IEA. (2023). Tracking Clean Energy Progress 2023. https://www.iea.org/reports/tracking-clean-energy-progress-2023.

Insana, A., & Barla, M. (2020). Experimental and numerical investigations on the energy performance of a thermo-active tunnel. Renewable Energy, 152, 781–792. https://doi.org/10.1016/j.renene.2020.01.086

Kalogirou, (2003). The potential of solar industrial process heat applications. Applied Energy, 76(4), 337–361. https://doi.org/10.1016/S0306-2619(02)00176-9

Kalogirou, (2004). Solar thermal collectors and applications. In Progress in Energy and Combustion Science (Vol. 30, Number 3, pp. 231–295). https://doi.org/10.1016/j.pecs.2004.02.001

Kalogirou, S. A., Lloyd, S., Ward, J., & Eleftheriou, P. (1994). Design and performance characteristics of a parabolic-trough solar-collector system. Applied Energy, 47(4), 341–354. https://doi.org/10.1016/0306-2619(94)90041-8

Katzenbach R., Clauss F., Leppla S., & Ruppert T. (2013). Potentials of environmental protection by geotechnical engineering. In Proceedings of the 15th European Conference on Soil Mechanics and Geotechnical Engineering. IOS Press. https://doi.org/10.3233/978-1-61499-199-1-247

Kumar, L., Hasanuzzaman, M., & Rahim, N. A. (2019). Global advancement of solar thermal energy technologies for industrial process heat and its future prospects: A review. In Energy Conversion and Management (Vol. 195, pp. 885–908). Elsevier Ltd. https://doi.org/10.1016/j.enconman.2019.05.081

Kumar, & Shekhar, S. (2014). Computing Building Rooftop Solar Potential For Photovoltaics. https://doi.org/10.13140/2.1.4787.7446

Kurian, J., & Karthi, L. (2023). Building integrated photovoltaics-an overview. Sustainability, Agri, Food and Environmental Research-DISCONTINUED, 10. https://doi.org/10.7770/safer-V10N1-art2495

Kürten, S., Mottaghy, D., & Ziegler, M. (2015). A new model for the description of the heat transfer for plane thermo-active geotechnical systems based on thermal resistances. Acta Geotechnica, 10(2), 219–229. https://doi.org/10.1007/s11440-014-0311-6

Laloui, L., & Di Donna, A. (2011). Understanding the behaviour of energy geo-structures. Proceedings of the Institution of Civil Engineers - Civil Engineering, 164(4), 184–191. https://doi.org/10.1680/cien.2011.164.4.184

Laloui, L., Moreni, M., & Vulliet, L. (2003). Comportement d'un pieu bi-fonction, fondation et échangeur de chaleur. Canadian Geotechnical Journal, 40(2), 388–402. https://doi.org/10.1139/t02-117

Laloui, L., Nuth, M., & Vulliet, L. (2006). Experimental and numerical investigations of the behaviour of a heat exchanger pile. International Journal for Numerical and Analytical Methods in Geomechanics, 30(8), 763–781. https://doi.org/10.1002/nag.499

Laloui, L., & Rotta Loria, A. F. (2020). Analysis and Design of Energy Geostructures Theoretical Essentials and Practical Application.

Laloui, L., & Sutman, M. (2019). Energy geostructures: A new era for geotechnical engineering practice. 17th European Conference on Soil Mechanics and Geotechnical Engineering, ECSMGE 2019 - Proceedings, 94–108. https://doi.org/10.32075/17ECSMGE-2019-1106

Lam SY. (2010). Ground movements due to excavation in clay: physical and analytical models, Ph.D. thesis, University of Cambridge.

Lavezzo, & Monti, S. (2012). Progettazione della residenza universitaria “Cesare Codegone” nell’area delimitata dalle vie borsellino. Relazione Geologica e Geotecnica.

Li, Z. (2023). Prospects of Photovoltaic Technology. Engineering, 21, 28–31. https://doi.org/10.1016/j.eng.2022.07.008

Liebel, H. T. (2012). Influence of Groundwater on Measurements of Thermal Properties in Fractured Aquifers. Norwegian University of Science and Technology, Trondheim, Norway.

Lind, L. (971). The rise and rise of geothermal heat pumps in New Zealand. https://www.researchgate.net/publication/316919670

Link, K., Lupi, N., & Siddiqi, G. (2015). Geothermal energy in Switzerland – Country update. In Proceedings World Geothermal Congress.

Loveridge, F., McCartney, J. S., Narsilio, G. A., & Sanchez, M. (2020). Energy geostructures: A review of analysis approaches, in situ testing and model scale experiments. Geomechanics for Energy and the Environment, 22, 100173. https://doi.org/10.1016/j.gete.2019.100173

Lund, J. W., & Boyd, T. L. (2016). Direct utilization of geothermal energy 2015 worldwide review. Geothermics, 60, 66–93. https://doi.org/10.1016/j.geothermics.2015.11.004

Laloui, L., & Loria, A. F. R. (2020). Analysis and design of energy geostructures: Theoretical essentials and practical application. Elsevier. https://doi.org/10.1016/B978-0-12-816223-1.00017-5

Mekhilef, S., Saidur, R., & Safari, A. (2011). A review on solar energy use in industries. Renewable and Sustainable Energy Reviews, 15(4), 1777–1790. https://doi.org/10.1016/j.rser.2010.12.018

Midttømme, K., & Roaldset, E. (1999). Thermal conductivity of sedimentary rocks: uncertainties in measurement and modelling. Geological Society, London, Special Publications, 158(1), 45–60. https://doi.org/10.1144/GSL.SP.1999.158.01.04

Mohamad, Z., Fardoun, F., & Meftah, F. (2021). A review on energy piles design, evaluation, and optimization. Journal of Cleaner Production, 292, 125802. https://doi.org/10.1016/j.jclepro.2021.125802ï

Moormann, C., Buhmann, P., Friedemann, W., Homuth, S., & Pralle, N. (2016). Tunnel geothermics – International experience with renewable energy concepts in tunnelling / Tunnelgeothermie – Internationale Erfahrungen zu regenerativen Energiekonzepten im

Tunnelbau. Geomechanics and Tunnelling, 9(5), 467–480. https://doi.org/10.1002/geot.201600048

Pandey, B., Banerjee, R., & Sharma, A. (2021). Coupled EnergyPlus and CFD analysis of PCM for thermal management of buildings. Energy and Buildings, 231, 110598. https://doi.org/10.1016/j.enbuild.2020.110598

Pearsall, N. M. (2017). Introduction to photovoltaic system performance. In The Performance of Photovoltaic (PV) Systems (pp. 1–19). Elsevier. https://doi.org/10.1016/B978-1-78242-336-2.00001-X

Poveromo, A., Insana, A., Papurello, D., & Barla, M. (2023). neural network approach for quick dimensioning of energy walls. Symposium on Energy Geotechnics 2023. https://doi.org/10.59490/seg.2023.521

Raina, G., & Sinha, S. (2023). Experimental investigations of front and rear side soiling on bifacial PV module under different installations and environmental conditions. Energy for Sustainable Development, 72, 301–313. https://doi.org/10.1016/j.esd.2023.01.001

Raymond, J.; Malo, M.; Tanguay, D.; Grasby, S.; Bakhteyar, F. Direct utilization of geothermal energy from coast to coast: a review of current applications and research in Canada. In Proceedings of the World Geothermal Congress 2015, Melbourne, Australia, 16–24 April 2015

Reddy, V. J., Hariram, N. P., Ghazali, M. F., & Kumarasamy, S. (2024). Pathway to Sustainability: An Overview of Renewable Energy Integration in Building Systems. In Sustainability (Switzerland) (Vol. 16, Number 2). Multidisciplinary Digital Publishing Institute (MDPI). https://doi.org/10.3390/su16020638

Rees, S. W., Adjali, M. H., Zhou, Z., Davies, M., & Thomas, H. R. (2000). Ground heat transfer effects on the thermal performance of earth-contact structures. Renewable and Sustainable Energy Reviews, 4(3), 213–265. https://doi.org/10.1016/S1364-0321(99)00018-0

Rhodes, C. J. (2010). Solar Energy: Principles and Possibilities. Science Progress, 93(1), 37–112. https://doi.org/10.3184/003685010X12626410325807

Rotta Loria, A. F. (2020). Energy geostructures: Theory and application. E3S Web of Conferences, 205, 01004. https://doi.org/10.1051/e3sconf/202020501004

Rotta Loria, A. F., & Laloui, L. (2017). Displacement interaction among energy piles bearing on stiff soil strata. Computers and Geotechnics, 90, 144–154. https://doi.org/10.1016/j.compgeo.2017.06.008

Rybach, L. (1995). Thermal waters in deep Alpine tunnels. Geothermics, 24(5–6), 631–637. https://doi.org/10.1016/0375-6505(95)00029-1

Saggu, R. (2019). Strain Distribution in Geothermal Energy Piles: A Parametric Study (pp. 129–137). https://doi.org/10.1007/978-981-13-2227-3_16

Salciarini, D., Gerola, M., De Feudis, S., Lupattelli, A., Dalla Santa, G., Capati, G., Rafai, M., Tihana, J., Scerbo, M., Di Donna, A., Ravera, E., Nicolino, M., Insana, A., Mroueh, H., & Barla, M. (2026). Database-driven analysis of energy geostructures using a global dataset: Diffusion, efficiency, and environmental performance. Renewable Energy, 256. https://doi.org/10.1016/j.renene.2025.124373

Sanner, B. (2016). Shallow geothermal energy – history , development , current status , and future prospects. European Geothermal Congress 2016, Pp. 19–24, Strasbourg, France.

Sarbu, I., & Sebarchievici, C. (2016). Solar Heating and Cooling: Fundamentals, Experiments and Applications. Elsevier: Oxford, UK.

Schneider, M. (2010). Geotu6 – a geothermal research project for tunnels, Tunnel 2 (2010) 14–21.

Shafagh I. (2019). Analytical investigations into thermal resistance of diaphragm wall heat exchangers. Proceedings of the European Geothermal Congress, 1–6.

Shafagh, I., & Loveridge, F. (2020). Developing analysis approaches for energy walls. E3S Web of Conferences, 205. https://doi.org/10.1051/e3sconf/202020506005

Shafagh, I., Rees, S., Urra Mardaras, I., Curto Janó, M., & Polo Carbayo, M. (2020). A Model of a Diaphragm Wall Ground Heat Exchanger. Energies, 13(2), 300. https://doi.org/10.3390/en13020300

Shin, S., & Shin, H. (2023). Aging of perovskite solar cells: a mini review. Materials Today Energy, 37, 101381. https://doi.org/10.1016/j.mtener.2023.101381

Smaisim, G. F., AbdulHussein, W. A., & Abed, A. M. (2022). Enhancement of heat transfer from solar thermal collector using nanofluid. Open Engineering, 12(1), 968–976. https://doi.org/10.1515/eng-2022-0337

Smith, B. L., Woodhouse, M., Horowitz, K. A. W., Silverman, T. J., Zuboy, J., & Margolis, R. M. (2021). Photovoltaic (PV) Module Technologies: 2020 Benchmark Costs and Technology Evolution Framework Results (NREL/TP-7A40-78173). National Renewable Energy Laboratory: Golden, CO.

Soga, K., & Rui, Y. (2016). Energy geostructures. In Advances in Ground-Source Heat Pump Systems (pp. 185–221). Elsevier Inc. https://doi.org/10.1016/B978-0-08-100311-4.00007-8

Sonal Vaghela, Ankitkumar S. Patel, Jayraj V. Solanki, & Kamlesh Damdoo. (2024). Optimizing Renewable Energy Integration in Green Building Projects: Addressing Barriers and

Enhancing Energy Performance. International Research Journal on Advanced Engineering Hub (IRJAEH), 2(08), 2179–2183. https://doi.org/10.47392/irjaeh.2024.0296

Stefansson, V. (2005). World geothermal assessment. In: Proceedings World Geothermal Congress.

Suman, S., Khan, Mohd. K., & Pathak, M. (2015). Performance enhancement of solar collectors—A review. Renewable and Sustainable Energy Reviews, 49, 192–210. https://doi.org/10.1016/j.rser.2015.04.087

Sun, Liu, D., Flor, J.-F., Shank, K., Baig, H., Wilson, R., Liu, H., Sundaram, S., Mallick, T. K., & Wu, Y. (2020). Analysis of the daylight performance of window integrated photovoltaics systems. Renewable Energy, 145, 153–163. https://doi.org/10.1016/j.renene.2019.05.061

Sun, Xia, C., & Zhang, G. (2013). Heat transfer model and design method for geothermal heat exchange tubes in diaphragm walls. Energy and Buildings, 61, 250–259. https://doi.org/10.1016/j.enbuild.2013.02.017

Tester, J. W., Drake, E. M., Golay, M. W., Driscoll, M. J., & Peters, W. A. (2005). Sustainable Energy – Choosing Among Options. MIT Press: Cambridge, Massachusetts, USA.

European Commission, Directorate-General for Energy. (1999). Blue Book on Geothermal Resources: A Strategic Plan for the Development of European Geothermal Sector. European Commission: Brussels, Belgium.

Tony, P., Suckling, & Smith. (2002). Environmentally friendly geothermal piles at Keble College, Oxford, UK.

Tsagarakis, K. P., Efthymiou, L., Michopoulos, A., Mavragani, A., Anđelković, A. S., Antolini, F., Bacic, M., Bajare, D., Baralis, M., Bogusz, W., Burlon, S., Figueira, J., Genç, M. S., Javed, S., Jurelionis, A., Koca, K., Ryżyński, G., Urchueguia, J. F., & Žlender, B. (2020). A review of the legal framework in shallow geothermal energy in selected European countries: Need for guidelines. Renewable Energy, 147, 2556–2571. https://doi.org/10.1016/j.renene.2018.10.007

United Nations Environment Programme. (2024). Global Status Report for Buildings and Construction: Beyond foundations: Mainstreaming sustainable solutions to cut emissions from the buildings sector. Nairobi. https://doi.org/10.59117/20.500.11822/45095.

Vieira, A., Alberdi-Pagola, M., Christodoulides, P., Javed, S., Loveridge, F., Nguyen, F., Cecinato, F., Maranha, J., Florides, G., Prodan, I., Van Lysebetten, G., Ramalho, E., Salciarini, D., Georgiev, A., Rosin-Paumier, S., Popov, R., Lenart, S., Erbs Poulsen, S., & Radioti, G. (2017). Characterisation of Ground Thermal and Thermo-Mechanical Behaviour

for Shallow Geothermal Energy Applications. Energies, 10(12), 2044. https://doi.org/10.3390/en10122044

Wang, G., Cai, Y., Jiang, H., Liu, F., Yi, K., & Wang, D. (2023). Combinatorial tuning of work function and optical properties in CuZnSe thin films for efficient bifacial CdTe solar cells. Solar Energy Materials and Solar Cells, 255, 112312. https://doi.org/10.1016/j.solmat.2023.112312

Wilhelm, J., & Rybach, L. (2003). The geothermal potential of Swiss Alpine tunnels. Geothermics, 32(4–6), 557–568. https://doi.org/10.1016/S0375-6505(03)00061-0

Wilson, G. M., Al-Jassim, M., Metzger, W. K., Glunz, S. W., Verlinden, P., Xiong, G., Mansfield, L. M., Stanbery, B. J., Zhu, K., Yan, Y., Berry, J. J., Ptak, A. J., Dimroth, F., Kayes, B. M., Tamboli, A. C., Peibst, R., Catchpole, K., Reese, M. O., Klinga, C. S., … Sulas-Kern, D. B. (2020). The 2020 photovoltaic technologies roadmap. Journal of Physics D: Applied Physics, 53(49), 493001. https://doi.org/10.1088/1361-6463/ab9c6a

Winston, R. (1974). Principles of solar concentrators of a novel design. Solar Energy, 16(2), 89–95. https://doi.org/10.1016/0038-092X(74)90004-8

Xia, C., Sun, M., Zhang, G., Xiao, S., & Zou, Y. (2012). Experimental study on geothermal heat exchangers buried in diaphragm walls. Energy and Buildings, 52, 50–55. https://doi.org/10.1016/j.enbuild.2012.03.054

Yang, N., Shi, W., & Zhou, Z. (2023). Research on Application and International Policy of Renewable Energy in Buildings. In Sustainability (Switzerland) (Vol. 15, Number 6). Multidisciplinary Digital Publishing Institute (MDPI). https://doi.org/10.3390/su15065118

Yousef, B. A. A., Mahmoud, M., Aljaghoub, H., Abdelkareem, M. A., Alami, A. H., & Olabi, A. G. (2023). Phase change materials in solar photovoltaics: Bibliometric analysis, role in achieving sustainability, challenges and barriers. Thermal Science and Engineering Progress, 45. https://doi.org/10.1016/j.tsep.2023.102082

ZANELDIN, E. (2024). Potential uses of renewable energy in construction: Advantages and challenges. Renewable Energy: Generation and Application, 43, 66–72. https://doi.org/10.21741/9781644903216-9

Zhao, C., Yu, S., Tang, W., Yuan, X., Zhou, H., Qi, T., Zheng, X., Ning, D., Ma, M., Zhu, J., Zhang, J., Yang, C., & Li, W. (2023). Advances in CIGS thin film solar cells with emphasis on the alkali element post-deposition treatment. Materials Reports: Energy, 3(3), 100214. https://doi.org/10.1016/j.matre.2023.100214

Zheng, J., Ma, F.-J., Liao, C., Bing, J., Tang, S., Soufiani, A. M., Lee Chin, R., Xue, C., Qu, J., Yang, L., Mahmud, M. A., Sun, Z., Leung, T. L., Wang, G., Cairney, J. M., Bremner, S.,

McKenzie, D. R., Huang, S., & Ho-Baillie, A. W. Y. (2023). Efficient perovskite solar cell on steel enabled by diffusion barrier and surface passivation. Cell Reports Physical Science, 4(9), 101543. https://doi.org/10.1016/j.xcrp.2023.101543

Ziyadanogullari, N. B., Yucel, H. L., & Yildiz, C. (2018). Thermal performance enhancement of flat-plate solar collectors by means of three different nanofluids. Thermal Science and Engineering Progress, 8, 55–65. https://doi.org/10.1016/j.tsep.2018.07.005